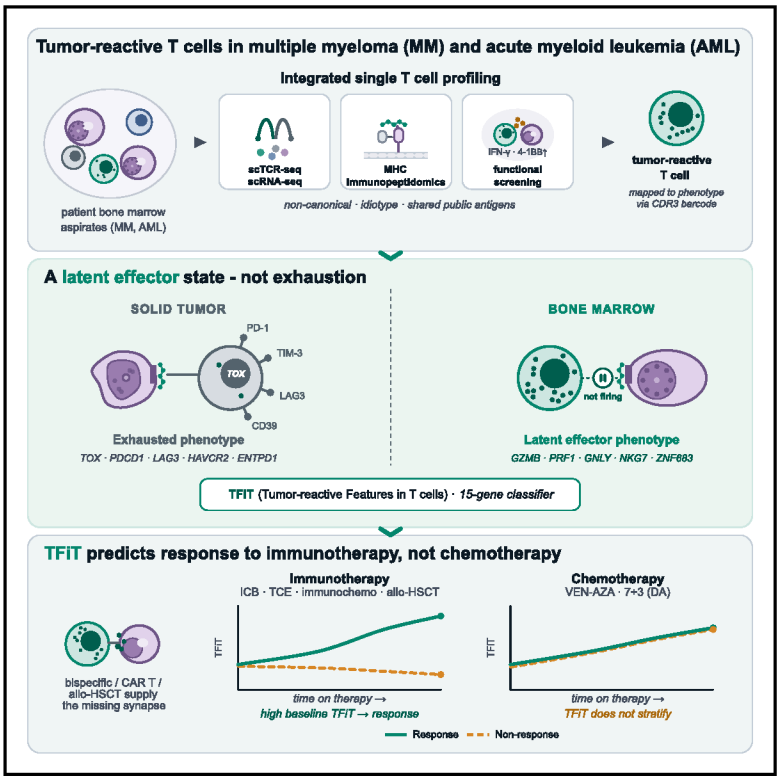
Cancer Cell

Article

Latent effector T cells mediate immunotherapy responses in the bone marrow microenvironment

Graphical abstract



Highlights

- Bone marrow tumor-reactive T cells in MM and AML are distinct from solid tumor TILs
- A shared immunopeptidome drives convergent T cell responses across MM and AML
- TFiT stratifies immunotherapy, but not chemotherapy, response in MM and AML
- Latent effector T cells in bone marrow are activatable by immunotherapy

Authors

Niklas Kehl, Tim R. Wagner, Simon Steiger, ..., Michael Platten, Stefan B. Eichmüller, Mirco J. Friedrich

Correspondence

mirco.friedrich@dkfz.de

In brief

Kehl et al. characterize tumor-reactive T cells in the bone marrow of patients with multiple myeloma and AML. These cells adopt an effector state distinct from exhausted solid tumor TILs. The TFiT classifier stratifies immunotherapy, but not chemotherapy, response, identifying a latent, therapeutically engageable anti-tumor compartment.

Kehl et al., 2026, Cancer Cell *44*, 1779–1798
September 14, 2026 © 2026 The Author(s). Published by Elsevier Inc.
https://doi.org/10.1016/j.ccell.2026.07.011

CellPress

Cancer Cell

CellPress
OPEN ACCESS

Article

Latent effector T cells mediate immunotherapy responses in the bone marrow microenvironment

Niklas Kehl,[1,2,3,4,22] Tim R. Wagner,[1,2,3,4,22] Simon Steiger,[5,6,22] Tamara Boschert,[2,7,8,9,22] Michael Kilian,[10] Antonia Schach,[1,2,3,4,11] Julius J. Michel,[1,2,3,4] Kane Foster,[12] Gabrielle M. Hernandez,[13] Claudia Ctortecka,[13] Anna D. Metzler,[1,2,3,4,11] Alanna Kirschner,[1,2,3,4,11] Arne Van der Vreken,[1,2,3,4] Dominik Humer,[1,2,3,4] René Onken,[1,2,3,4] Sven Cuntz,[1,2,3,4] Julian Zoller,[1,2,3,4] Cornelius Funk,[1,2,3,4] Selina Neunhäuser,[4] Maximilian Mönnig,[4] Bruno Schönfelder,[14] Simon Renders,[2,3,4,15] Claudia Maldonado Torres,[2,7,8,9] Lilli S. Sester,[4,16] Jan H. Frenking,[4,16] Franziska Werner,[14] Wolfram Osen,[14] Katharina Lindner,[2,7,8] Ezgi Sen,[5,6] Sabrina Schumacher,[5,6] Daria Galas-Filipowicz,[12] Evie Fitzsimons,[12] Edward W. Green,[2,7,8,9] Patrick Schmidt,[14,17] John M. Lindner,[18] Sebastian Uhrig,[17,19] Lukas Bunse,[2,7,8,9] Benny Chain,[12] Hartmut Goldschmidt,[4,16] Niels Weinhold,[4] Stefan Fröhling,[2,17,19,20] Tim Sauer,[4] Simon Raffel,[4] Jennifer G. Abelin,[13] Steven A. Carr,[13] Kwee Yong,[12] Andreas Trumpp,[2,3,15] Carsten Müller-Tidow,[4,17] Karsten Rippe,[5,6,23] Marc S. Raab,[4,16,23] Michael Platten,[2,7,8,9,21,23] Stefan B. Eichmüller,[2,14,23] and Mirco J. Friedrich[1,2,3,4,13,24,*]

[1]German Cancer Research Center (DKFZ), JRG Hematology and Immune Engineering, Heidelberg, Germany
[2]German Cancer Consortium (DKTK), Core Center Heidelberg, Heidelberg, Germany
[3]Heidelberg Institute for Stem Cell Technology and Experimental Medicine (HI-STEM gGmbH), Heidelberg, Germany
[4]Department of Hematology, Oncology and Rheumatology, Heidelberg University Hospital, Heidelberg, Germany
[5]German Cancer Research Center (DKFZ), Division of Chromatin Networks, Heidelberg, Germany
[6]BioQuant, Heidelberg, Germany
[7]German Cancer Research Center (DKFZ), CCU Neuroimmunology and Brain Tumor Immunology, Heidelberg, Germany
[8]Department of Neurology, Medical Faculty Mannheim, MCTN, University of Heidelberg, Mannheim, Germany
[9]Helmholtz Institute for Translational Oncology (HI-TRON) Mainz, German Cancer Research Center (DKFZ), Mainz, Germany
[10]Ann Romney Center for Neurologic Diseases, Brigham and Women's Hospital, Harvard Medical School, Boston, MA, USA
[11]Faculty of Biosciences, Heidelberg University, Heidelberg, Germany
[12]Department of Haematology, Cancer Institute, University College London, London, UK
[13]Broad Institute of MIT and Harvard, Cambridge, MA, USA
[14]German Cancer Research Center (DKFZ), GMP and Cell Therapy Group, Heidelberg, Germany
[15]Division of Stem Cells and Cancer, German Cancer Research Center (DKFZ), Heidelberg, Germany
[16]Heidelberg Myeloma Center, Heidelberg University Hospital, Heidelberg, Germany
[17]National Center for Tumor Diseases (NCT), NCT Heidelberg, a partnership between DKFZ and Heidelberg University Hospital, Heidelberg, Germany
[18]BioMed X Institute, Heidelberg, Germany
[19]Division of Translational Medical Oncology, German Cancer Research Center (DKFZ), Heidelberg, Germany
[20]Division of Translational Precision Medicine, Institute of Human Genetics, Heidelberg University, Heidelberg, Germany
[21]DKFZ-Hector Cancer Institute at University Medical Center Mannheim, Mannheim, Germany
[22]These authors contributed equally
[23]Senior author
[24]Lead contact
*Correspondence: mirco.friedrich@dkfz.de
https://doi.org/10.1016/j.ccell.2026.07.011

SUMMARY

T cell-mediated immune surveillance is critical for cancer control, yet its role in bone marrow malignancies remains poorly understood. Here, we integrate TCR profiling, HLA immunopeptidomics, and functional screening to characterize tumor-reactive T cells in the bone marrow of patients with multiple myeloma (MM) and acute myeloid leukemia (AML). These cells are transcriptionally defined by a conserved effector program distinct from the exhausted phenotype of tumor-reactive T cells in solid cancers. Immunopeptidomic profiling reveals a partially shared antigen landscape enriched for noncanonical peptides driving convergent TCR responses. We develop *TFiT* (tumor-reactive features in T cells), a transcriptional classifier that identifies these cells and stratifies immunotherapy, but not chemotherapy, response across independent MM and AML cohorts, supporting its specificity for T cell-mediated tumor control. These findings reveal a latent but activatable anti-tumor T cell compartment in bone marrow malignancies and provide a framework for engaging endogenous immunity in MM and AML.

This is an open access article under the CC BY license (http://creativecommons.org/licenses/by/4.0/).

INTRODUCTION

T cells can mediate durable tumor control, yet their efficacy in bone-marrow-resident malignancies remains highly variable and poorly understood.[1–3] While disease-associated T cells are frequently observed in the bone marrow of patients with multiple myeloma (MM) and acute myeloid leukemia (AML), the frequency, antigen specificity, and clinical relevance of tumor-reactive T cells in these diseases remain elusive.[4–6] Prior studies have demonstrated that most T cells within the tumor microenvironment are bystanders with no overt anti-tumor activity and that *bona fide* tumor-reactive clonotypes are rare and difficult to identify, particularly outside the setting of immune checkpoint blockade (ICB) or in the context of highly immunogenic disease.[7–9] In contrast to solid tumors, where the landscape of tumor-specific T cell receptors (TCRs) and their functional correlates is increasingly defined,[10–13] MM and AML lack a unifying model of endogenous antitumor T cell immunity.[4–6,14,15] While neoantigens derived from gene fusions[16,17] and cancer-associated antigens (CAAs)[18] have been proposed and tested as actionable targets in selected hematologic malignancies, the prevalence and immunological relevance of shared public antigens or recurrent, cross-disease targets—distinct from private neoantigens—remain incompletely characterized.[19–21]

Here, we integrate high-sensitivity TCR profiling with HLA immunopeptidomes and functional single-cell screening to define the antigen specificity, transcriptional phenotype, and clinical relevance of tumor-reactive bone marrow T cells (BMTs) from patients with MM and AML. By combining antigen-agnostic assays with peptide-guided interrogation of patient-derived T cells, we identify patient- and disease-spanning features of functionally identified tumor-reactive lymphocytes, uncover shared immunogenic peptides derived from both canonical and noncanonical sources, and link the abundance and functional state of these cells to therapeutic response across multiple treatment modalities.

RESULTS

Identification of tumor-reactive T cells in the bone marrow of patients with MM and AML

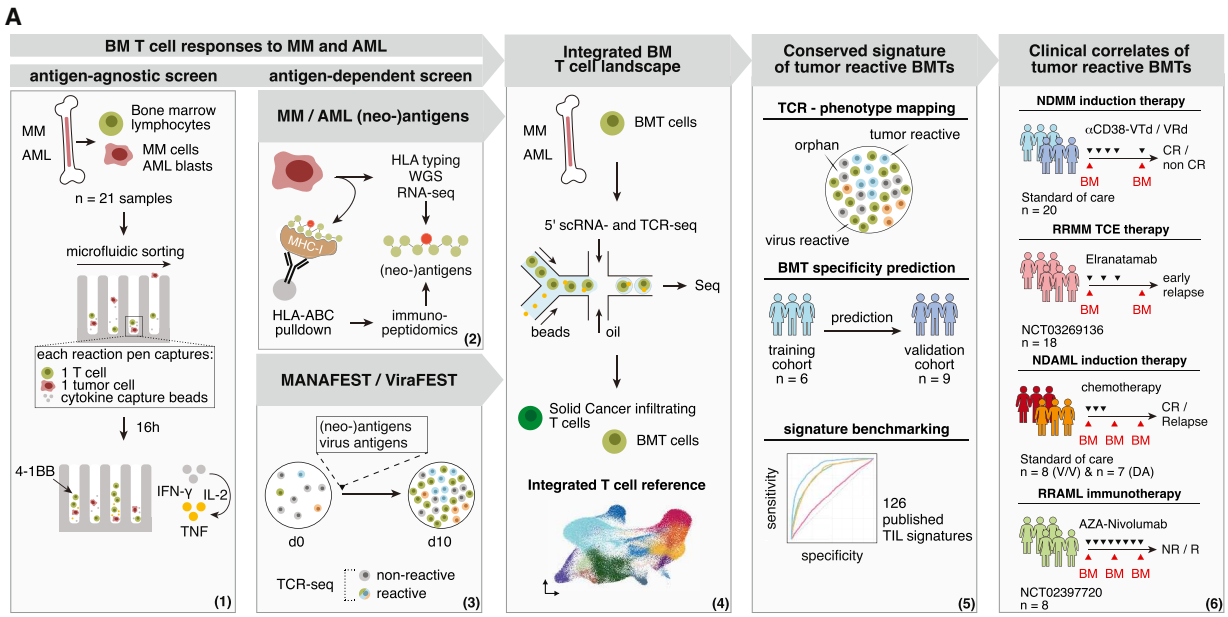
The detection and characterization of tumor-reactive T cells in bone-marrow-resident malignancies is hampered by marrow infiltration by malignant cells, lymphodepletion from high-dose chemotherapy regimens, and the complexity of the bone marrow microenvironment.[22,23] To identify such clonotypes and define their phenotypic and functional states *in situ*, we performed integrated *ex vivo* profiling of BMTs from a total of 21 patients with newly diagnosed MM (NDMM, $n = 15$) and AML ($n = 6$) of bone marrow aspirates obtained at initial diagnosis. The myeloma cohort was subjected to parallel single-cell transcriptomic, TCR profiling, and functional analyses (Figure 1A; Table S1).

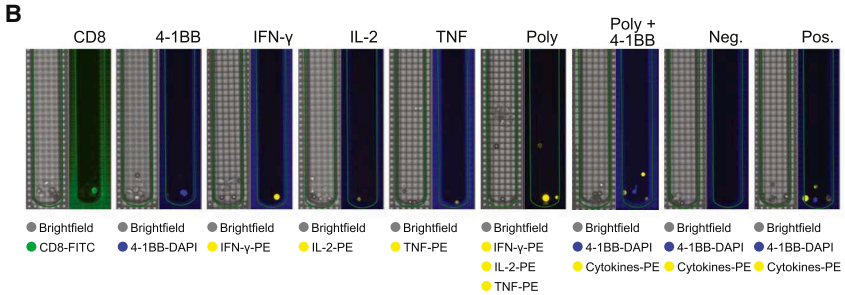
To establish a high-resolution map of BMT phenotypes and their TCR clonotypes, we applied single-cell RNA sequencing (scRNA-seq) combined with single-cell V(D)J sequencing (scVDJ-seq) for simultaneous assessment of gene expression and paired TCR identity (Figures S1A–S1D). We recovered 186,060 high-quality transcriptomes representing 135,398 unique TCR clonotypes across an extended NDMM patient cohort of $n = 20$ patients (Figures S1E–S1I), and we integrated our hematological malignancy and healthy BMT datasets with a published pan-cancer TIL reference atlas[24] across 16 cancer types to enable high-confidence phenotypic annotation and allow direct comparisons with solid cancer tumor-infiltrating lymphocytes (TILs), . This unified atlas enabled common reference-based clustering (Figures S1B–S1F) and annotation across entities, treatment stages, and tissue compartments and revealed marked compositional differences between solid cancer TILs and BMTs; notably, exhausted and progenitor-exhausted T cells played a substantially more pronounced role in the solid tumor compartment compared to the bone marrow microenvironment (Figures S2A–S2E). Unsupervised clustering of BMTs within this integrated framework resolved 15 phenotypic subsets, defined by canonical marker genes including *CCR7*, *TCF7*, *TOX*, *PDCD1*, *ENTPD1*, *LAG3*, *HAVCR2*, *TIGIT*, *GZMB*, and *GZMK* (Figures S1E and S1F). Major populations comprised $CD8^+$ effector-memory ($CD8^+$ eEM) and terminally differentiated effectors ($CD8^+$ TermEff), which together constituted the highest proportion in most patients, and $CD8^+$ naive ($CD8^+$ N) T cells, alongside naive and memory $CD4^+$ subsets and regulatory T cells, consistent with previous studies in untreated MM and AML[25–29] (Figures S1C–S1F and S2A–S2D; Table S1). Minor populations included MAIT and interferon-stimulated gene (ISG)-expressing T cells.

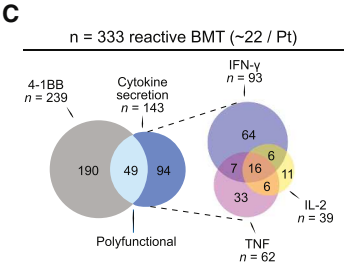
To identify functionally tumor-reactive T cells in both diseases, we employed a dual screening strategy: (1) an antigen-agnostic forward screen exposing single BMTs to patient-autologous MM or AML cells in microfluidic chambers and (2) an antigen-informed reverse screen based on whole-genome sequencing (WGS)-, RNA-seq-predicted, and immunopeptidomics-defined tumor antigens, applying a functional expansion assay (MANAFEST/ViraFEST) to detect antigen-responsive T cells[10,30–32](Figure 1A).

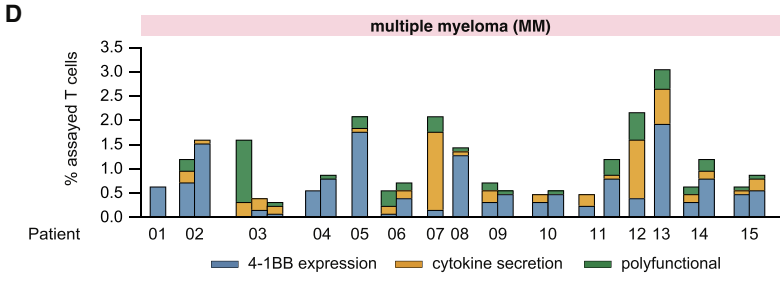
In the forward screen, single BMTs were co-incubated with autologous primary tumor cells for 16 h. The microfluidic assay simultaneously captured cytokine secretion (interleukin [IL]-2, interferon gamma [IFN-γ], tumor necrosis factor [TNF]) and surface upregulation of CD137 (4-1BB) upon tumor cell contact (Figure 1B). Given the median count and distribution of unique BMT clonotypes in our patient biopsies determined by concurrently performed scTCR-seq, and considering the benchmarks of our screening approach, the minimal frequency of an individual TCR to be detected at least once with ≥95% probability is approximately 0.2% (or 42 cells per clone). Across all patients and 42,262 BMTs functionally screened, we identified 333 BMTs demonstrating at least one signal of tumor reactivity, which were retrieved and subjected to paired TCRα/β sequencing (Figures 1B and 1C; Table S2; Figures S3A and S3B; Data S1). IFN-γ was the most frequently secreted cytokine, followed by TNF and IL-2. A subset of T cells exhibited polyfunctionality, with simultaneous cytokine secretion and CD137 expression (Figure 1C). Tumor-reactive BMTs were detected in nearly all patients, but their abundance and functional profiles varied across individuals and disease entities (Figures 1D and 1E; Table S2). MM samples displayed a higher overall frequency of tumor-reactive cells than AML, particularly among $CD8^+$ polyfunctional T cells co-expressing CD137 (Figures 1F and 1G; Table S2). Notably, IL-2-only-secreting cells were exclusively $CD4^+$ (Figure 1G). Using the CDR3 sequence as a unique clonal barcode to map these

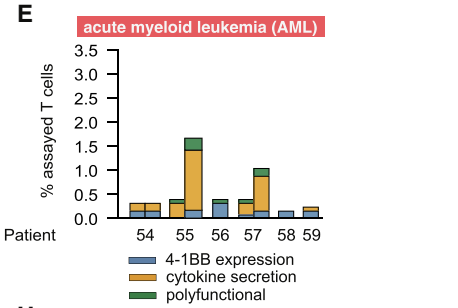
CellPress
OPEN ACCESS

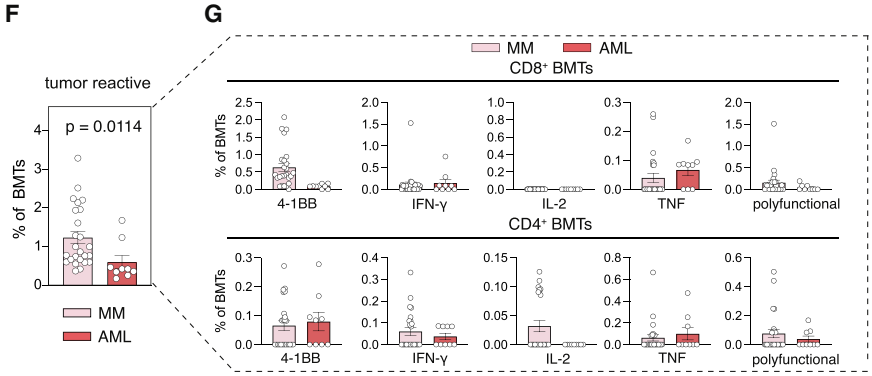


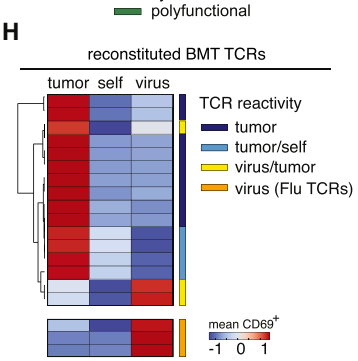












(legend on next page)

functionally identified TCRs to the scRNA/VDJ-seq dataset,[33,34] we found that the abundance of tumor-reactive clones correlated with canonical transcriptional programs; less expanded tumor-reactive T cells expressed lymphoid progenitor markers such as *SELL* and *IL7R*, while highly expanded reactive clones expressed cytotoxic effector genes including *GZMB*, *GNLY*, *PRF1*, and *NKG7* (Figures S4A and S4B).

To validate the tumor specificity of recovered TCRs, we reconstructed clonotypes via mRNA-based TCR re-expression in patient-autologous peripheral blood T cells (Figures S4C–S4G). TCRs were selected for functional validation based on the following criteria: (1) full V(D)J sequencing coverage of both α and β chains; (2) identification of unique TCRα/β chain pairings (in cases where two alpha chains were detected for a single clone, observed in ∼30% of human T cells due to incomplete allelic exclusion at the TRA locus, all recovered αβ combinations were tested); (3) TCR surface expression rates exceeding 30% following mRNA electroporation; and (4) availability of sufficient purity-sorted autologous malignant plasma cells or AML blasts from the same patient to perform cellular specificity assays. A subsequently performed orthogonal co-culture assay used upregulation of CD69 as an early activation marker to validate MHC class I-dependent TCR responses in each patient against autologous tumor cells, with anti-HLA-ABC blocking antibodies confirming HLA dependence (Figure 1H: Figures S3, S5A–S5D, and S6A–S6C). However, investigation of *ex vivo* cytotoxicity by LDH-release assay was not possible due to severely limited post-thawing viability of primary patient malignant cell samples (Figures S7A–S7J). Tumor-reactive TCRs showed selective activation upon tumor cell co-culture but not against autologous healthy peripheral blood mononuclear cells (PBMCs) or viral peptide pools, though a subset of TCRs demonstrated cross-reactivity with either viral antigens or healthy PBMCs (Figures S8A and S8B).

Noncanonical immunopeptidomes and shared antigen vulnerabilities in MM and AML

Having identified tumor-reactive TCRs with selective activity against autologous malignant cells, we next aimed to delineate the antigenic landscape that underlies these specificities *in vivo*. Building on emerging insights into the immunogenic potential of aberrant transcript processing,[35,36] including recent evidence of mis-splicing-derived neoepitopes in splicing factor-mutant leukemias, we hypothesized that hematological malignancies, despite their comparatively low tumor mutational burden (TMB) relative to solid tumors (∼1–2 mutations/Mb), may give rise to immunogenic noncanonical antigens as a byproduct of transcriptional and translational dysregulation.[21] To explore this, we conducted systematic HLA class I immunopeptidomics on primary tumor samples from 11 patients with MM and 6 patients with AML in our cohort, each informed by prior HLA typing (Table S3).

Using LC-MS/MS analysis of HLA-I immunoprecipitates, we identified 17,161 unique peptide sequences across the cohort. Integration with curated annotations of upstream/downstream open reading frames (ORFs), long noncoding RNAs (lncRNAs), pseudogenes, and CAAs revealed that a substantial fraction of HLA-I-bound peptides were derived from noncanonical translational events[37,38] (Figure 2A; Table S3). Notably, only a single classical mutation-derived neoantigen was detected across the entire cohort, underscoring that in these low-TMB malignancies, the immunopeptidome is shaped predominantly by non-canonical and cancer-associated antigen sources rather than somatic mutations. Noncanonical peptides were observed across all patients and accounted for a major fraction of the tumor immunopeptidome, although the number and composition of presented peptides varied markedly between individuals and entities, reflecting high inter-individual heterogeneity of HLA-I antigen presentation (Figure 2A). CAAs were identified in both diseases but contributed a modest fraction of the total peptide pool (∼5%–10%) and were more frequently detected in MM[39] (Figure 2A; Table S3). To assess potential normal tissue expression of identified antigens, we cross-referenced peptides mapping to canonical protein-coding genes against the HLA Ligand Atlas,[40] which contains immunopeptidome data from a panel of benign human tissues. This comparison revealed selective enrichment on malignant cells relative to normal tissues for

Figure 1. Integrated discovery and functional validation of tumor-reactive T cells and antigens in the bone marrow of patients with multiple myeloma and acute myeloid leukemia

(A) Schematic overview of the pipeline for identifying tumor-reactive bone marrow T cells (BMTs) in multiple myeloma (MM) and acute myeloid leukemia (AML). Steps include (1) functional co-culture assays with autologous tumor cells in microfluidic chambers; (2) tumor antigen discovery via whole-genome sequencing (WGS), RNA-seq, and HLA class I immunopeptidomics; (3) immunopeptidome-informed MANAFEST (mutation-associated neoantigen functional expansion of specific T cells) and ViraFEST assays; (4) 5′ single-cell RNA and TCR sequencing of BMTs and integration with tumor-infiltrating T cells of solid cancers[24] to construct an integrated reference of cancer-associated T cell phenotypes; (5) TCR-phenotype mapping to single-cell transcriptome data and generation of a conserved transcriptional signature of tumor-reactive BMTs; and (6) clinical association with independent patient cohorts and therapeutic settings.

(B) Representative images from the antigen-agnostic functional screen. Single BMTs were co-cultured with autologous tumor cells (MM or AML) for 16 h in nanowell chambers containing cytokine-capture antibodies and monitored for surface CD137 (4-1BB) upregulation and secretion of IFN-γ, IL-2, and TNF. Tumor-reactive cells were individually retrieved and subjected to paired TCRα/β sequencing.

(C) Venn diagram summarizing functional characteristics of 333 tumor-reactive MM BMTs polyfunctionality was defined as concurrent CD137 expression and secretion of ≥1 cytokine.

(D and E) Distribution of tumor-reactive events across as percentage of assayed T cells in $n = 25$ MM (D) and $n = 9$ AML (E) screening runs. Functional categories defined as in (C).

(F) Frequency of tumor-reactive BMTs as a proportion of total BMTs per experimental run. Statistical comparison between MM ($n = 25$ individual experimental runs) and AML ($n = 9$ individual experimental runs) by unpaired two-tailed *t* test with Welch's correction (mean ± SEM).

(G) Proportion of tumor-reactive BMTs stratified by $CD4^+$ or $CD8^+$ lineage. Mean ± SEM shown for MM ($n = 25$ individual experimental runs) and AML ($n = 9$ individual experimental runs).

(H) Heatmap summarizing tumor specificity testing for $n = 19$ representative reconstituted BMT-derived TCRs, each tested against autologous tumor cells (tumor), healthy PBMCs (self), and a viral peptide pool (virus). Data represent CD69-positive events shown as mean across $n = 3$ experimental replicates per TCR scaled per row. See also Figures S1–S8; Tables S1 and S2; Data S1.

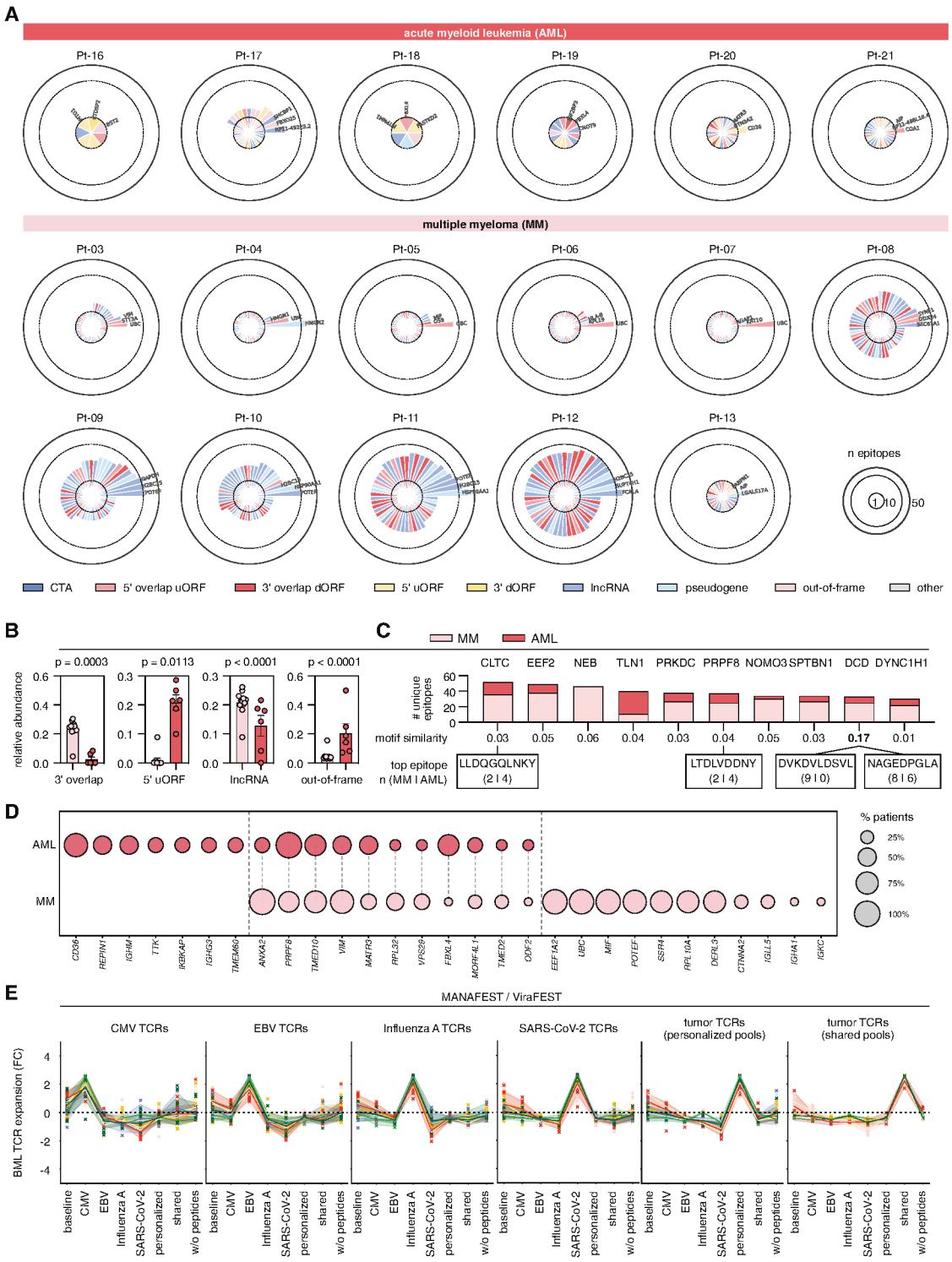


Figure 2. Noncanonical antigen landscapes in MM and AML revealed by HLA class I immunopeptidomics

(A) Circular bar plots illustrating the diversity and source composition of HLA-class-I-bound peptides identified in individual AML (top) and MM (bottom) patients. Epitope sources include cancer-associated antigens (CAAs), upstream and downstream noncanonical open reading frames (nuORFs), lncRNA-derived peptides, pseudogene-derived peptides, and immunoglobulin/BCR-derived sequences. Total of 17,161 unique peptides across the cohort.

(B) Relative abundance of noncanonical epitope categories in MM $n = 11$ and AML $n = 6$ patients. Statistical comparisons by unpaired two-tailed t tests (mean ± SEM).

(legend continued on next page)

the majority of tested antigens; of 69 unique CAA epitopes, 13 (18.8%) were found to be naturally presented on healthy cells, with bone marrow presentation described for six of these (Table S3; Figures S9A–S9C).

The noncanonical antigen landscape diverged systematically between MM and AML. AML samples predominantly presented peptides from 5′-untranslated-region-derived upstream ORFs (uORFs), while MM samples were enriched for 3′-overlapping downstream ORFs (dORFs), lncRNA-encoded peptides, and pseudogene-derived sequences. These differences remained statistically significant after normalization for total peptide counts (Figure 2B; Table S3).

However, we identified a subset of noncanonical peptides that were recurrently detected across both diseases. For example, a peptide derived from *DCD*, a gene normally expressed in epithelial tissues and aberrantly activated in hematological cancers, was HLA presented in 8 of 11 MM patients and all 6 AML samples.[41] Additional recurrently presented peptides derived from *CTNNA2*, *ODF2*, the RNA/DNA-binding protein *MATR3*, and the chromatin-associated *MORF4L1* gene were detected across both diseases, echoing recent reports of conserved HLA-presented peptides arising from splicing factor mutations[21,35,36] and suggesting that convergent antigen processing pathways may operate across genetically and clinically distinct malignancies, potentially through shared stress or epigenetic mechanisms that deregulate RNA translation (Figures 2C and 2D).

Beyond non-canonical upstream ORF (nuORF)-derived peptides, we also identified several peptides originating from the immunoglobulin protein complex in MM samples as HLA-I-bound antigens presented by malignant plasma cells (Figure 2D).

To systematically investigate this phenomenon, we performed *in silico* assembly of the malignant B cell receptor (BCR) repertoire by reconstructing the dominant myeloma clonotype in each patient. We then predicted peptide sequences with high binding affinity to each patient's autologous HLA class I allotypes and generated individualized BCR-derived peptide libraries for targeted immunopeptidomic mapping (Figure S9D; Table S4). In one patient (Pt-11), we identified a naturally presented peptide (LYKFNNKEYL) derived from the hypermutated *IGKV* chain, specifically within complementarity-determining region 1 (CDR1). This peptide was eluted from the HLA class I complex and matched a variant detected at 40% variant allele frequency in the dominant MM clone, providing direct evidence of BCR-derived peptide presentation in MM (Figure S9E). Together with prior reports on immunoglobulin-derived antigens in lymphomas and idiotype vaccinations, these data underscore the potential of clonotypic immunoglobulin sequences as a personalized neoantigen source uniquely accessible in B cell-derived malignancies.[42–48]

To complement our antigen-agnostic forward TCR screening approach and broaden coverage of the BMT specificity landscape, we next sought to retrospectively identify TCRs reactive to the identified tumor antigens as well as those recognizing common viral epitopes. We performed MANAFEST and ViraFEST assays in nine patients for whom both immunopeptidomic data and viable BMTs were available.[10,30–32] T cells were stimulated with personalized peptide pools comprising all detected non-canonical and CAA peptides from each patient's immunopeptidome, supplemented by a shared tumor antigen pool of recurrently detected peptides, alongside defined viral epitope libraries. The number of peptides tested per patient ranged from 25 to 68, depending on immunopeptidomics yield. Peptides were tested in pools, as is standard for the MANAFEST assay, which relies on antigen-driven clonal expansion over 10 days followed by ultra-deep TCRβ sequencing to identify significantly expanded clonotypes. We identified 123 tumor-antigen-specific (mutation-associated antigen [MANA]-specific) TCRs across all individuals: 88 reactive to private antigens and 35 targeting shared tumor epitopes. In parallel, we detected 104 CMV-specific, 86 EBV-specific, 88 influenza-A-specific, and 88 SARS-CoV-2-specific TCRs (Figure 2E; Figure S3; Table S4). No overlap was observed between tumor-reactive and virus-specific TCRs. Convergent TCR selection is well established in the context of viral immunity, where population-wide exposure to conserved epitopes drives the emergence of public TCRs.[49,50] Beyond the expected virus-specific public TCRβ sequences expanding similarly across individuals, we also identified several shared TCRβ sequences across patients in response to common tumor-derived peptides in the MANAFEST assay, suggesting that convergent selection may occur in response to recurrently presented tumor antigens (Table S4).

Together, these findings reveal a complex yet structured tumor antigen landscape in AML and MM, shaped by disease-specific translational programs and partially conserved epitopes. The near-absence of classical mutation-derived neoantigens and the recurrent presentation of nuORF-derived peptides, CAAs, and clonotypic-idiotype-derived neoepitopes define alternative sources of tumor-specific peptides for TCR recognition in low-TMB bone marrow malignancies.

Mapping of tumor-specific TCRs and convergent selection

To resolve antigen specificities of the tumor-reactive TCRs identified in our screens, we performed a peptide-library-based TCR:epitope deconvolution approach adapted from the T-FINDER system.[51] We assembled personalized antigen libraries composed of all detected patient-specific and shared

(C) Stacked bars show the number of unique HLA-presented peptide sequences derived from each of the 10 most frequently sampled source proteins, ranked by total unique sequences (PTM variants collapsed; keratin contaminants excluded). Each bar is partitioned by the patient group in which sequences were detected: MM-only, shared (detected in ≥1 patient of both entities), and AML-only. Below each bar: intra-protein motif similarity of its epitopes and selected single most broadly presented ("top") epitopes, with the number of MM and AML patients presenting it (n, MM | AML).
(D) Bubble plot, where each protein is scored by the percentage of patients per entity in whom ≥1 epitope from that protein was detected (MM $n = 11$, AML $n = 6$); circle area is proportional to that percentage. Proteins are grouped along the *x* axis as AML-restricted (detected only in AML patients), shared (detected in both entities), or MM-restricted (detected only in MM patients).
(E) Summary of MANAFEST and ViraFEST assay results across $n = 9$ NDMM patients with matched immunopeptidome data. Significantly expanded TCRβ clonotypes per condition were identified by bootstrapped enrichment (FEST algorithm). Personalized peptide pools comprised 25–68 peptides per patient, tested in pools. See also Figures S3 and S9; Tables S3 and S4.

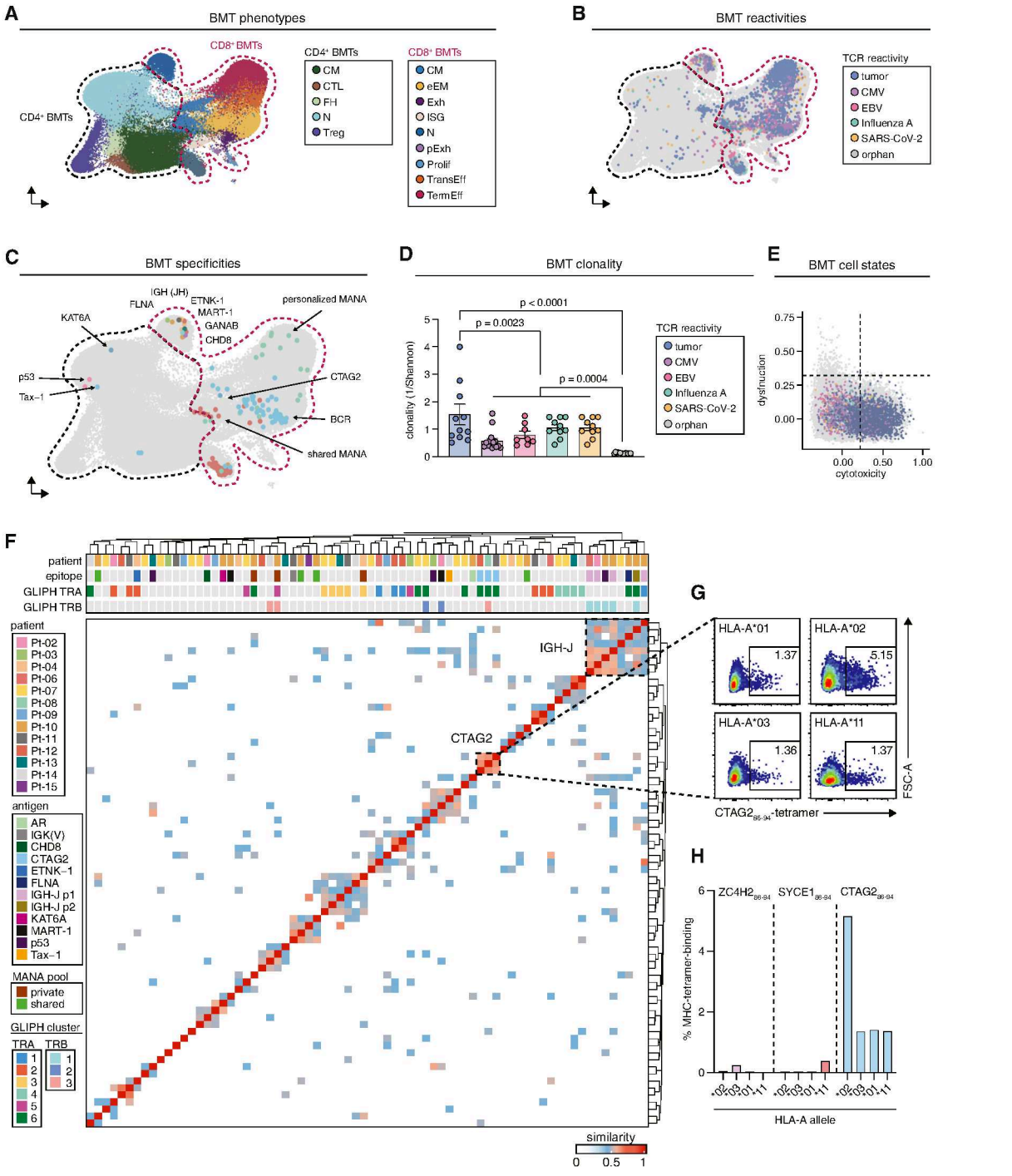


Figure 3. Mapping antigen specificity, clonal architecture, and convergent TCR selection across the bone marrow T cell landscape

(A) Representative UMAP of BMTs reference-based cluster annotation. Colored by cluster.

(B) UMAP projection of BMTs with TCR specificity overlay. Specificity categories: tumor-reactive (functionally validated by antigen-agnostic screening, MANA-specific by MANAFEST, or deorphanized to cognate antigen) and virus-specific (SARS-CoV-2, influenza A, CMV, EBV). Orphan cells (no attributed specificity) shown in gray. A total of 2,243 tumor-reactive T cells were back-projected across 15 patients.

(C) UMAP of deorphanized BMTs colored by matched cognate peptide antigen.

(D) TCR clonality (inverse Shannon diversity) as bar chart (mean ± SEM) in cohort of n = 15 NDMM patients stratified by specificity group, where available. Statistical comparisons by one-way ANOVA with Tukey's post hoc test.

(E) Scatterplot of cytotoxicity versus dysfunction module scores[52] across BMTs of n = 15 NDMM patients, color-coded by antigen specificity. Bystander cells in gray.

(legend continued on next page)

peptides identified by immunopeptidomics, additionally including predicted BCR-derived neoepitopes in MM cases. Lentivirally transduced Jurkat reporter cells expressing individual tumor-reactive TCRs were co-cultured with patient-derived B lymphoblastoid cell lines (B-LCLs), which served as HLA-matched autologous antigen-presenting cells (Figures S10A–S10D). Of the 51 antigen-agnostically identified TCRs, 43 had confirmed paired α/β sequences compatible with the T-FINDER reporter platform; using CD69 upregulation as a readout of TCR activation relative to the irrelevant peptide control TET93, we successfully deorphanized 11 TCRs to their individual cognate antigens (Figures S10E and S10F; Tables S4 and S5). We further investigated endogenous T cell recognition of the *IGKV*-derived neoepitope identified in Pt-11 using this approach and recovered three independent endogenous TCR clonotypes capable of recognizing different minimal epitopes of the naturally presented *IGKV* peptide (LYKFNNKEYL) (Figure S10G; Tables S4 and S5).

To map tumor-specific TCRs within the broader immune architecture of the bone marrow, we integrated the functional data from our antigen-agnostic and antigen-informed assays with baseline BMT transcriptomes. By leveraging the unique CDR3 nucleotide sequences of validated TCRs as clonal barcodes, we retrospectively traced them to their baseline transcriptional states in the scRNA/VDJ-seq dataset, to enable resolution of native *in vivo* phenotypes independent of stimulation-induced transcriptional perturbation[33,34] (Figure 3A; Figure S2).

Across 15 patients, we back-projected 2,243 T cells from the identified and validated tumor-reactive clonotypes (Figure 3B; Figure S3; Table S5). Tumor-reactive T cells constituted approximately 1.29% of all bone-marrow-infiltrating T cells at diagnosis, aligning with frequencies observed in our functional screening as well as in solid tumors.[7,11] In contrast, the majority of TCRs not classified as tumor-reactive mapped to $CD4^+$ subsets or matched empirically defined viral antigen-recognizing TCRs (CMV, EBV, influenza A, and SARS-CoV-2). These distributions are consistent with published descriptions of virus-specific immune landscapes in healthy bone marrow,[53–55] although they likely also reflect technical enrichment inherent to our screening strategy: the antigen-agnostic microfluidic assay captures cytokine secretion (IFN-γ and TNF) and 4-1BB upregulation—readouts that preferentially detect $CD8^+$ effector T cells with immediate cytotoxic capacity—while the MANAFEST assay uses predominantly HLA-class-I-restricted peptides, further enriching for $CD8^+$ responses (Figures 3A–3C). Tumor-specific TCRs exhibited significantly higher clonality than viral or orphan TCRs (Figure 3D), suggesting antigen-driven local expansion. These expanded clones also displayed transcriptional states associated with cytotoxicity when scored with published signatures of T cell effector function (Figure 3E). In contrast, virus-specific TCRs largely resembled non-expanded bystanders with lower cytotoxic potential and a more quiescent phenotype, as previously reported[7,56] (Figures 3A, 3B, and 3D).

Given that certain tumor antigens were recurrently presented across patients, we next investigated whether chronic exposure to shared tumor-associated epitopes could drive convergent selection, i.e., the emergence of TCRs with similar antigen-binding motifs across individuals.[49,50] We defined convergent TCRs as those sharing at least one V gene and a homologous CDR3 amino acid sequence with another patient-derived clone, irrespective of nucleotide sequence (i.e., public rearrangements). Using pairwise CDR3 similarity scoring based on BLOSUM45 local alignment, normalized to self-alignment scores, we applied bootstrapped similarity thresholds and motif clustering, cross-validated with GLIPH,[57] to identify multiple TCR networks exhibiting high inter-patient similarity indicative of convergent recognition (Figure 3F; Figure S11A).

Among tumor-reactive TCRs, we identified two representative clusters of convergent clonotypes. The first comprised three MM patients (Pt-02, Pt-06, and Pt-12) sharing a homologous TCRβ CDR3 sequence specific for the immunoglobulin heavy-chain joining segment (*IGHJ*), a tumor-associated antigen highly expressed in plasma cell malignancies but absent in healthy non-B cells[58] (Figure 3F). The second cluster featured a shared TCRα CDR3 motif across Pt-06, Pt-08, and Pt-11, with variable yet overlapping TCRβ sequences (Figure 3F; Figure S11A). Using HLA profiling data and tumor cells from Pt-08, we validated $CTAG2_{86\text{-}94}$ (RLLELHITM) as the cognate antigen of this clonotype, confirming antigen specificity across patients with non-overlapping HLA haplotypes (Figures S11B and S11C). To assess the breadth of this shared reactivity, we performed peptide-MHC tetramer staining for $CTAG2_{86\text{-}94}$ and three other recurrent HLA-class-I-presented epitopes using BMTs from patients across four distinct HLA haplotypes (Figures S12A and S12B). $CTAG2_{86\text{-}94}$-reactive T cells were detected in multiple individuals across different HLA supergroups, with preferential but not exclusive binding to HLA-A*02 (Figures 3G and 3H; Figure S12B). These data indicate HLA promiscuity of the $CTAG2_{86\text{-}94}$ epitope, a property of certain antigens that enables cross-patient immune recognition despite HLA diversity.[59] Notably, the frequency of $CTAG2_{86\text{-}94}$-specific T cells exceeded that of other shared antigens tested, suggesting its potential as an actionable therapeutic target (Figures 3F–3H).

Together, these data demonstrate that tumor-specific T cell responses in MM are not entirely private but can involve public TCR motifs and shared tumor antigens with broad HLA-restricted epitope presentation, features that may be exploitable for off-the-shelf immunotherapeutic approaches.

(F) Network visualization of pairwise TCR CDR3αβ sequence similarity. Similarity was computed by BLOSUM45 local alignment normalized to self-alignment scores; edges shown only above the 95th percentile of a bootstrapped background distribution (>100,000 non-annotated TCR pairwise comparisons). Nodes colored by patient of origin. Cross-validated with GLIPH-based clustering. Inset sequence logos show convergent CDR3 motifs exceeding the 99th percentile threshold.

(G) Representative flow cytometry plots of peptide-MHC tetramer staining for $CTAG2_{86\text{-}94}$ (RLLELHITM) across HLA-A supergroups (*01, *02, *03, and *11).

(H) Quantification of tetramer-positive BMTs for shared immunopeptidome-derived antigens across HLA-A supergroups, demonstrating binding promiscuity of selected epitopes. See also Figures S2, S3, and S10–S12; Tables S4 and S5.

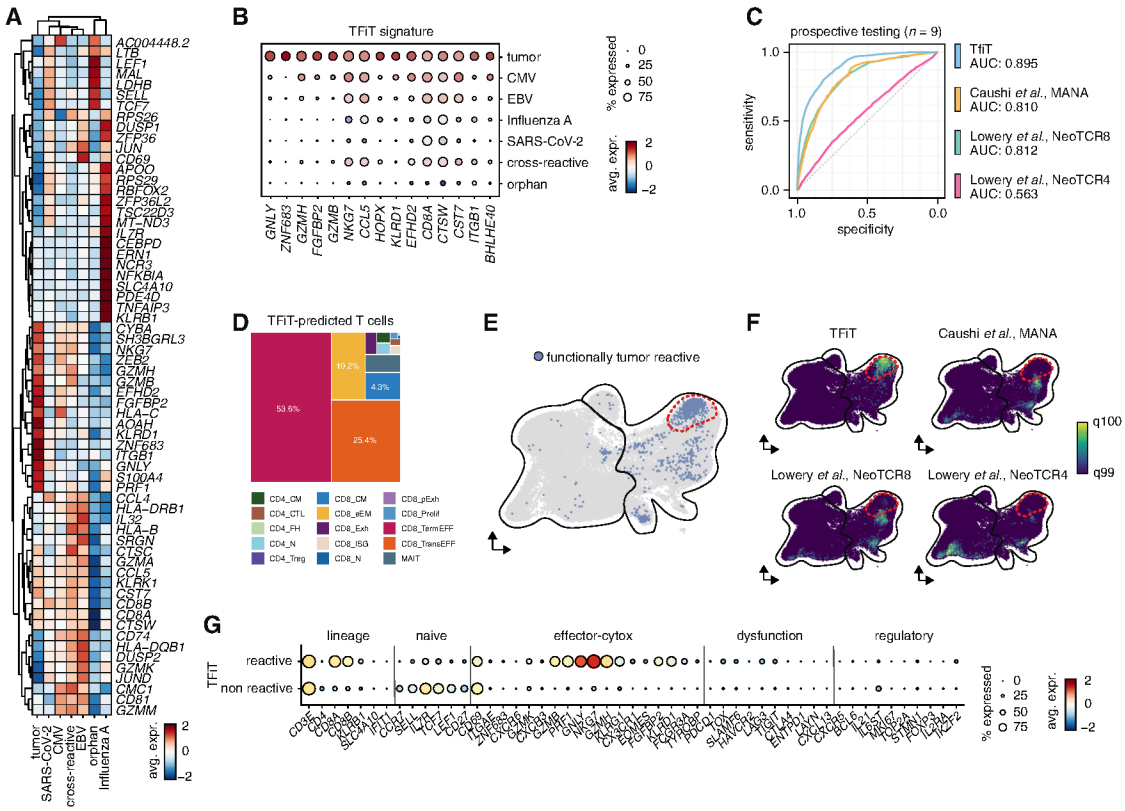


Figure 4. TFiT—a conserved transcriptional classifier distinguishing tumor-reactive from virus-reactive and bystander bone marrow T cells

(A) Scaled heatmap of top differentially expressed genes between tumor-reactive, virus-reactive (CMV, EBV, influenza A, and SARS-CoV-2), and orphan BMTs across $n = 15$ NDMM patients. Genes ranked by $\log_2$ fold change within each category.

(B) Dot plot of TFiT signature gene expression across reactivity categories in the classifier training cohort ($n = 6$ patients, 947 tumor-reactive cells). Dot size indicates percentage of cells expressing each gene; color indicates scaled mean expression.

(C) Receiver operating characteristic (ROC) analysis comparing predictive performance of transcriptional classifiers for tumor-reactive TCR identification: TFiT (AUC = 0.895), MANA (Caushi et al., 2021[10]; AUC = 0.810), NeoTCR_8 (Lowery et al., 2022[12]; AUC = 0.812), and NeoTCR_4 (Lowery et al., 2022[12]; AUC = 0.563). Evaluated in the independent prospective validation cohort ($n = 9$ patients; 1,302 cells). Statistical analysis as described in STAR Methods section.

(D) Treemap visualization of T cell cluster composition by percentage of TFiT-based tumor-reactive predicted T cells (total of 26,269 cells) in $n = 15$ NDMM patients. Colored by T cell cluster.

(E) UMAP of T-cell-reference-based cluster annotation in $n = 15$ NDMM patients overlaid with tumor-reactive T cells ($n = 2,243$ cells after reference-based QC; $n = 100$ scVDJ clonotypes) highlighted in blue.

(F) Feature plot highlighting top 1% of signature expressing T cells in atlas dataset of tumor-associated T cells of hematological and solid cancers ($n = 188,101$ cells).[24]

(G) Dot plot of canonical T cell phenotype marker gene expression in TFiT-positive (predicted tumor-reactive) and TFiT-negative (non reactive) BMTs in $n = 15$ NDMM patients. Markers include cytotoxic effector genes (*GZMB*, *PRF1*, *GNLY*, and *NKG7*), tissue-residency markers (*ZNF683*), and exhaustion-associated genes (*TOX*, *ENTPD1*, *PDCD1*, *LAG3*, *HAVCR2*, and *TIGIT*). See also Figures S4 and S13; Table S6.

Conserved transcriptional programs define tumor-reactive T cells in the bone marrow

To determine whether tumor-reactive BMTs share conserved transcriptional features that distinguish them from virus-specific or bystander T cells, we performed differential gene expression analysis between tumor-reactive, virus-reactive, and orphan BMTs. Tumor-reactive T cells displayed a predominant cytotoxic effector phenotype, marked by high expression of *GZMB*, *GZMH*, *GNLY*, *PRF1*, and *NKG7*, alongside tissue-residency markers such as *ZNF683* (Figures 4A and 4B; Figures S13A and S4A). These features were not shared with virus-reactive TCRs.

To systematically define the transcriptional features of tumor-reactive BMTs, we generated a classifier based on genes that consistently distinguished tumor-specific from virus-specific T cells across patients. Using iterative feature selection, model training, and retrospective receiver operating characteristic (ROC) analysis on a reference dataset of 947 tumor-reactive cells from six patients (with the remaining patients as a holdout cohort for benchmarking), we identified a robust 15-gene signature with high predictive accuracy (AUC = 0.979) (Figures 4B and 4C; Table S6). We termed this classifier TFiT (tumor-reactive features in T cells). As expected, TFiT-classified T cells predominantly mapped to a $CD8^+$ effector T cell phenotype, although they were not confined to a single cluster, further supporting the use of signature-based classification over cluster-restricted phenotyping (Figure 4D).

When benchmarked on the same dataset, TFiT outperformed 122 existing signatures derived from neoantigen- or

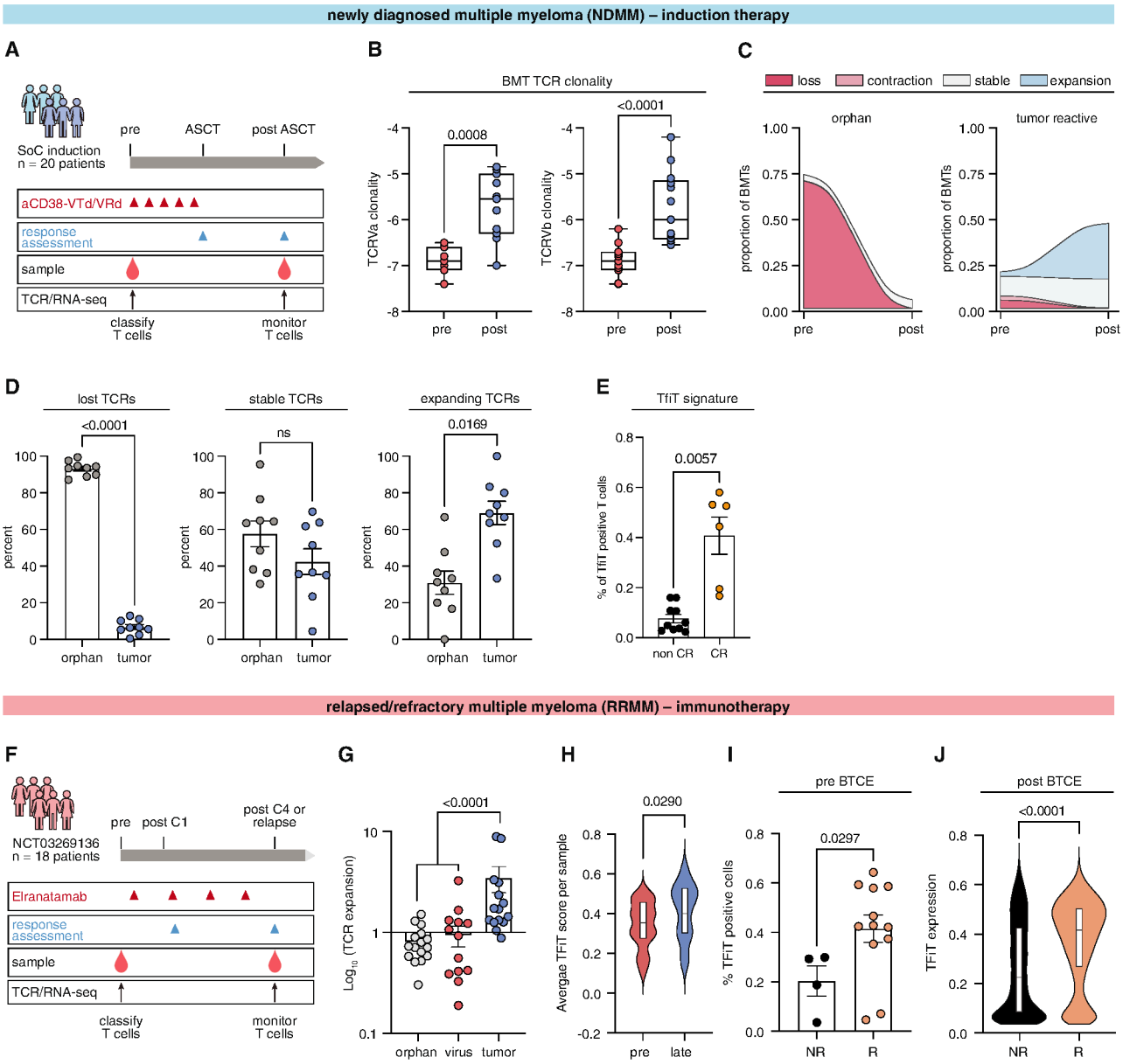


Figure 5. Longitudinal dynamics and clinical relevance of tumor-reactive BMTs during MM induction therapy and bispecific antibody treatment

(A) Experimental workflow and sampling timeline for 20 newly diagnosed MM (NDMM) patients treated with SOC induction therapy followed by autologous stem cell transplantation (ASCT). BMTs were profiled by scRNA-seq and scTCR-seq pre-treatment and post-ASCT.

(B) TCR clonality (inverse Shannon diversity) based on TCRα/β usage, assessed pre-treatment, and 100 days post-ASCT (CARDAMON trial)[64] in $n = 11$ NDMM patients. Boxplot showing median ± IQR; whiskers indicate 10–90 percentile. Statistical analysis by two-tailed paired t test.

(C) Representative alluvial plots showing clonal dynamics of individual TCR clonotypes pre- and post-treatment, colored by TFiT-assigned reactivity category.

(D) Clonal dynamics across $n = 9$ patients with paired pre- and post-treatment samples. Mean ± SEM. Statistically significant changes in clonotype frequency determined by bootstrap resampling, corrected for multiple comparisons (Benjamini-Hochberg method).

(E) Frequency of TFiT-positive BMTs at baseline stratified by clinical response to quadruple induction therapy (non-CR, CR; $n = 16$ patients). Mean ± SEM. Statistical comparison by unpaired t test with Welch's correction.

(F) Experimental workflow for scRNA-seq and scTCR-seq profiling of 18 relapsed/refractory MM patients treated with the BCMA×CD3 bispecific antibody elranatamab (MagnetisMM-1 trial, NCT03269136). Bone marrow samples collected pre-treatment and post-cycle 4 (~90 days) or at relapse.

(G) Longitudinal tracking of TCR clonotype frequencies stratified by TFiT-predicted reactivity ($n = 16$ patients with paired samples). Mean ± SEM. Statistical analysis by repeated-measures two-way ANOVA with Tukey's post hoc test.

(H) Average TFiT score per patient ($n = 16$) pre-treatment and after four cycles of bispecific antibody therapy. Violin plot with overlaid boxplot showing median ± IQR; whiskers indicate 10–90 percentile. Statistical comparison by unpaired t test with Welch's correction.

(legend continued on next page)

MANA-specific T cells, including MANA[10] (Caushi et al., 2021; AUC = 0.810), NeoTCR_8[12] (Lowery et al., 2022; AUC = 0.812), and NeoTCR_4[12] (Lowery et al., 2022; AUC = 0.563) (Figure S13B; [10–13,52,60,61] Table S6). To evaluate prospective performance, we applied TFiT to an independent validation cohort of 1,302 T cells from nine additional patients. TFiT again outperformed all comparator models, achieving an AUC of 0.895 (Figure 4C; Figure S13C; Table S6), confirming its generalizability across patients.

Critically, the transcriptional identity of tumor-reactive BMTs diverged fundamentally from that of tumor-reactive TILs in solid cancers. By integrating our bone marrow datasets with a pan-solid-cancer TIL reference atlas,[47] we found that validated tumor-reactive T cells in the bone marrow mapped to the cytotoxic effector compartment rather than to the exhausted or progenitor-exhausted clusters that characterize tumor-reactive TILs in solid tumors (Figures 4E and 4F). Bone marrow tumor-reactive T cells lacked the canonical exhaustion signature defined by high co-expression of *TOX*, *ENTPD1* (CD39), *PDCD1* (PD-1), *LAG3*, and *HAVCR2* (TIM-3) that is the hallmark of neoantigen-reactive TILs in melanoma, non-small cell lung cancer (NSCLC), and other solid cancers. Instead, these cells maintained active expression of cytotoxic effector genes while lacking markers of terminal exhaustion, consistent with a state of latent competence: transcriptionally equipped for cytotoxicity but not engaged in sustained tumor elimination *in vivo* (Figure 4G).

This distinction is further supported by the non-overlap between TFiT and established solid-tumor reactivity signatures. When we applied NeoTCR8[12] and MANA,[10] they primarily did not capture our bone marrow tumor-reactive T cells (Figures 4C and 4E). We therefore hypothesize that bone marrow tumor-reactive T cells and solid tumor TILs operate under distinct transcriptional programs shaped by their respective microenvironments, rather than representing the same biology detected with different sensitivity.

Together, these data establish a conserved transcriptional blueprint of antitumor T cell responses in the bone marrow that is fundamentally distinct from the exhaustion-defined programs in solid cancers. TFiT captures bone-marrow-resident T cells that are both transcriptionally equipped for cytotoxicity and enriched for *bona fide* tumor recognition. Because tumor-reactive T cells in these malignancies are rare and do not form a single discrete cluster on standard dimensionality reduction projections (Figures 4D and 4F), this classifier derived from differential expression analysis across functionally defined categories provides a more reliable identification strategy than visual or clustering-based approaches.

Pre-existing tumor-reactive T cells correlate with clinical response in multiple myeloma

In solid tumors, efforts to predict anti-tumor immune responses have focused on TCR clonality, neoantigen-specificity, or exhaustion markers—mostly in samples collected post-immunotherapy exposure.[10–13,52,60–63] By contrast, little is known about how endogenous tumor-specific T cells shape therapeutic outcomes in patients with multiple myeloma.

To address this, we analyzed longitudinal BMT samples from patients with NDMM undergoing current standard-of-care induction chemotherapy (daratumumab, bortezomib, thalidomide, dexamethasone [Dara-VTd] or bortezomib, lenalidomide, and dexamethasone [VRD]; see Table S1). We performed paired scRNA/VDJ-seq and bulk TCRα/β-seq on vitally preserved bone marrow samples collected before and after induction therapy for direct tracking of tumor-reactive T cell clones using their CDR3 nucleotide sequence as a clonal barcode (Figure 5A). Overall, T cell counts remained stable across time points (Figure S13D); however, post-treatment samples showed significantly increased clonality (Figure 5B), consistent with antigen-driven responses during or after treatment. To assess the behavior of tumor-reactive T cells specifically, we classified all detected TCRs at baseline using the TFiT signature and tracked their clonal dynamics. Across the cohort, tumor-reactive TCRs were more likely than bystander or orphan clones to persist or significantly expand following therapy (Figures 5C and 5D). In contrast, virus-specific and orphan TCRs were more frequently lost or remained static. We next asked whether the abundance of tumor-reactive T cells at diagnosis could predict clinical response to induction therapy. Patients who achieved a complete response (CR) or better exhibited a higher abundance of TFiT-classified tumor-reactive cells in pretreatment bone marrow (Figure 5E). Together, these data suggest that tumor-reactive TCRs are selectively preserved during treatment and are associated with response to induction (immunochemo-)therapy in MM.

Given the observed association between baseline tumor-reactive T cells and response to induction therapy, we next asked whether this relationship would be further amplified in the context of active immunotherapy, specifically bispecific T cell engagers (bsAbs), which directly depend on the presence of functional, cytotoxic T cells for therapeutic efficacy.

To explore this, we longitudinally profiled bone marrow T cell responses in 18 clinical trial patients with relapsed/refractory MM (r/r MM) treated with the BCMA × CD3 bispecific antibody elranatamab.[65–67] Bone marrow samples were collected at baseline (pre-treatment) and post-cycle 4 (∼90 days) or at relapse and analyzed by integrated scRNA/VDJ-seq (Figures 5F and 5G). Classification of TCRs using TFiT identified tumor-reactive T cells in all r/r MM patients, albeit at variable frequencies. Following bsAb administration, we observed selective expansion of tumor-reactive clones, while orphan and virus-specific TCRs remained largely unchanged (Figure 5G). TFiT expression increased during treatment (Figures 5H–5J), and a high baseline frequency of TFiT$^+$ tumor-reactive T cells correlated with clinical response in terms of early relapse (Figure 5I), both by proportion of TFiT$^+$-classified cells at baseline, mirroring our observations in newly diagnosed MM patients treated with induction therapy.

(I) Pre-treatment frequency of TFiT$^+$ BMTs per patient (n = 16) stratified by clinical response (early relapse before four cycles) to bispecific antibody therapy after four cycles. Mean ± SEM shown. Statistical comparison by unpaired t test with Welch's correction.
(J) Single-cell TFiT expression in single cells (total n = 68,348 cells) comparing clinical responders and non-responders after four treatment cycles. Violin plot with overlaid boxplot showing median ± IQR; whiskers indicate 10–90 percentile. Statistical comparison by unpaired t test with Welch's correction. See also Figure S13; Table S1.

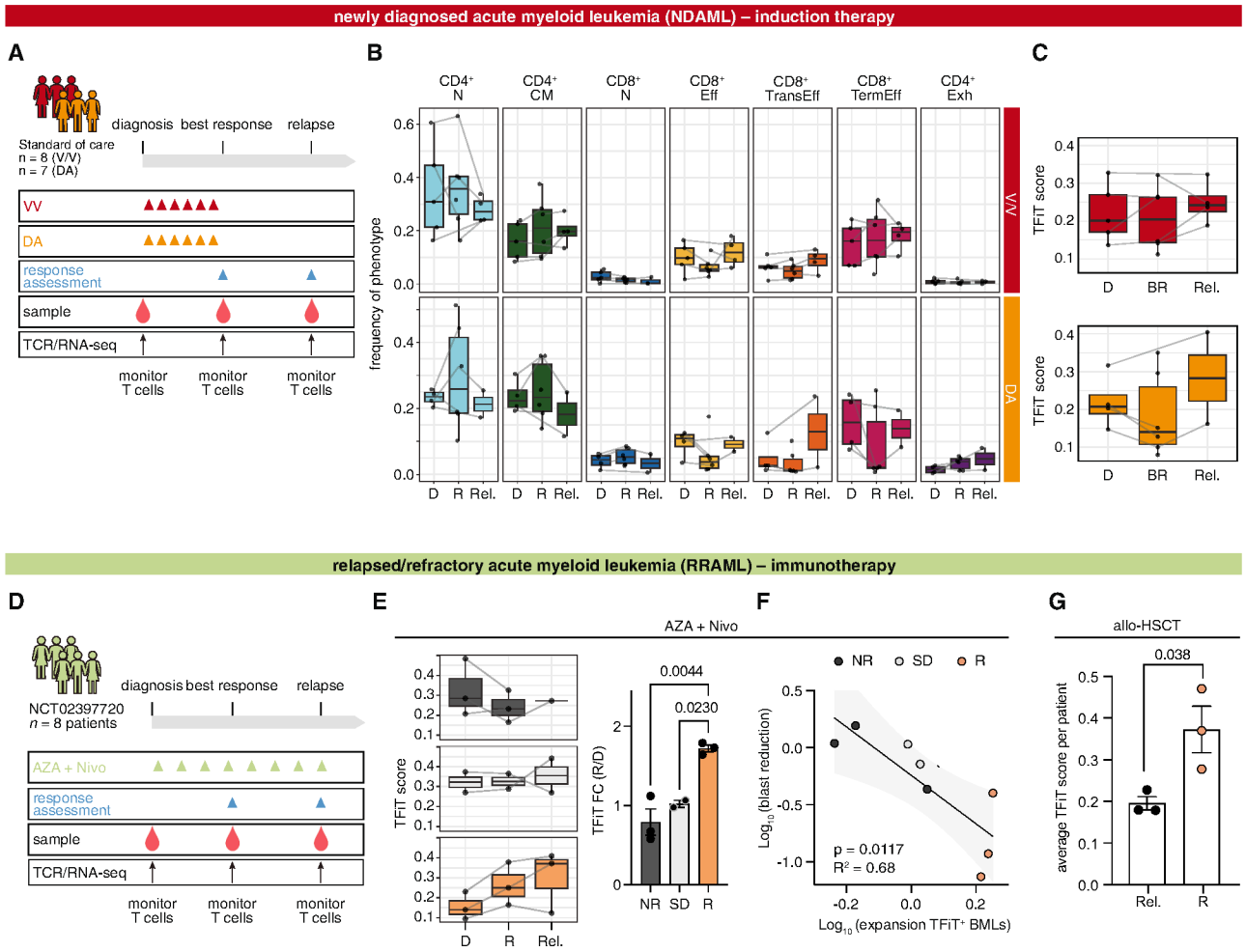


Figure 6. TFiT predicts immunotherapy response in relapsed/refractory AML but not response to standard intensive chemotherapy

(A) Experimental workflow for scRNA-seq and scTCR-seq profiling of 16 newly diagnosed AML (ND AML) patients pre-treatment at complete response and at relapse treated with non-intensive induction chemotherapy with Vidaza/Venetoclax (VV, *n* = 8) or intensive induction chemotherapy with daunorubicin and cytarabine (DA, *n* = 7).

(B) Bone marrow T cell subtype dynamics of ND AML patients across time points split by treatment cohort. Boxplot showing median ± IQR; whiskers indicate 10–90 percentile. n = total of VV, *n* = 8; DA, *n* = 7 patients as per sample availability at time points: diagnosis (D), best response (BR), and relapse (Rel.).

(C) Longitudinal dynamic of average TFiT expression per ND AML sample split by therapeutic regimen. Boxplot showing median ± IQR; whiskers indicate 10–90 percentile. n = total of VV, *n* = 8; DA, *n* = 7 patients as per sample availability at time points: diagnosis (D), best response (BR), and relapse (Rel.).

(D) Experimental workflow for scRNA-seq and scTCR-seq profiling of eight relapsed/refractory AML (RR AML) patients pre-treatment, during treatment, and post-treatment treated with the azacitidine (AZA) + nivolumab (Nivo) within the AARON trial (NCT02397720).[68]

(E) Left: longitudinal dynamic of average TFiT expression per sample split by response category. Boxplot showing median ± IQR; whiskers indicate 10–90 percentile. Right: fold change between time points A and B in frequency of TFiT$^+$ BMTs stratified by clinical response in total *n* = 8 RR AML patients. Mean ± SEM per reponse category shown. Statistical comparison by unpaired *t* test with Welch's correction.

(F) Linear correlation of TFiT$^+$ BMT expansion (log10FC of average TFiT expression between pre- and best response) and blast reduction by flow cytometry (log10FC of blast reduction between pre and best response) across *n* = 8 RR AML patients. X-Y scatterplot with line showing linear regression fit (shaded area: 95% confidence interval [CI]). Pearson correlation coefficient shown (R^2 = 0.68, *p* = 0.0117). Data points color-coded by patient's best response.

(G) Average TFiT score per patient in *n* = 6 AML patients post-allogeneic stem cell transplantation (allo-HSCT)[14] split by response status (complete response [CR] or relapse post-allo-HSCT). Mean ± SEM. Statistical significance was assessed using a linear mixed-effects model with donor as a random effect. See also Figure S13; Table S1.

Tumor-reactive T cells associate with responses to immunotherapy, but not chemotherapy, in AML

Given the predictive value of tumor-reactive T cells in MM and their association with response to both immunochemotherapy and bispecific antibodies, we next assessed whether this framework extends to AML.

To this end, we prospectively assembled and performed single-cell 5′ GEX and VDJ sequencing on BMTs from a cohort of 15 newly diagnosed AML patients treated with standard intensive and non-intensive chemotherapy: eight with venetoclax-azacitidine (VV) and seven with daunorubicin-cytarabine (DA), stratified into eight patients achieving complete remission and

seven with refractory disease (Figure 6A; Table S1). Patients span all ELN 2022 risk categories (seven favorable, four adverse, four intermediate), with matched longitudinal sampling at diagnosis, best response, and relapse. Across all time points, we profiled 247,394 high-quality bone marrow T cells (Figure 6A). Analysis of T cell subset dynamics revealed an increase in terminally differentiated $CD8^+$ effector T cells with therapy and at relapse in both treatment arms. VV-treated patients additionally showed a shift from naive to memory $CD4^+$ T cells, while naive $CD8^+$ T cells were present at very low frequencies across all patients and time points, consistent with the immunosuppressive and disrupted bone marrow microenvironment in AML (Figure 6B).

Critically, and in contrast to MM, TFiT did not predict response to chemotherapy in this cohort (Figure 6C), which we hypothesize reflects that in patients receiving cytotoxic chemotherapy such as VV or DA, the primary mechanism of blast clearance is rapid, direct pharmacological killing of malignant cells rather than endogenous T cell-mediated tumor elimination.

However, the curative potential of allogeneic stem cell transplantation demonstrates that AML is fundamentally amenable to T cell-mediated immune control,[69] and the limited but real responses to ICB suggest that endogenous tumor-reactive T cells may contribute to anti-leukemia immunity when appropriately activated, even if their spontaneous efficacy is constrained by the immunosuppressive marrow niche and the low neoantigen burden characteristic of AML.[68,70,71] To test whether tumor-reactive T cells underlie the rare responses to ICB, we re-analyzed paired scRNA-seq and scTCR-seq data from the phase 2 AARON trial (NCT02397720)[71] of azacitidine plus nivolumab in relapsed/refractory (r/r) AML. This cohort comprised longitudinal bone marrow samples from eight patients, including three clinical responders, three non-responders, and two with stable disease[68] (Figure 6D).

We applied TFiT to this dataset to determine whether pre-existing tumor-reactive T cells associate with clinical anti-leukemia response. TFiT-positive cells were detectable at baseline and showed selective expansion in clinical responders following therapy. In contrast, non-responders exhibited minimal or no expansion of tumor-reactive T cells, while patients with stable disease showed intermediate dynamics (Figure 6E). Across the cohort, the magnitude of tumor-reactive T cell expansion—as inferred by TFiT—correlated with both flow cytometric blast reduction and overall clinical response (R^2 = 0.68, p = 0.0117), while baseline tumor burden did not correlate with TFiT at diagnosis (Figure S13E), providing further support for the predictive relevance of BMTs with features of tumor reactivity (Figure 6F).

In a complementary analysis of six AML patients post-allogeneic stem cell transplantation (allo-HSCT),[14] a low average TFiT score was associated with early relapse after transplantation (Figure 6G). This finding is noteworthy in light of recent work that identified clonally expanded $ZNF683^+$ $GZMB^+$ $CD8^+$ cytotoxic T lymphocytes as mediators of the graft-versus-leukemia (GvL) effect following donor lymphocyte infusion in AML.[23] The $ZNF683^+$ effector phenotype described in that study overlaps with the TFiT transcriptional program, which also includes *ZNF683* as a defining feature of bone marrow tumor-reactive T cells, suggesting that GvL-mediating T cells and endogenous tumor-reactive T cells identified by TFiT may share a common transcriptional identity shaped by the bone marrow microenvironment.

These findings establish tumor-reactive BMTs as a mechanistic correlate of response to immunotherapy in AML and MM and validate the TFiT signature as a broadly applicable tool for their detection. Importantly, the specificity of TFiT for immunotherapy-mediated responses—but not chemotherapy-driven blast clearance—supports its biological validity as a marker of T cell-mediated tumor control rather than a nonspecific prognostic indicator. Our approach provides tools for tracking endogenous antitumor immunity across disease states and therapeutic modalities and offers a proof of concept for using the transcriptional features of functionally relevant T cell populations to guide patient stratification and immunotherapy development in bone marrow malignancies.

DISCUSSION

This study provides a framework for characterizing the nature, specificity, and functional relevance of T cell responses in the bone marrow microenvironment in MM and AML. By combining high-sensitivity TCR sequencing, single-cell transcriptomics, HLA immunopeptidomics, and functional T cell screening, we identify a functionally defined population of tumor-reactive T cells residing in the bone marrow of patients with these two biologically distinct cancers. Our findings indicate that endogenous tumor-reactive T cells in MM and AML are transcriptionally equipped for cytotoxicity and can be functionally activated *in vitro*, yet appear to exist in a latent state that limits spontaneous tumor elimination *in vivo*.[4,14,72,73]

The low frequency of tumor-reactive T cells in MM and AML, particularly in treatment-naive settings, has historically limited their systematic characterization. To address this, we applied a dual strategy combining single-cell functional assays and immunopeptidome-informed expansion assays to identify tumor-reactive clonotypes *in situ* and validate their specificity *in vitro*.

We focused on AML and MM as representative bone-marrow-resident malignancies because they are the two most common cancers that arise within and remain confined to the bone marrow compartment, yet they differ fundamentally in cellular origin—myeloid versus plasma cell—and in their response profiles to immunotherapy. Bispecific T cell engagers have transformed the treatment landscape in MM and are under active clinical investigation in AML, while checkpoint blockade has shown limited single-agent efficacy in both diseases.[68,70,71] The bone marrow constitutes a unique immunological niche with its own resident T cell compartment, distinct cytokine milieu, and antigen presentation dynamics,[74,75] and we reasoned that studying cancers native to this compartment would yield the most coherent picture of endogenous anti-tumor T cell surveillance within the bone marrow. That we found substantial conservation in both the antigen repertoire and the transcriptional programs of tumor-reactive T cells across two biologically distinct diseases suggests that common principles of immune surveillance may operate in bone-marrow-resident malignancies more broadly, although formal validation in additional entities remains necessary.

A central conceptual finding of this study is that tumor-reactive T cells in the bone marrow exist in a state of latent competence;

they are transcriptionally equipped for cytotoxicity, yet do not appear to be actively engaged in sustained tumor elimination *in vivo*.[73] This interpretation is supported by the observation that MANA-reactive TCRs—which recognize antigens definitively presented on patient tumor cells—predominantly map to naive transcriptional states, suggesting that many tumor-reactive T cells may never have been productively primed in the bone marrow despite cognate antigen availability. Several features of the bone marrow microenvironment may explain this latency. First, unlike solid tumors where T cells and tumor cells are structurally confined together in a compact mass with high local antigen density, tumor cells and T cells in the bone marrow coexist within a shared hematopoietic compartment, potentially limiting the sustained antigen encounter required for productive T cell priming. Second, the low TMB of AML and MM (~1–2 mutations/Mb) means that many tumor-reactive T cells recognize overexpressed self-antigens or non-canonical peptides with potentially suboptimal affinity, sufficient to generate a functional readout in sensitive assays but insufficient to drive the sustained signaling required for full exhaustion or autonomous tumor elimination. Third, the bone marrow niche may lack the co-stimulatory context required for effective T cell priming, in contrast to the solid tumor microenvironment where continuous antigen encounter drives T cells along the canonical exhaustion trajectory.[2,76]

This framework has direct therapeutic implications. It provides a mechanistic explanation for the clinical observation that ICB, which acts on chronically stimulated, checkpoint-dependent T cells, has limited efficacy in MM[77,78] and AML[68,70,71]; there is no fully exhausted, checkpoint-dependent T cell population to "unblock," and the barrier to effective endogenous immunity is insufficient initial priming rather than exhaustion. Conversely, therapies that bypass the need for natural priming, such as bispecific T cell engagers (which provide a synthetic immunological synapse), CAR T cells, or allogeneic transplantation (where donor T cells arrive pre-activated), have demonstrated transformative efficacy in these diseases.[1,66,69] In relapsed disease, we find that non-response to immunotherapy is characterized by a failure of tumor-reactive T cells to expand or acquire effector phenotypes. This observation supports a model in which the pre-existing functional state and clonal composition of the T cell repertoire—rather than the reversal of exhaustion per se—shape therapeutic responsiveness to T cell-engaging therapies in bone marrow malignancies. These findings complement prior evidence from solid tumors, suggesting that successful immunotherapy may depend on either recruitment of novel TCRs or reactivation of pre-existing tumor-reactive T cells within the tumor microenvironment[13] while highlighting that the mechanistic underpinnings of response may differ fundamentally between solid and bone-marrow-resident cancers.

The transcriptional identity of tumor-reactive T cells in the bone marrow diverges fundamentally from that of tumor-reactive TILs in solid cancers, a distinction that has important implications for biomarker development and therapeutic strategy. By integrating our bone marrow datasets with a pan-solid-cancer TIL reference atlas,[24] we demonstrate that bone marrow tumor-reactive T cells map to the cytotoxic effector compartment rather than to the exhausted or progenitor-exhausted clusters that characterize tumor-reactive TILs. The TFiT signature captures this cytotoxic effector program in the absence of canonical exhaustion markers and outperforms existing signatures trained on solid tumor TILs. The inclusion of *ZNF683* (Hobit) as a defining feature of TFiT is noteworthy in light of recent work by Maurer and colleagues,[23] who identified clonally expanded ZNF683$^+$ GZMB$^+$ CD8$^+$ cytotoxic T lymphocytes as mediators of the GvL effect following donor lymphocyte infusion in AML. The convergence between the ZNF683$^+$ effector phenotype of GvL-mediating T cells and the TFiT transcriptional program suggests that endogenous tumor-reactive T cells and donor-derived GvL effectors may share a common transcriptional identity shaped by the bone marrow microenvironment, despite their distinct origins.

The specificity of TFiT as a biomarker of T cell-mediated tumor control—rather than a generic prognostic marker—is supported by several converging lines of evidence. First, baseline tumor burden (blast percentage in AML, plasma cell percentage in MM) does not correlate with TFiT at diagnosis, arguing against TFiT being a surrogate for disease bulk and instead supporting its specificity as a marker of tumor-reactive T cells. Second, TFiT does not predict response to standard intensive chemotherapy in AML patients treated with venetoclax-azacitidine or daunorubicin-cytarabine, where the primary mechanism of blast clearance is direct pharmacological killing rather than endogenous T cell-mediated tumor elimination. That TFiT selectively stratifies outcomes in immunotherapy contexts, such as checkpoint inhibitors, bispecific antibodies, and immunochemotherapy, across independent cohorts but not in chemotherapy settings reinforces its mechanistic specificity for immune-mediated tumor control. Unlike surrogate markers such as tumor mutational burden or clonal hematopoiesis, TFiT provides a prospective, immune-intrinsic measure of anti-tumor immunity anchored in the transcriptional phenotype of bone-marrow-resident T cells. Its ability to stratify patients across multiple therapeutic modalities and independent cohorts suggests that transcriptional profiling of bone marrow T cells may serve as both a mechanistic correlate and a clinically actionable biomarker.

Our HLA class I immunopeptidomic analysis reveals a partially shared antigen landscape in MM and AML. Classical mutation-derived neoantigens were near-absent: only a single neoantigen was detected across the entire cohort, reflecting the low TMB of these cancers. Instead, the tumor immunopeptidome was dominated by non-canonical peptides derived from uORFs, dORFs, lncRNAs, and pseudogenes, alongside CAAs and, in MM, idiotype-derived BCR neoepitopes. Some of these antigens are recognized by tumor-reactive TCRs with convergent motifs across patients, supporting the existence of public T cell responses targeting conserved epitopes. These findings are consistent with recent work identifying non-mutational immunogenic drivers in myeloid malignancies, such as mis-splicing-derived neoantigens,[21] and with pan-cancer evidence that nuORF-derived peptides represent a broadly relevant source of tumor antigens across melanoma, CLL, and glioblastoma.[37] Our study extends this paradigm by showing that conserved, aberrantly expressed antigens elicit endogenous T cell responses with a conserved cytotoxic effector transcriptional program, even in the absence of strong mutational signals. Cross-referencing identified epitopes against the HLA Ligand Atlas revealed that the majority of tested antigens showed

selective enrichment on malignant cells relative to normal tissues. Future studies leveraging systematic Ribo-seq-based filtering from multiple normal tissues will be critical for distinguishing tumor-enriched from ubiquitously translated non-canonical peptides before therapeutic translation.

From a translational perspective, our approach integrates transcriptional state, antigen presentation, and TCR motif convergence to increase the pre-test likelihood of identifying tumor-specific TCRs in cancers with low immunogenicity. This framework could inform the rational design and treatment monitoring of TCR-engineered T cells, bispecific antibodies, or T cell-engaging regimens, particularly in patients with limited mutational targets or poor responses to current therapies.

Limitations of the study

Several limitations should be noted. First, our functional discovery relies on *ex vivo* assays, which may not fully capture the complexity of *in vivo* bone marrow immune surveillance; future studies generating functional *in vivo* data will help to elucidate how the complete bone marrow microenvironment distinctly perturbs tumor T cell interaction *in vivo*.

Second, although our workflow is in principle compatible with HLA-class-II-restricted epitopes—and we did identify several tumor-reactive $CD4^+$ T cells—we focused primarily on HLA-class-I-restricted responses and therefore likely underrepresent $CD4^+$ T cell-mediated immunity.

Third, complete deorphanization of all identified TCRs to their individual cognate antigens was not achievable, reflecting the inherent difficulty and cost of TCR:antigen pairing at scale. Our functional data establish *ex vivo* activation and MHC-class-I-dependent recognition of autologous tumor cells but do not constitute direct evidence of tumor-cell killing. A definitive demonstration that the identified non-canonical antigens are endogenously processed and presented at a density sufficient for TCR-T cell-mediated cytotoxicity would require deconvolution of antigen pools to individual peptides and testing against translation-competent versus knockout target cells and remains an open question for future work; direct anti-myeloma cytotoxicity assays were further constrained by the inherently limited *ex vivo* viability of primary myeloma cells.

Fourth, because antigen identification (immunopeptidomic mass spectrometry) and TCR identification (microfluidic co-culture) were performed in separate assays, TCRs recovered in one screen may not be primarily directed against the peptides recovered in the other; antigen assignments should be interpreted with this sampling and technical bias in mind.

Fifth, a substantial portion of functional TCR matches, including database- and MANAFEST/ViraFEST-derived assignments, could be resolved only by CDR3 amino acid sequence rather than full paired α/β chains, introducing a degree of imprecision that should be considered when interpreting functional back-projections onto the single-cell data.

Sixth, our screening approach likely underestimates the true frequency of tumor-reactive T cells; the antigen-agnostic microfluidic assay preferentially captures $CD8^+$ effector T cells with immediate effector readouts, and the MANAFEST assay relies predominantly on HLA-class-I-restricted peptides, together enriching for $CD8^+$ responses. The $\sim$1.29% frequency we report should therefore be regarded as a lower bound.

Finally, the low baseline abundance of tumor-reactive T cells, even in eventual clinical responders, underscores the need for strategies that amplify or sustain these populations *in vivo* and highlights that TFiT-based stratification is a prognostic tool rather than a therapeutic intervention. Relatedly, our study centers on the bone marrow niche and, in particular, on multiple myeloma, which informed the derivation of the TFiT signature and the bulk of the functional validation. While our data indicate that comparable mechanisms of immune surveillance operate in AML, further work is needed to delineate T cell-mediated recognition and control of AML blasts across the complex therapeutic settings in which immunotherapy currently has only a limited role.

In summary, we define conserved programs and specificities of tumor-reactive T cells in MM and AML and identify transcriptional correlates of clinical response to immunotherapy. The integration of functional screening, immunopeptidomics, TCR validation, and transcriptional profiling provides a resource for decoding endogenous anti-tumor immunity in bone marrow malignancies and a framework for developing immunotherapies tailored to the distinct immune biology of these diseases.

RESOURCE AVAILABILITY

Lead contact

Further information and requests for resources and reagents should be directed to and will be fulfilled by the lead contact, Mirco J. Friedrich (mirco.friedrich@dkfz.de).

Materials availability

Reconstituted TCR plasmids generated in this study are available from the lead contact upon reasonable request and completion of a Material Transfer Agreement. Patient-derived primary tumor materials are subject to the original informed consent and institutional regulations and are not generally available. This study did not generate new unique reagents that require formal deposit.

Data and code availability

The original mass spectra, peptide spectrum matches, and the protein sequence database used for searches have been deposited in the public proteomics repository MassIVE (https://massive.ucsd.edu) with the identifier MSV000094359 and are accessible at ftp://massive.ucsd.edu/v07/MSV000094359/. This dataset will be made public upon publication of the peer-reviewed manuscript. All annotated single-cell RNA/V(D)J-sequencing data from newly diagnosed multiple myeloma patients undergoing standard-of-care induction therapy can be accessed at Gene Expression Omnibus (GEO; GSE242883). This dataset will be made public upon acceptance of the manuscript. All annotated single-cell RNA/V(D)J-sequencing data from external cohorts can be accessed as described in the STAR Methods section. All further data and code generated within this study is available upon reasonable request.

ACKNOWLEDGMENTS

This study was supported by the Deutsche José Carreras Leukämie-Stiftung (DJCLS, PI: M.J.F.; Project ID DJCLS 01ZI/2022); the Dr. Rolf M. Schwiete Stiftung (PI: M.J.F.; Project ID 2025-018); the Else Kröner-Fresenius-Stiftung (PI: M.J.F.; Project ID 2025_EKMS.52); the Stiftung Deutsche Krebshilfe (PI: M.J.F.; Project ID 70117225); the Dietmar Hopp Foundation (PI: M.J.F. and A.T.); and the Deutsche Forschungsgemeinschaft (DFG, German Research Foundation) - SFB 1709/1 2025 - 533056198. This study was further supported by the Federal Ministry of Education and Research (BMBF) and the Ministry of Science Baden-Württemberg within the framework of the Excellence Strategy of the Federal and State Governments of Germany (PI: M.J.F.; Project ID ExU 6.1.12 and PI: J.Z.; Project ID HARMONY - ExU 6.1.49). We are grateful to the

DKFZ Sample Processing Lab, the Next Generation Sequencing Core Facility of the Genomics and Proteomics Core Facility, and the Omics IT and Data Management Core Facility for their technical support. We thank the Clinical Myeloma Registry and Biobank at Heidelberg University Hospital, funded by the Dietmar Hopp Foundation. This study includes samples provided by the NCT Cell and Liquid Biobank (NCT CLB), a member of the Biomaterial Bank Heidelberg (BMBH). This work was supported in part by the National Cancer Institute (NCI) Clinical Proteomic Tumor Analysis Consortium (grants U24CA270823 and U01CA271402 to S.A.C.) and the Dr. Miriam and Sheldon G. Adelson Medical Research Foundation (to S.A.C.). K.F. is supported by the Cancer Research UK Early Detection and Diagnosis Programme (C9203). K.Y. is supported by the UCL/UCLH Biomedical Research Centre. B.C. is supported by Cancer Research UK, the Rosetrees Trust, and the UCLH Biomedical Research Centre. M.P. is supported by the European Research Council (ERC Advanced Grant CENTRIC Brain, Project ID 101141901, "Characterizing and harnessing tumor-reactive T cells in the brain") and the Deutsche Forschungsgemeinschaft (DFG, German Research Foundation) under Germany's Excellence Strategy – EXC-3018/1 – 533587280. S.R. is supported by the Deutsche Forschungsgemeinschaft (DFG, German Research Foundation) – Emmy Noether Programme – Project ID RA3166/1. M.K. is supported by the German National Academy of Sciences Leopoldina (Project ID LPDS 2022-13). N.K. is supported by the International Myeloma Society and the Paula and Rodger Riney Foundation Career Development Award. E.W.G. is supported by the German Ministry of Education and Research (National Center for Tumor Diseases Heidelberg, NCT 3.0 Program "Precision Immunotherapy of Brain Tumors") and the DKTK program (to M.P.). T.B. is supported by the Helmholtz Institute for Translational Oncology Mainz (HI-TRON Mainz) and by a German Cancer Consortium DKTK-DKFZ Joint Funding Project Award (TRUST, to M.P.).

AUTHOR CONTRIBUTIONS

N.K., T.R.W., and T.B. designed and performed experiments, analyzed, and interpreted data. S. Steiger and N.K. analyzed and interpreted scRNA/VDJ-seq data. M.K., N.K., S. Schumacher, J.J.M., and M.J.F. performed single-cell experiments and analyses. E.S. performed single-cell sequencing and analyses. K.F., D.G.-F., E.F., B.C., and K.Y. analyzed longitudinal VDJ-seq data. T.B., K.L., B.S., F.W., C.M.T., A.S., A.D.M., A.K., A.V.d.V., D.H., R.O., and J.M.L. performed TCR cloning and functional testing. S. Renders, L.S.S., J.H.F., and T.S. analyzed clinical data. S.C., J.Z., and C.F. researched and analyzed clinical metadata. S.N., M.M., S. Raffel, and T.S. performed sequencing and metadata analyses on AML samples. G.M.H., C.C., J.G.A., and S.A.C. performed HLA-I ligandome analyses. S.U. and S.F. performed HLA binding predictions. W.O. and P.S. contributed to antigen validation. N.W., E.W.G., L.B., C.M.-T., H.G., K.R., M.S.R., M.P., A.T., and S.B.E. were involved in study design and data interpretation. M.J.F. conceptualized and supervised the study. N.K. and M.J.F. wrote the paper with input from all co-authors.

DECLARATION OF INTERESTS

N.K., M.J.F., and S. Steiger are co-inventors on a European provisional patent application filed by the German Cancer Research Center (DKFZ) relating to this work. M.J.F. reports speaker honoraria from Pfizer, Roche, and Eli Lilly. S.A.C. is a member of the scientific advisory boards of Kymera, PTM BioLabs, Seer, and PrognomIQ. M.P. and E.W.G. are founders of Tcelltech.

STAR★METHODS

Detailed methods are provided in the online version of this paper and include the following:

- KEY RESOURCES TABLE
- EXPERIMENTAL MODEL AND STUDY PARTICIPANT DETAILS
  - Human participants
  - Processing of human bone marrow samples
  - Cell lines
- METHOD DETAILS
  - Antigen-agnostic screening of tumor-reactive T cells
  - Export and TCR sequencing of tumor-reactive T cells
  - HLA class I immunopeptidomics on CD138+ multiple myeloma cells
  - Antigen-dependent screening of tumor and virus-specific T cells
  - Validation of tumor-reactivity by autologous co-cultures
  - Testing of cytotoxicity of tumor-reactive T cells
  - Epitope mapping of tumor-reactive TCRs
  - Antigen HLA promiscuity testing using tetramers
  - Single-cell transcriptome/V(D)J analyses
  - Integration of external and internal datasets and generation of a unified pan-entity reference map of cancer associated T cells
  - Differential gene expression and signature derivation
  - Analysis of newly diagnosed MM samples during induction therapy
  - Analysis of longitudinal relapsed/refractory MM samples during bispecific antibody therapy
  - Analysis of newly diagnosed AML samples during induction chemotherapy
  - Analysis of longitudinal r/r AML samples during AZA/nivolumab therapy
  - Analysis of AML samples after allogeneic stem cell transplantation
  - Deep TCRB sequencing of clinical trial samples (CARDAMON trial)
  - Whole-genome sequencing of tumor cells and germline controls
  - Prediction of immunoglobulin-derived neoepitopes in multiple myeloma
  - Data visualization
- QUANTIFICATION AND STATISTICAL ANALYSIS

SUPPLEMENTAL INFORMATION

Supplemental information can be found online at https://doi.org/10.1016/j.ccell.2026.07.011.

Received: July 23, 2025
Revised: March 30, 2026
Accepted: July 17, 2026
Published: August 10, 2026

REFERENCES

1. June, C.H., O'Connor, R.S., Kawalekar, O.U., Ghassemi, S., and Milone, M.C. (2018). CAR T cell immunotherapy for human cancer. Science *359*, 1361–1365. https://doi.org/10.1126/science.aar6711.
2. van der Leun, A.M., Thommen, D.S., and Schumacher, T.N. (2020). CD8(+) T cell states in human cancer: insights from single-cell analysis. Nat. Rev. Cancer *20*, 218–232. https://doi.org/10.1038/s41568-019-0235-4.
3. Waldman, A.D., Fritz, J.M., and Lenardo, M.J. (2020). A guide to cancer immunotherapy: from T cell basic science to clinical practice. Nat. Rev. Immunol. *20*, 651–668. https://doi.org/10.1038/s41577-020-0306-5.
4. Welters, C., Lammoglia Cobo, M.F., Stein, C.A., Hsu, M.-T., Ben Hamza, A., Penter, L., Chen, X., Buccitelli, C., Popp, O., Mertins, P., et al. (2022). Immune Phenotypes and Target Antigens of Clonally Expanded Bone Marrow T Cells in Treatment-Naïve Multiple Myeloma. Cancer Immunol. Res. *10*, 1407–1419. https://doi.org/10.1158/2326-6066.CIR-22-0434.
5. Perumal, D., Imai, N., Laganà, A., Finnigan, J., Melnekoff, D., Leshchenko, V.V., Solovyov, A., Madduri, D., Chari, A., Cho, H.J., et al. (2020). Mutation-derived Neoantigen-specific T-cell Responses in Multiple Myeloma. Clin. Cancer Res. *26*, 450–464. https://doi.org/10.1158/1078-0432.CCR-19-2309.
6. Kehl, N., Kilian, M., Michel, J., Wagner, T.R., Uhrig, S., Brobeil, A., Sester, L.-S., Blobner, S., Steiger, S., Hundemer, M., et al. (2022). IgE type multiple myeloma exhibits hypermutated phenotype and tumor reactive T cells. J. Immunother. Cancer *10*, e005815. https://doi.org/10.1136/jitc-2022-005815.
7. Simoni, Y., Becht, E., Fehlings, M., Loh, C.Y., Koo, S.L., Teng, K.W.W., Yeong, J.P.S., Nahar, R., Zhang, T., Kared, H., et al. (2018). Bystander CD8(+) T cells are abundant and phenotypically distinct in human tumour infiltrates. Nature *557*, 575–579. https://doi.org/10.1038/s41586-018-0130-2.

8. Duhen, T., Duhen, R., Montler, R., Moses, J., Moudgil, T., de Miranda, N.F., Goodall, C.P., Blair, T.C., Fox, B.A., McDermott, J.E., et al. (2018). Co-expression of CD39 and CD103 identifies tumor-reactive CD8 T cells in human solid tumors. Nat. Commun. *9*, 2724. https://doi.org/10.1038/s41467-018-05072-0.

9. Yarchoan, M., Hopkins, A., and Jaffee, E.M. (2017). Tumor Mutational Burden and Response Rate to PD-1 Inhibition. N. Engl. J. Med. *377*, 2500–2501. https://doi.org/10.1056/NEJMc1713444.

10. Caushi, J.X., Zhang, J., Ji, Z., Vaghasia, A., Zhang, B., Hsiue, E.H.C., Mog, B.J., Hou, W., Justesen, S., Blosser, R., et al. (2021). Transcriptional programs of neoantigen-specific TIL in anti-PD-1-treated lung cancers. Nature *596*, 126–132. https://doi.org/10.1038/s41586-021-03752-4.

11. Oliveira, G., Stromhaug, K., Klaeger, S., Kula, T., Frederick, D.T., Le, P.M., Forman, J., Huang, T., Li, S., Zhang, W., et al. (2021). Phenotype, specificity and avidity of antitumour CD8(+) T cells in melanoma. Nature *596*, 119–125. https://doi.org/10.1038/s41586-021-03704-y.

12. Lowery, F.J., Krishna, S., Yossef, R., Parikh, N.B., Chatani, P.D., Zacharakis, N., Parkhurst, M.R., Levin, N., Sindiri, S., Sachs, A., et al. (2022). Molecular signatures of antitumor neoantigen-reactive T cells from metastatic human cancers. Science *375*, 877–884. https://doi.org/10.1126/science.abl5447.

13. Yost, K.E., Satpathy, A.T., Wells, D.K., Qi, Y., Wang, C., Kageyama, R., McNamara, K.L., Granja, J.M., Sarin, K.Y., Brown, R.A., et al. (2019). Clonal replacement of tumor-specific T cells following PD-1 blockade. Nat. Med. *25*, 1251–1259. https://doi.org/10.1038/s41591-019-0522-3.

14. Mathioudaki, A., Wang, X., Sedloev, D., Huth, R., Kamal, A., Hundemer, M., Liu, Y., Vasileiou, S., Lulla, P., Müller-Tidow, C., et al. (2024). The remission status of AML patients after allo-HCT is associated with a distinct single-cell bone marrow T-cell signature. Blood *143*, 1269–1281. https://doi.org/10.1182/blood.2023021815.

15. Rajasagi, M., Shukla, S.A., Fritsch, E.F., Keskin, D.B., DeLuca, D., Carmona, E., Zhang, W., Sougnez, C., Cibulskis, K., Sidney, J., et al. (2014). Systematic identification of personal tumor-specific neoantigens in chronic lymphocytic leukemia. Blood *124*, 453–462. https://doi.org/10.1182/blood-2014-04-567933.

16. Zamora, A.E., Crawford, J.C., Allen, E.K., Guo, X.-Z.J., Bakke, J., Carter, R.A., Abdelsamed, H.A., Moustaki, A., Li, Y., Chang, T.-C., et al. (2019). Pediatric patients with acute lymphoblastic leukemia generate abundant and functional neoantigen-specific CD8+ T cell responses. Sci. Transl. Med. *11*, eaat8549. https://doi.org/10.1126/scitranslmed.aat8549.

17. Biernacki, M.A., Foster, K.A., Woodward, K.B., Coon, M.E., Cummings, C., Cunningham, T.M., Dossa, R.G., Brault, M., Stokke, J., Olsen, T.M., et al. (2020). CBFB-MYH11 fusion neoantigen enables T cell recognition and killing of acute myeloid leukemia. J. Clin. Investig. *130*, 5127–5141. https://doi.org/10.1172/JCI137723.

18. Chapuis, A.G., Egan, D.N., Bar, M., Schmitt, T.M., McAfee, M.S., Paulson, K.G., Voillet, V., Gottardo, R., Ragnarsson, G.B., Bleakley, M., et al. (2019). T cell receptor gene therapy targeting WT1 prevents acute myeloid leukemia relapse post-transplant. Nat. Med. *25*, 1064–1072. https://doi.org/10.1038/s41591-019-0472-9.

19. Schumacher, T.N., and Schreiber, R.D. (2015). Neoantigens in cancer immunotherapy. Science *348*, 69–74. https://doi.org/10.1126/science.aaa4971.

20. Cai, Y., Li, D., Lv, D., Yu, J., Ma, Y., Jiang, T., Ding, N., Liu, Z., Li, Y., and Xu, J. (2024). MHC-I-presented non-canonical antigens expand the cancer immunotherapy targets in acute myeloid leukemia. Sci. Data *11*, 831. https://doi.org/10.1038/s41597-024-03660-y.

21. Kim, W.J., Crosse, E.I., De Neef, E., Etxeberria, I., Sabio, E.Y., Wang, E., Bewersdorf, J.P., Lin, K.-T., Lu, S.X., Belleville, A., et al. (2025). Mis-splicing-derived neoantigens and cognate TCRs in splicing factor mutant leukemias. Cell *188*, 3422–3440.e24. *0*. https://doi.org/10.1016/j.cell.2025.03.047.

22. Podar, K., Chauhan, D., and Anderson, K.C. (2009). Bone marrow microenvironment and the identification of new targets for myeloma therapy. Leukemia *23*, 10–24. https://doi.org/10.1038/leu.2008.259.

23. Maurer, K., Park, C.Y., Mani, S., Borji, M., Raths, F., Gouin, K.H., Penter, L., Jin, Y., Zhang, J.Y., Shin, C., et al. (2025). Coordinated immune networks in leukemia bone marrow microenvironments distinguish response to cellular therapy. Sci. Immunol. *10*, eadr0782. https://doi.org/10.1126/sciimmunol.adr0782.

24. Chu, Y., Dai, E., Li, Y., Han, G., Pei, G., Ingram, D.R., Thakkar, K., Qin, J.-J., Dang, M., Le, X., et al. (2023). Pan-cancer T cell atlas links a cellular stress response state to immunotherapy resistance. Nat. Med. *29*, 1550–1562. https://doi.org/10.1038/s41591-023-02371-y.

25. Pilcher, W.C., Yao, L., Gonzalez-Kozlova, E., Pita-Juarez, Y., Karagkouni, D., Acharya, C.R., Michaud, M.E., Hamilton, M., Nanda, S., Song, Y., et al. (2026). A single-cell atlas characterizes dysregulation of the bone marrow immune microenvironment associated with outcomes in multiple myeloma. Nat. Cancer *7*, 224–246. https://doi.org/10.1038/s43018-025-01072-4.

26. Boiarsky, R., Haradhvala, N.J., Alberge, J.-B., Sklavenitis-Pistofidis, R., Mouhieddine, T.H., Zavidij, O., Shih, M.-C., Firer, D., Miller, M., El-Khoury, H., et al. (2022). Single cell characterization of myeloma and its precursor conditions reveals transcriptional signatures of early tumorigenesis. Nat. Commun. *13*, 7040. https://doi.org/10.1038/s41467-022-33944-z.

27. Dang, M., Wang, R., Lee, H.C., Patel, K.K., Becnel, M.R., Han, G., Thomas, S.K., Hao, D., Chu, Y., Weber, D.M., et al. (2023). Single cell clonotypic and transcriptional evolution of multiple myeloma precursor disease. Cancer Cell *41*, 1032–1047.e4. https://doi.org/10.1016/j.ccell.2023.05.007.

28. Gottschlich, A., Thomas, M., Grünmeier, R., Lesch, S., Rohrbacher, L., Igl, V., Briukhovetska, D., Benmebarek, M.-R., Vick, B., Dede, S., et al. (2023). Single-cell transcriptomic atlas-guided development of CAR-T cells for the treatment of acute myeloid leukemia. Nat. Biotechnol. *41*, 1618–1632. https://doi.org/10.1038/s41587-023-01684-0.

29. Alrasheed, N., Lee, L., Ghorani, E., Henry, J.Y., Conde, L., Chin, M., Galas-Filipowicz, D., Furness, A.J.S., Chavda, S.J., Richards, H., et al. (2020). Marrow-Infiltrating Regulatory T Cells Correlate with the Presence of Dysfunctional CD4(+)PD-1(+) Cells and Inferior Survival in Patients with Newly Diagnosed Multiple Myeloma. Clin. Cancer Res. *26*, 3443–3454. https://doi.org/10.1158/1078-0432.CCR-19-1714.

30. Chan, H.Y., Zhang, J., Garliss, C.C., Kwaa, A.K., Blankson, J.N., and Smith, K.N. (2020). A T Cell Receptor Sequencing-Based Assay Identifies Cross-Reactive Recall CD8+ T Cell Clonotypes Against Autologous HIV-1 Epitope Variants. Front. Immunol. *11*, 591. https://doi.org/10.3389/fimmu.2020.00591.

31. Danilova, L., Anagnostou, V., Caushi, J.X., Sidhom, J.W., Guo, H., Chan, H.Y., Suri, P., Tam, A., Zhang, J., Asmar, M.E., et al. (2018). The Mutation-Associated Neoantigen Functional Expansion of Specific T Cells (MANAFEST) Assay: A Sensitive Platform for Monitoring Antitumor Immunity. Cancer Immunol. Res. *6*, 888–899. https://doi.org/10.1158/2326-6066.CIR-18-0129.

32. Dykema, A.G., Zhang, B., Woldemeskel, B.A., Garliss, C.C., Cheung, L.S., Choudhury, D., Zhang, J., Aparicio, L., Bom, S., Rashid, R., et al. (2021). Functional characterization of CD4+ T cell receptors crossreactive for SARS-CoV-2 and endemic coronaviruses. J. Clin. Investig. *131*, e146922. https://doi.org/10.1172/JCI146922.

33. Fischer, D.S., Ansari, M., Wagner, K.I., Jarosch, S., Huang, Y., Mayr, C.H., Strunz, M., Lang, N.J., D'Ippolito, E., Hammel, M., et al. (2021). Single-cell RNA sequencing reveals ex vivo signatures of SARS-CoV-2-reactive T cells through "reverse phenotyping.". Nat. Commun. *12*, 4515. https://doi.org/10.1038/s41467-021-24730-4.

34. Fuchs, Y.F., Sharma, V., Eugster, A., Kraus, G., Morgenstern, R., Dahl, A., Reinhardt, S., Petzold, A., Lindner, A., Löbel, D., and Bonifacio, E. (2019). Gene Expression-Based Identification of Antigen-Responsive CD8+ T

Cells on a Single-Cell Level. Front. Immunol. *10*, 2568. https://doi.org/10.3389/fimmu.2019.02568.

35. Stanley, R.F., and Abdel-Wahab, O. (2022). Dysregulation and therapeutic targeting of RNA splicing in cancer. Nat. Cancer *3*, 536–546. https://doi.org/10.1038/s43018-022-00384-z.

36. Bradley, R.K., and Anczuków, O. (2023). RNA splicing dysregulation and the hallmarks of cancer. Nat. Rev. Cancer *23*, 135–155. https://doi.org/10.1038/s41568-022-00541-7.

37. Ouspenskaia, T., Law, T., Clauser, K.R., Klaeger, S., Sarkizova, S., Aguet, F., Li, B., Christian, E., Knisbacher, B.A., Le, P.M., et al. (2022). Unannotated proteins expand the MHC-I-restricted immunopeptidome in cancer. Nat. Biotechnol. *40*, 209–217. https://doi.org/10.1038/s41587-021-01021-3.

38. Laumont, C.M., Vincent, K., Hesnard, L., Audemard, É., Bonneil, É., Laverdure, J.-P., Gendron, P., Courcelles, M., Hardy, M.-P., Côté, C., et al. (2018). Noncoding regions are the main source of targetable tumor-specific antigens. Sci. Transl. Med. *10*, eaau5516. https://doi.org/10.1126/scitranslmed.aau5516.

39. Almeida, L.G., Sakabe, N.J., deOliveira, A.R., Silva, M.C.C., Mundstein, A.S., Cohen, T., Chen, Y.T., Chua, R., Gurung, S., Gnjatic, S., et al. (2009). CTdatabase: a knowledge-base of high-throughput and curated data on cancer-testis antigens. Nucleic Acids Res. *37*, D816–D819. https://doi.org/10.1093/nar/gkn673.

40. Marcu, A., Bichmann, L., Kuchenbecker, L., Kowalewski, D.J., Freudenmann, L.K., Backert, L., Mühlenbruch, L., Szolek, A., Lübke, M., Wagner, P., et al. (2021). The HLA Ligand Atlas. A resource of natural HLA ligands presented on benign tissues. J. Immunother. Cancer *9*, e002071. https://doi.org/10.1136/jitc-2020-002071.

41. Stocki, P., Wang, X.N., Morris, N.J., and Dickinson, A.M. (2011). HSP70 natively and specifically associates with an N-terminal dermcidin-derived peptide that contains an HLA-A*03 antigenic epitope. J. Biol. Chem. *286*, 12803–12811. https://doi.org/10.1074/jbc.M110.179630.

42. Medina, A., Jiménez, C., Sarasquete, M.E., González, M., Chillón, M.C., Balanzategui, A., Prieto-Conde, I., García-Álvarez, M., Puig, N., González-Calle, V., et al. (2020). Molecular profiling of immunoglobulin heavy-chain gene rearrangements unveils new potential prognostic markers for multiple myeloma patients. Blood Cancer J. *10*, 14. https://doi.org/10.1038/s41408-020-0283-8.

43. Khodadoust, M.S., Olsson, N., Chen, B., Sworder, B., Shree, T., Liu, C.L., Zhang, L., Czerwinski, D.K., Davis, M.M., Levy, R., et al. (2019). B-cell lymphomas present immunoglobulin neoantigens. Blood *133*, 878–881. https://doi.org/10.1182/blood-2018-06-845156.

44. Kwak, L.W., Campbell, M.J., Czerwinski, D.K., Hart, S., Miller, R.A., and Levy, R. (1992). Induction of Immune Responses in Patients with B-Cell Lymphoma against the Surface-Immunoglobulin Idiotype Expressed by Their Tumors. N. Engl. J. Med. *327*, 1209–1215. https://doi.org/10.1056/NEJM199210223271705.

45. Trojan, A., Schultze, J.L., Witzens, M., Vonderheide, R.H., Ladetto, M., Donovan, J.W., and Gribben, J.G. (2000). Immunoglobulin framework-derived peptides function as cytotoxic T-cell epitopes commonly expressed in B-cell malignancies. Nat. Med. *6*, 667–672. https://doi.org/10.1038/76243.

46. Xiaoling, G., Ying, L., Jing, L., Huifang, L., Xia, Z., Qingqing, F., and Ping, Z. (2005). Induction of anti B-cell malignance CTL response by subfamily-shared peptides derived from variable domain of immunoglobulin heavy chain. Cancer Immunol. Immunother. *54*, 1106–1114. https://doi.org/10.1007/s00262-005-0696-z.

47. Weng, J., Baio, F.E., Moriarty, K.E., Torikai, H., Wang, H., Liu, Z., Maiti, S.N., Gwak, D., Popescu, M.S., Cha, S.-C., et al. (2016). Targeting B-cell malignancies through human B-cell receptor specific CD4 $^{+}$ T cells. OncoImmunology *5*, e1232220. https://doi.org/10.1080/2162402X.2016.1232220.

48. Sabdia, M.B., Patch, A.-M., Tsang, H., and Gandhi, M.K. (2022). Neoantigens – the next frontier in precision immunotherapy for B-cell lymphoproliferative disorders. Blood Rev. *56*, 100969. https://doi.org/10.1016/j.blre.2022.100969.

49. Parameswaran, P., Liu, Y., Roskin, K.M., Jackson, K.K.L., Dixit, V.P., Lee, J.-Y., Artiles, K.L., Zompi, S., Vargas, M.J., Simen, B.B., et al. (2013). Convergent Antibody Signatures in Human Dengue. Cell Host Microbe *13*, 691–700. https://doi.org/10.1016/j.chom.2013.05.008.

50. Venturi, V., Chin, H.Y., Asher, T.E., Ladell, K., Scheinberg, P., Bornstein, E., Van Bockel, D., Kelleher, A.D., Douek, D.C., Price, D.A., and Davenport, M.P. (2008). TCR β-Chain Sharing in Human CD8+ T Cell Responses to Cytomegalovirus and EBV. J. Immunol. *181*, 7853–7862. https://doi.org/10.4049/jimmunol.181.11.7853.

51. Cetin, M., Pinamonti, V., Schmid, T., Boschert, T., Mellado Fuentes, A., Kromer, K., Lerner, T., Zhang, J., Herzig, Y., Ehlert, C., et al. (2024). T-FINDER: A highly sensitive, pan-HLA platform for functional T cell receptor and ligand discovery. Sci. Adv. *10*, eadk3060. https://doi.org/10.1126/sciadv.adk3060.

52. Li, H., van der Leun, A.M., Yofe, I., Lubling, Y., Gelbard-Solodkin, D., van Akkooi, A.C.J., van den Braber, M., Rozeman, E.A., Haanen, J.B.A.G., Blank, C.U., et al. (2019). Dysfunctional CD8 T Cells Form a Proliferative, Dynamically Regulated Compartment within Human Melanoma. Cell *176*, 775–789.e18. https://doi.org/10.1016/j.cell.2018.11.043.

53. Emerson, R.O., DeWitt, W.S., Vignali, M., Gravley, J., Hu, J.K., Osborne, E.J., Desmarais, C., Klinger, M., Carlson, C.S., Hansen, J.A., et al. (2017). Immunosequencing identifies signatures of cytomegalovirus exposure history and HLA-mediated effects on the T cell repertoire. Nat. Genet. *49*, 659–665. https://doi.org/10.1038/ng.3822.

54. Okhrimenko, A., Grün, J.R., Westendorf, K., Fang, Z., Reinke, S., Von Roth, P., Wassilew, G., Kühl, A.A., Kudernatsch, R., Demski, S., et al. (2014). Human memory T cells from the bone marrow are resting and maintain long-lasting systemic memory. Proc. Natl. Acad. Sci. USA *111*, 9229–9234. https://doi.org/10.1073/pnas.1318731111.

55. Mazo, I.B., Honczarenko, M., Leung, H., Cavanagh, L.L., Bonasio, R., Weninger, W., Engelke, K., Xia, L., McEver, R.P., Koni, P.A., et al. (2005). Bone Marrow Is a Major Reservoir and Site of Recruitment for Central Memory CD8+ T Cells. Immunity *22*, 259–270. https://doi.org/10.1016/j.immuni.2005.01.008.

56. Snyder, T.M., Gittelman, R.M., Klinger, M., May, D.H., Osborne, E.J., Taniguchi, R., Zahid, H.J., Kaplan, I.M., Dines, J.N., Noakes, M.T., et al. (2025). Magnitude and dynamics of the T-cell response to SARS-CoV-2 infection at both individual and population levels. Front. Immunol. *15*, 1488860. https://doi.org/10.3389/fimmu.2024.1488860.

57. Glanville, J., Huang, H., Nau, A., Hatton, O., Wagar, L.E., Rubelt, F., Ji, X., Han, A., Krams, S.M., Pettus, C., et al. (2017). Identifying specificity groups in the T cell receptor repertoire. Nature *547*, 94–98. https://doi.org/10.1038/nature22976.

58. Meeuwsen, M.H., Wouters, A.K., Jahn, L., Hagedoorn, R.S., Kester, M.G.D., Remst, D.F.G., Morton, L.T., Van Der Steen, D.M., Kweekel, C., De Ru, A.H., et al. (2022). A broad and systematic approach to identify B cell malignancy-targeting TCRs for multi-antigen-based T cell therapy. Mol. Ther. *30*, 564–578. https://doi.org/10.1016/j.ymthe.2021.08.010.

59. Dhodapkar, K., and Dhodapkar, M. (2016). Harnessing shared antigens and T-cell receptors in cancer: Opportunities and challenges. Proc. Natl. Acad. Sci. USA *113*, 7944–7945. https://doi.org/10.1073/pnas.1608860113.

60. Miller, B.C., Sen, D.R., Al Abosy, R., Bi, K., Virkud, Y.V., LaFleur, M.W., Yates, K.B., Lako, A., Felt, K., Naik, G.S., et al. (2019). Subsets of exhausted CD8(+) T cells differentially mediate tumor control and respond to checkpoint blockade. Nat. Immunol. *20*, 326–336. https://doi.org/10.1038/s41590-019-0312-6.

61. Tirosh, I., Izar, B., Prakadan, S.M., Wadsworth, M.H., Treacy, D., Trombetta, J.J., Rotem, A., Rodman, C., Lian, C., Murphy, G., et al. (2016). Dissecting the multicellular ecosystem of metastatic melanoma by single-cell RNA-seq. Science *352*, 189–196. https://doi.org/10.1126/science.aad0501.

62. Wu, T.D., Madireddi, S., de Almeida, P.E., Banchereau, R., Chen, Y.J.J., Chitre, A.S., Chiang, E.Y., Iftikhar, H., O'Gorman, W.E., Au-Yeung, A., et al. (2020). Peripheral T cell expansion predicts tumour infiltration and clinical response. Nature *579*, 274–278. https://doi.org/10.1038/s41586-020-2056-8.

63. Sade-Feldman, M., Yizhak, K., Bjorgaard, S.L., Ray, J.P., De Boer, C.G., Jenkins, R.W., Lieb, D.J., Chen, J.H., Frederick, D.T., Barzily-Rokni, M., et al. (2018). Defining T Cell States Associated with Response to Checkpoint Immunotherapy in Melanoma. Cell *175*, 998–1013.e20. https://doi.org/10.1016/j.cell.2018.10.038.

64. Yong, K., Wilson, W., de Tute, R.M., Camilleri, M., Ramasamy, K., Streetly, M., Sive, J., Bygrave, C.A., Benjamin, R., Chapman, M., et al. (2023). Upfront autologous haematopoietic stem-cell transplantation versus carfilzomib-cyclophosphamide-dexamethasone consolidation with carfilzomib maintenance in patients with newly diagnosed multiple myeloma in England and Wales (CARDAMON): a randomised, phase 2, non-inferiority trial. Lancet Haematol. *10*, e93–e106. https://doi.org/10.1016/S2352-3026(22)00350-7.

65. Bahlis, N.J., Raje, N.S., Costello, C., Dholaria, B.R., Solh, M.M., Levy, M.Y., Tomasson, M.H., Dube, H., Liu, F., Liao, K.H., et al. (2021). Efficacy and safety of elranatamab (PF-06863135), a B-cell maturation antigen (BCMA)-CD3 bispecific antibody, in patients with relapsed or refractory multiple myeloma (MM). J. Clin. Oncol. *39*, 8006. https://doi.org/10.1200/JCO.2021.39.15_suppl.8006.

66. Bahlis, N.J., Costello, C.L., Raje, N.S., Levy, M.Y., Dholaria, B., Solh, M., Tomasson, M.H., Damore, M.A., Jiang, S., Basu, C., et al. (2023). Elranatamab in relapsed or refractory multiple myeloma: the MagnetisMM-1 phase 1 trial. Nat. Med. *29*, 2570–2576. https://doi.org/10.1038/s41591-023-02589-w.

67. Friedrich, M.J., Neri, P., Kehl, N., Michel, J., Steiger, S., Kilian, M., Leblay, N., Maity, R., Sankowski, R., Lee, H., et al. (2023). The pre-existing T cell landscape determines the response to bispecific T cell engagers in multiple myeloma patients. Cancer Cell *41*, 711–725.e6. https://doi.org/10.1016/j.ccell.2023.02.008.

68. Abbas, H.A., Hao, D., Tomczak, K., Barrodia, P., Im, J.S., Reville, P.K., Alaniz, Z., Wang, W., Wang, R., Wang, F., et al. (2021). Single cell T cell landscape and T cell receptor repertoire profiling of AML in context of PD-1 blockade therapy. Nat. Commun. *12*, 6071. https://doi.org/10.1038/s41467-021-26282-z.

69. Horowitz, M.M., Gale, R.P., Sondel, P.M., Goldman, J.M., Kersey, J., Kolb, H.J., Rimm, A.A., Ringdén, O., Rozman, C., and Speck, B. (1990). Graft-versus-leukemia reactions after bone marrow transplantation. Blood *75*, 555–562. https://doi.org/10.1182/blood.V75.3.555.555.

70. Davids, M.S., Kim, H.T., Bachireddy, P., Costello, C., Liguori, R., Savell, A., Lukez, A.P., Avigan, D., Chen, Y.-B., McSweeney, P., et al. (2016). Ipilimumab for Patients with Relapse after Allogeneic Transplantation. N. Engl. J. Med. *375*, 143–153. https://doi.org/10.1056/NEJMoa1601202.

71. Daver, N., Garcia-Manero, G., Basu, S., Boddu, P.C., Alfayez, M., Cortes, J.E., Konopleva, M., Ravandi-Kashani, F., Jabbour, E., Kadia, T., et al. (2019). Efficacy, Safety, and Biomarkers of Response to Azacitidine and Nivolumab in Relapsed/Refractory Acute Myeloid Leukemia: A Nonrandomized, Open-Label, Phase II Study. Cancer Discov. *9*, 370–383. https://doi.org/10.1158/2159-8290.CD-18-0774.

72. Shasha, C., Glass, D.R., Moelhman, E., Islas, L., Tian, Y., Chour, T., Xu, G., Szeto, G.L., Peng, T., Song, X., et al. (2025). Hallmarks of T-cell exhaustion and antigen experience are absent in multiple myeloma from diagnosis to maintenance therapy. Blood *145*, 3113–3123. https://doi.org/10.1182/blood.2024025655.

73. Friedrich, M.J., and Raab, M.S. (2025). When the silence speaks: T-cell dysfunction in myeloma. Blood *145*, 3064–3066. https://doi.org/10.1182/blood.2025029262.

74. de Jong, M.M.E., Kellermayer, Z., Papazian, N., Tahri, S., Hofste op Bruinink, D., Hoogenboezem, R., Sanders, M.A., van de Woestijne, P.C., Bos, P.K., Khandanpour, C., et al. (2021). The multiple myeloma microenvironment is defined by an inflammatory stromal cell landscape. Nat. Immunol. *22*, 769–780. https://doi.org/10.1038/s41590-021-00931-3.

75. Kawano, Y., Moschetta, M., Manier, S., Glavey, S., Görgün, G.T., Roccaro, A.M., Anderson, K.C., and Ghobrial, I.M. (2015). Targeting the bone marrow microenvironment in multiple myeloma. Immunol. Rev. *263*, 160–172. https://doi.org/10.1111/imr.12233.

76. Thommen, D.S., and Schumacher, T.N. (2018). T Cell Dysfunction in Cancer. Cancer Cell *33*, 547–562. https://doi.org/10.1016/j.ccell.2018.03.012.

77. Usmani, S.Z., Schjesvold, F., Oriol, A., Karlin, L., Cavo, M., Rifkin, R.M., Yimer, H.A., LeBlanc, R., Takezako, N., McCroskey, R.D., et al. (2019). Pembrolizumab plus lenalidomide and dexamethasone for patients with treatment-naive multiple myeloma (KEYNOTE-185): a randomised, open-label, phase 3 trial. Lancet Haematol. *6*, e448–e458. https://doi.org/10.1016/S2352-3026(19)30109-7.

78. Mateos, M.-V., Blacklock, H., Schjesvold, F., Oriol, A., Simpson, D., George, A., Goldschmidt, H., Larocca, A., Chanan-Khan, A., Sherbenou, D., et al. (2019). Pembrolizumab plus pomalidomide and dexamethasone for patients with relapsed or refractory multiple myeloma (KEYNOTE-183): a randomised, open-label, phase 3 trial. Lancet Haematol. *6*, e459–e469. https://doi.org/10.1016/S2352-3026(19)30110-3.

79. Satija, R., Hoffman, P., and Butler, A. (2025). SeuratData: Install and Manage Seurat Datasets R package version 0.2.2.9002. https://github.com/satijalab/seurat-data.

80. Hao, Y., Stuart, T., Kowalski, M.H., Choudhary, S., Hoffman, P., Hartman, A., Srivastava, A., Molla, G., Madad, S., Fernandez-Granda, C., and Satija, R. (2024). Dictionary learning for integrative, multimodal and scalable single-cell analysis. Nat. Biotechnol. *42*, 293–304. https://doi.org/10.1038/s41587-023-01767-y.

81. Hao, Y., Hao, S., Andersen-Nissen, E., Mauck, W.M., Zheng, S., Butler, A., Lee, M.J., Wilk, A.J., Darby, C., Zager, M., et al. (2021). Integrated analysis of multimodal single-cell data. Cell *184*, 3573–3587.e29. https://doi.org/10.1016/j.cell.2021.04.048.

82. Hafemeister, C., and Satija, R. (2019). Normalization and variance stabilization of single-cell RNA-seq data using regularized negative binomial regression. Genome Biol. *20*, 296. https://doi.org/10.1186/s13059-019-1874-1.

83. Choudhary, S., and Satija, R. (2022). Comparison and evaluation of statistical error models for scRNA-seq. Genome Biol. *23*, 27. https://doi.org/10.1186/s13059-021-02584-9.

84. Germain, P.-L., Lun, A., Garcia Meixide, C., Macnair, W., and Robinson, M.D. (2021). Doublet identification in single-cell sequencing data using scDblFinder. F1000Res. *10*, 979. https://doi.org/10.12688/f1000research.73600.2.

85. Korsunsky, I., Nathan, A., Millard, N., and Raychaudhuri, S. (2022). presto: Fast Functions for Differential Expression using Wilcox and AUC. R package version 1.0.0.

86. Aibar, S., González-Blas, C.B., Moerman, T., Huynh-Thu, V.A., Imrichova, H., Hulselmans, G., Rambow, F., Marine, J.-C., Geurts, P., Aerts, J., et al. (2017). SCENIC: single-cell regulatory network inference and clustering. Nat. Methods *14*, 1083–1086. https://doi.org/10.1038/nmeth.4463.

87. Robin, X., Turck, N., Hainard, A., Tiberti, N., Lisacek, F., Sanchez, J.-C., and Müller, M. (2011). pROC: an open-source package for R and S+ to analyze and compare ROC curves. BMC Bioinf. *12*, 77. https://doi.org/10.1186/1471-2105-12-77.

88. Bolotin, D.A., Poslavsky, S., Mitrophanov, I., Shugay, M., Mamedov, I.Z., Putintseva, E.V., and Chudakov, D.M. (2015). MiXCR: software for comprehensive adaptive immunity profiling. Nat. Methods *12*, 380–381. https://doi.org/10.1038/nmeth.3364.

89. Lefranc, M.-P. (2011). IMGT, the International ImMunoGeneTics Information System. Cold Spring Harb. Protoc. *2011*, 595–603. https://doi.org/10.1101/pdb.top115.

90. Shugay, M., Bagaev, D.V., Zvyagin, I.V., Vroomans, R.M., Crawford, J.C., Dolton, G., Komech, E.A., Sycheva, A.L., Koneva, A.E., Egorov, E.S., et al. (2018). VDJdb: a curated database of T-cell receptor sequences with known antigen specificity. Nucleic Acids Res. *46*, D419–D427. https://doi.org/10.1093/nar/gkx760.

91. Tickotsky, N., Sagiv, T., Prilusky, J., Shifrut, E., and Friedman, N. (2017). McPAS-TCR: a manually curated catalogue of pathology-associated T cell receptor sequences. Bioinformatics *33*, 2924–2929. https://doi.org/10.1093/bioinformatics/btx286.

92. Huang, H., Wang, C., Rubelt, F., Scriba, T.J., and Davis, M.M. (2020). Analyzing the Mycobacterium tuberculosis immune response by T-cell receptor clustering with GLIPH2 and genome-wide antigen screening. Nat. Biotechnol. *38*, 1194–1202. https://doi.org/10.1038/s41587-020-0505-4.

93. Gu, Z., Eils, R., and Schlesner, M. (2016). Complex heatmaps reveal patterns and correlations in multidimensional genomic data. Bioinformatics *32*, 2847–2849. https://doi.org/10.1093/bioinformatics/btw313.

94. Csárdi, G., and Nepusz, T. (2006). The igraph software package for complex network research. Complex Syst. *1695*, 1–9.

95. Bodenhofer, U., Bonatesta, E., Horejš-Kainrath, C., and Hochreiter, S. (2015). msa: an R package for multiple sequence alignment. Bioinformatics *31*, 3997–3999. https://doi.org/10.1093/bioinformatics/btv494.

96. Wagih, O. (2017). ggseqlogo: a versatile R package for drawing sequence logos. Bioinformatics *33*, 3645–3647. https://doi.org/10.1093/bioinformatics/btx469.

97. Szolek, A., Schubert, B., Mohr, C., Sturm, M., Feldhahn, M., and Kohlbacher, O. (2014). OptiType: precision HLA typing from next-generation sequencing data. Bioinformatics *30*, 3310–3316. https://doi.org/10.1093/bioinformatics/btu548.

98. Reynisson, B., Alvarez, B., Paul, S., Peters, B., and Nielsen, M. (2020). NetMHCpan-4.1 and NetMHCIIpan-4.0: improved predictions of MHC antigen presentation by concurrent motif deconvolution and integration of MS MHC eluted ligand data. Nucleic Acids Res. *48*, W449–W454. https://doi.org/10.1093/nar/gkaa379.

99. Chen, C., Li, Z., Huang, H., Suzek, B.E., and Wu, C.H.; UniProt Consortium (2013). A fast Peptide Match service for UniProt Knowledgebase. Bioinformatics *29*, 2808–2809. https://doi.org/10.1093/bioinformatics/btt484.

100. The UniProt Consortium (2017). UniProt: the universal protein knowledgebase. Nucleic Acids Res. *45*, D158–D169. https://doi.org/10.1093/nar/gkw1099.

101. Hunter, J.D. (2007). Matplotlib: A 2D graphics environment. Comput. Sci. Eng. *9*, 90–95. https://doi.org/10.1109/MCSE.2007.55.

102. Abelin, J.G., Bergstrom, E.J., Rivera, K.D., Taylor, H.B., Klaeger, S., Xu, C., Verzani, E.K., Jackson White, C., Woldemichael, H.B., Virshup, M., et al. (2023). Workflow enabling deepscale immunopeptidome, proteome, ubiquitylome, phosphoproteome, and acetylome analyses of sample-limited tissues. Nat. Commun. *14*, 1851. https://doi.org/10.1038/s41467-023-37547-0.

103. Klaeger, S., Apffel, A., Clauser, K.R., Sarkizova, S., Oliveira, G., Rachimi, S., Le, P.M., Tarren, A., Chea, V., Abelin, J.G., et al. (2021). Optimized Liquid and Gas Phase Fractionation Increases HLA-Peptidome Coverage for Primary Cell and Tissue Samples. Mol. Cell. Proteomics *20*, 100133. https://doi.org/10.1016/j.mcpro.2021.100133.

104. Phulphagar, K.M., Ctortecka, C., Jacome, A.S.V., Klaeger, S., Verzani, E.K., Hernandez, G.M., Udeshi, N.D., Clauser, K.R., Abelin, J.G., and Carr, S.A. (2023). Sensitive, high-throughput HLA-I and HLA-II immunopeptidomics using parallel accumulation-serial fragmentation mass spectrometry. Mol. Cell. Proteomics *22*, 100563. https://doi.org/10.1016/j.mcpro.2023.100563.

105. Djureinovic, D., Hallström, B.M., Horie, M., Mattsson, J.S.M., La Fleur, L., Fagerberg, L., Brunnström, H., Lindskog, C., Madjar, K., Rahnenführer, J., et al. (2016). Profiling cancer testis antigens in non–small-cell lung cancer. JCI Insight *1*, e86837. https://doi.org/10.1172/jci.insight.86837.

106. Levin, N., Paria, B.C., Vale, N.R., Yossef, R., Lowery, F.J., Parkhurst, M.R., Yu, Z., Florentin, M., Cafri, G., Gartner, J.J., et al. (2021). Identification and Validation of T-cell Receptors Targeting *RAS* Hotspot Mutations in Human Cancers for Use in Cell-based Immunotherapy. Clin. Cancer Res. *27*, 5084–5095. https://doi.org/10.1158/1078-0432.CCR-21-0849.

107. Kim, S.P., Vale, N.R., Zacharakis, N., Krishna, S., Yu, Z., Gasmi, B., Gartner, J.J., Sindiri, S., Malekzadeh, P., Deniger, D.C., et al. (2022). Adoptive Cellular Therapy with Autologous Tumor-Infiltrating Lymphocytes and T-cell Receptor-Engineered T Cells Targeting Common p53 Neoantigens in Human Solid Tumors. Cancer Immunol. Res. *10*, 932–946. https://doi.org/10.1158/2326-6066.CIR-22-0040.

108. Malekzadeh, P., Pasetto, A., Robbins, P.F., Parkhurst, M.R., Paria, B.C., Jia, L., Gartner, J.J., Hill, V., Yu, Z., Restifo, N.P., et al. (2019). Neoantigen screening identifies broad TP53 mutant immunogenicity in patients with epithelial cancers. J. Clin. Investig. *129*, 1109–1114. https://doi.org/10.1172/JCI123791.

109. Yokota, R., Kaminaga, Y., and Kobayashi, T.J. (2017). Quantification of Inter-Sample Differences in T-Cell Receptor Repertoires Using Sequence-Based Information. Front. Immunol. *8*, 1500. https://doi.org/10.3389/fimmu.2017.01500.

110. Thakkar, N., and Bailey-Kellogg, C. (2019). Balancing sensitivity and specificity in distinguishing TCR groups by CDR sequence similarity. BMC Bioinf. *20*, 241. https://doi.org/10.1186/s12859-019-2864-8.

111. Vujovic, M., Degn, K.F., Marin, F.I., Schaap-Johansen, A.-L., Chain, B., Andresen, T.L., Kaplinsky, J., and Marcatili, P. (2020). T cell receptor sequence clustering and antigen specificity. Comput. Struct. Biotechnol. J. *18*, 2166–2173. https://doi.org/10.1016/j.csbj.2020.06.041.

112. Thomas, N., Heather, J., Ndifon, W., Shawe-Taylor, J., and Chain, B. (2013). Decombinator: a tool for fast, efficient gene assignment in T-cell receptor sequences using a finite state machine. Bioinformatics *29*, 542–550. https://doi.org/10.1093/bioinformatics/btt004.

113. Horak, P., Heining, C., Kreutzfeldt, S., Hutter, B., Mock, A., Hüllein, J., Fröhlich, M., Uhrig, S., Jahn, A., Rump, A., et al. (2021). Comprehensive Genomic and Transcriptomic Analysis for Guiding Therapeutic Decisions in Patients with Rare Cancers. Cancer Discov. *11*, 2780–2795. https://doi.org/10.1158/2159-8290.CD-21-0126.

STAR★METHODS

KEY RESOURCES TABLE

REAGENT or RESOURCE	SOURCE	IDENTIFIER
Antibodies		
Anti-HLA-A,B,C (clone W6/32), purified (immunoprecipitation)	Bio X Cell	Cat# BP0079; RRID:AB_3720016
Anti-HLA-ABC blocking antibody (clone W6/32)	Life Technologies/Thermo Fisher Scientific	Cat# MA1-19027; RRID:AB_1076699
Brilliant Violet 421 anti-human CD137 (4-1BB)	BioLegend	Cat# 309820; RRID:AB_2563830
FITC anti-human CD8	BioLegend	Cat# 344704; RRID:AB_1877178
LEGENDplex Human Th Panel detection antibodies	BioLegend	Cat# 741036; RRID:AB_3711477
LEGENDplex Streptavidin-PE	BioLegend	Cat# 740452
Human IFN-γ, IL-2, and TNF-α capture beads (LEGENDplex)	BioLegend	Cat# 740545, Cat# 740934, Cat# 740711
mTRBC (anti-mouse TCRβ constant region)-PE	BioLegend	Cat# 109208; RRID:AB_313431
Anti-human CD69-PE-Cy7 (clone FN50)	BioLegend	Cat# 310912; RRID:AB_314847
Anti-human CD137-APC (clone 4B4-1)	BioLegend	Cat# 309810; RRID:AB_830672
Anti-human CD3 (clone OKT3)	Thermo Fisher Scientific	Cat# 16-0037-85; RRID:AB_468855
Anti-human CD2 PerCP-Cy5.5 (clone RPA-2.10)	BioLegend	Cat# 300216; RRID:AB_2561923
Anti-human CD20 PE (clone 2H7)	BioLegend	Cat# 302306; RRID:AB_314254
Anti-human CD69 APC-Cy7 (clone FN50)	BioLegend	Cat# 310912; RRID:AB_314849
Anti-human CD3 PE-Cy7 (clone UCHT1)	BioLegend	Cat# 300420; RRID:AB_439781
Anti-HA.11 APC (clone 16B12)	BioLegend	Cat# 901524; RRID:AB_2734658
Anti-human CD3 Pacific Blue (clone HIT3a)	BioLegend	Cat# 300330; RRID:AB_0551436
Anti-human CD138 (clone MI15)	BD Biosciences	Cat# 569110; RRID:AB_3684784
Anti-human CD3 BV510 (clone OKT3)	BD Biosciences	Cat# 566779; RRID:AB_2869862
Anti-human CD69 RB613 (clone FN50)	BD Biosciences	Cat# 571124; RRID:AB_3686253
Anti-human CD137/4-1BB BV750 (clone 4B4-1)	BD Biosciences	Cat# 569693; RRID:AB_3685237
Human TruStain FcX (Fc Receptor Blocking Solution/Fc block)	BD Biosciences/ BioLegend	Cat# 422302; RRID:AB_2818986
TotalSeq-C0251 anti-human Hashtag 1 Antibody	BioLegend	Cat# 394661; RRID:AB_2801031
TotalSeq-C0252 anti-human Hashtag 2 Antibody	BioLegend	Cat# 394663; RRID:AB_2801032
TotalSeq-C0253 anti-human Hashtag 3 Antibody	BioLegend	Cat# 394665; RRID:AB_2801033
TotalSeq-C0254 anti-human Hashtag 4 Antibody	BioLegend	Cat# 394667; RRID:AB_2801034
TotalSeq-C0256 anti-human Hashtag 6 Antibody	BioLegend	Cat# 394671; RRID:AB_2820042
TotalSeq-C0257 anti-human Hashtag 7 Antibody	BioLegend	Cat# 394673; RRID:AB_2820043
TotalSeq-C0258 anti-human Hashtag 8 Antibody	BioLegend	Cat# 394675; RRID:AB_2820044
TotalSeq-C0259 anti-human Hashtag 9 Antibody	BioLegend	Cat# 394677; RRID:AB_2820045
Biological samples		
Human bone marrow aspirates (NDMM, *n* = 15/20; NDAML, *n* = 6/15)	This paper/Heidelberg University Hospital	N/A
Human peripheral blood/PBMC samples	This paper/Heidelberg University Hospital	N/A
Chemicals, peptides, and recombinant proteins		
Bicoll separating solution	Biochrom	Cat# L6715-500ML
BSA	Sigma-Aldrich	Cat# A9647
RPMI-1640 Medium (GlutaMAX)	Gibco/Thermo Fisher Scientific	Cat# 61870-010

(*Continued on next page*)

Continued

REAGENT or RESOURCE	SOURCE	IDENTIFIER
DMEM	Gibco/Thermo Fisher Scientific	Cat# D6429-500ML
X-VIVO 20 medium	Lonza	Cat# 04-448Q
TexMACS Medium	Miltenyi Biotec	Cat# 130-097-196
P3 Primary Cell Nucleofector Solution (4D)	Lonza	Cat# V4XP-3032
Recombinant human IL-2	Novartis Pharmaceuticals	NDC 73776-022-01
Recombinant human IL-7	BioLegend	Cat# 581902
Recombinant human IL-15	BioLegend	Cat# 570302
CEFT peptide pool (≥70%, ∼120 nmol)	JPT Peptide Technologies	Cat# PM-CEFT-2
Retention Time Standards (iRTs)	JPT Peptide Technologies	Cat# RTK-1-10pmol
Flex-T HLA-A*01:01 Monomer UVX	BioLegend	Cat# 280001
Flex-T HLA-A*02:01 Monomer UVX	BioLegend	Cat# 280004
Flex-T HLA-A*03:01 Monomer UVX	BioLegend	Cat# 280005
Flex-T HLA-A*11:01 Monomer UVX	BioLegend	Cat# 280007
PE-streptavidin/APC-streptavidin	BioLegend	Cat# 740452, Cat#405207
D-Biotin	Thermo Fisher	Cat# B20656
Human T cell TransAct	Miltenyi Biotec	Cat# 130-111-160
Holo-transferrin	Sigma-Aldrich	Cat# T0665
CpG ODN 2006	InvivoGen	Cat# tlrl-2006
Gammabind Plus Sepharose beads	Sigma-Aldrich (Cytiva)	Cat# GE17-0886-01
RNAClean XP magnetic beads	Beckman Coulter	Cat# A63987
MagBind TotalPure NGS magnetic beads	Omega Bio-tek	Cat# M1378-01
Q5 Hot Start High-Fidelity 2×Master Mix	New England Biolabs	Cat# M0494
CloneAmp HiFi PCR Premix	Takara Bio/Thermo Fisher Scientific	Cat# 639298
BsaI restriction enzyme	New England Biolabs	Cat# R3733L
Tris-HCl pH 7.5	Invitrogen	Cat# 15567027
EDTA (0.5 M)	Invitrogen	Cat# 15575-038
NaCl	Sigma-Aldrich	Cat# 71386-1L
MgCl2	Sigma-Aldrich	Cat# 63069-100ML
Octyl β-D-glucopyranoside	Sigma-Aldrich	Cat# O8001-25G
PMSF	Sigma-Aldrich	Cat# 93482-250ML-F
Iodoacetamide	Thermo Fisher Scientific	Cat# A39271
Triton X-100	Sigma-Aldrich	Cat# T9284-500ML
cOmplete protease inhibitor tablet, EDTA-free	Sigma-Aldrich (Roche)	Cat# 11873580001
NaF	Sigma-Aldrich	Cat# S7920
Phosphatase Inhibitor Cocktail II	Sigma-Aldrich	Cat# P0044
Phosphatase Inhibitor Cocktail III	Sigma-Aldrich	Cat# P5726
Sodium Butyrate	Sigma-Aldrich	Cat# B5887
Suberoylanilide hydroxamic acid (SAHA)	Sigma-Aldrich	Cat# SML0061
Nicotinamide	Sigma-Aldrich	Cat# N3376
PR-619	Lifesensors	Cat# SI9619
Benzonase nuclease	Sigma-Aldrich	Cat# E1014-25KU
Dithiothreitol (DTT)	Thermo Fisher Scientific	Cat# A39255
Critical commercial assays		
CD138 MicroBeads, human	Miltenyi Biotec	Cat# 130-051-301; RRID:AB_3665843
CD33 MicroBeads, human	Miltenyi Biotec	Cat# 130-045-501
Pan T cell Isolation Kit, human	Miltenyi Biotec	Cat# 130-096-535; RRID:AB_3695577
$CD8^+$ T cell Isolation Kit, human	Miltenyi Biotec	Cat# 130-096-495; RRID:AB_3073903

(*Continued on next page*)

Continued

REAGENT or RESOURCE	SOURCE	IDENTIFIER
Dead Cell Removal Kit	Miltenyi Biotec	Cat# 130-090-101
EasySep Human B Cell Isolation Kit	STEMCELL Technologies	Cat# 17954
Chromium Next GEM Single Cell 5′ Reagent Kit v2 (Dual Index)	10× Genomics	Cat# PN-1000263
ImmunoSEQ hsTCRB Kit/ hsTCRB_v4b (UltraDeep)	Adaptive Biotechnologies	N/A
QIAamp DNA isolation kit	QIAGEN	Cat# 56304
T7 mScript Standard mRNA Production System	CellScript	Cat# C-MSC11625
TransIT-Virusgen Transfection Reagent	Mirus Bio	Cat# MIR6700
LDH cytotoxicity (release) assay	Promega	Cat# G7940
Annexin V-FITC Apoptosis kit/ Annexin V Binding Buffer	BD Biosciences	Cat# 556547; RRID:AB_2869082
4D-Nucleofector System reagents	Lonza	Cat# V4SP-3096
Deposited data		
HLA-I immunopeptidomics raw mass spectra, PSMs, and search database	This paper	MassIVE (https://massive.ucsd.edu)
scRNA/V(D)J-seq datasets	This paper	GEO: GSE242883
RRMM scRNA/V(D)J-seq (BCMA×CD3 TCE cohort)	Friedrich et al.[67]	GEO: GSE216571
Relapsed/refractory AML scRNA-seq	Abbas et al.[68]	European Genome-phenome Archive (EGA): EGAD00001007672
Healthy bone marrow scRNA-seq reference	SeuratData,[79] Satija Lab[80] Hao et al.[81]	GEO: GSE164378
Pan-cancer tumor-infiltrating T cell reference atlas (TREF)	Chu et al.[24]	https://singlecell.mdanderson.org/TCM/
AML post-allo-HCT bone marrow T cell dataset	Mathioudaki et al.[14]	Dataset kindly provided by A. Mathioudaki
Experimental models: Cell lines		
Patient-derived B lymphoblastoid cell lines (B-LCL)	This paper	N/A
HEK293T	ATCC	Cat# CRL-3216; RRID:CVCL_0063
B95-8 (EBV-producing marmoset line)	ATCC	Cat# CRL-1612; RRID:CVCL_1953
Oligonucleotides		
IVT forward primer (T7 promoter): 5′-TAATACGACTCACTATAGGGACC GGTGAATTCTAGCCAC-3′	This paper/Eurofins Genomics	N/A
IVT reverse primer: 5′-CGGGATCCAC GCCTATCA-3′	This paper/Eurofins Genomics	N/A
TCRseq primers 1 and 2; TCR amp primer mix	PhenomeX (Bruker Cellular Analysis)	Cat# 750-01001
TCR Index primers (N7XX and S5XX)	Illumina	Cat# 15052163
V(D)J-coding TCRα/β gene fragments (gene synthesis)	Twist Bioscience	N/A
Recombinant DNA		
pLVX-EF1α-IRES-Puro lentiviral expression vector	Takara Bio	Cat# 631253
pMD2.G (VSV-G envelope plasmid)	Addgene	RRID:Addgene_12259
psPAX2 (lentiviral packaging plasmid)	Addgene	RRID:Addgene_12260
Software and algorithms		
R v4.5.0	The R Foundation	https://www.r-project.org/
GraphPad Prism 10.0	GraphPad Software Inc.	N/A

(*Continued on next page*)

Continued

REAGENT or RESOURCE	SOURCE	IDENTIFIER
Cell Ranger v7.1/v10.0	10× Genomics	https://www.10xgenomics.com/support/software/cell-ranger/downloads
Seurat v5.0.1	Satija Lab[80,81]	https://cran.r-project.org/web/packages/Seurat/index.html
SCTransform (v2) v0.4.3	Satija Lab[82,83]	https://cran.r-project.org/web/packages/sctransform/index.html
scDblFinder	Germain et al.[84]	https://github.com/plger/scDblFinder
vegan v2.6-4	vegan developers	https://vegandevs.github.io/
presto v1.0.0	Raychaudhuri Lab[85]	https://github.com/immunogenomics/presto
pheatmap v1.0.12	CRAN	https://cran.r-project.org/web/packages/pheatmap/index.html
AUCell v1.24.0	Aibar S et al.[86]	https://bioconductor.org/packages/release/bioc/html/AUCell.html
pROC v1.18.5	Robin et al.[87]	https://cran.r-project.org/web/packages/pROC/index.html
MiXCR	MiLaboratories; Bolotin et al.[88]	https://mixcr.com/
IMGT/V-QUEST	IMGT[89]	https://www.imgt.org/
FEST/MANAFEST analysis tool	Johns Hopkins (stat-apps)[31]	http://www.stat-apps.onc.jhmi.edu/FEST/
Decombinator pipeline	Innate2Adaptive lab @ University College London, 2024	https://github.com/innate2adaptive/Decombinator
VDJdb (downloaded Jan 25, 2024)	Shugay et al.[90]	https://vdjdb.cdr3.net/
McPAS-TCR (downloaded Feb 1, 2024)	Tickotsky et al.[91]	http://friedmanlab.weizmann.ac.il/McPAS-TCR/
turboGliph/GLIPH[57,92]	HetzDra	https://github.com/HetzDra/turboGliph
ComplexHeatmap	Gu et al.[93]	https://github.com/jokergoo/ComplexHeatmap
igraph; ggraph	Csardi & Nepusz, 2006[94]	https://igraph.org/
msa; ggseqlogo	Bodenhofer et al.[95]; Wagih et al.[96]	https://omarwagih.github.io/ggseqlogo/
Spectrum Mill v8.01	Broad Institute	https://proteomics.broadinstitute.org/
OptiType v1.3.1	Szolek et al.[97]	https://github.com/FRED-2/Optitype
NetMHCpan v4.1[98]	DTU Health Tech	https://services.healthtech.dtu.dk/
PeptideMatch v1.0	Chen et al.[99]	N/A
UniProtKB[99,100]	UniProt Consortium	https://www.uniprot.org/
HLA Ligand Atlas	Marcu et al.[40]	https://hla-ligand-atlas.org
tidyverse; ggplot2	CRAN	https://www.tidyverse.org/
matplotlib (Python)	Hunter, 2007[101]	https://matplotlib.org/
FlowJo v10.6.1/v10.8.1/v10.10	BD Biosciences/Tree Star	N/A
BD FACSDiva Software	BD Biosciences	N/A
Image Analyzer 2.4.16.6	Bruker Cellular Analysis	N/A
Adobe Illustrator 2026	Adobe Inc.	N/A
Other		
Lightning optofluidic system; OptoSelect chip; NanoPen chambers	Bruker Cellular Analysis	N/A
BD FACSAria Fusion cell sorter	BD Biosciences	N/A
BD FACSCanto II	BD Biosciences	N/A
Cytek Aurora spectral flow cytometer	Cytek Biosciences	N/A
10× Genomics Chromium controller	10× Genomics	N/A
Illumina NovaSeq 6000 (S2/S4 flow cells)	Illumina	N/A
Illumina MiSeq	Illumina	N/A
timsTOF SCP mass spectrometer; nanoElute LC	Bruker	N/A
Vanquish *Neo* UHPLC System	Thermo Fisher Scientific	N/A

(*Continued on next page*)

Continued

REAGENT or RESOURCE	SOURCE	IDENTIFIER
4D-Nucleofector System	Lonza	N/A
SpectraMax iD3 microplate reader	Molecular Devices	N/A
Qubit 4 Fluorometer	Thermo Fisher Scientific	N/A

EXPERIMENTAL MODEL AND STUDY PARTICIPANT DETAILS

Human participants

Patients with newly diagnosed multiple myeloma

Bone marrow and peripheral blood samples were obtained from 20 patients at diagnosis (pre-treatment/baseline) and, when available, after induction (immuno-)chemotherapy. All participants provided written informed consent prior to sample collection. The study was conducted in accordance with the principles of the Declaration of Helsinki and the Belmont Report. Ethical approval for the collection, functional testing, and sequencing of human samples was granted by the Ethics Committee of Heidelberg University Medical Faculty (reference numbers S-096/2017, S-777/2024).

Patients with newly diagnosed acute myeloid leukemia (AML)

Bone marrow and peripheral blood samples were collected from 21 patients at diagnosis (pre-treatment/baseline). Written informed consent was obtained from all participants, and the study complied with the Declaration of Helsinki and the Belmont Report. Ethical approval for the collection, functional testing, and sequencing of human samples was granted by the Ethics Committee of Heidelberg University Medical Faculty (reference S-744/2024).

Patients enrolled in clinical trial NCT02315716

Bone marrow aspirates were collected from 14 patients at baseline (pre-treatment) and at day +100 following autologous stem cell transplantation (ASCT). Written informed consent was obtained from all participants prior to enrollment. The study adhered to the Declaration of Helsinki and the Belmont Report. Ethical approval for the collection, functional testing, and sequencing of human samples was granted by the appropriate UK research ethics committee (reference number 07/Q0502/17).

Patients enrolled in clinical trial NCT03269136

Samples were collected from 18 patients at diagnosis (pre-treatment/baseline) and either after three cycles of bispecific antibody therapy (post-bsAb cycle 3) or at relapse, whichever occurred first. All patients provided written informed consent for sample collection, tissue sequencing, and review of medical records. The original study was conducted in accordance with the Declaration of Helsinki and the Belmont Report, and was approved by the University of Calgary Institutional Review Board (Ethics ID: HREBA.CC-21-0248) and the resulting dataset re-analyzed for this study.

Processing of human bone marrow samples

Bone marrow aspirates were 1:1 diluted in preparation buffer (PBS with 0.1% BSA and 2 mM EDTA), and mononuclear cell separation was performed by density centrifugation (Bicoll separating solution, Biochrom) with diluted bone marrow cells (centrifugation 20 min, 1300g). Cells were carefully aspirated and washed with preparation buffer (centrifugation 5 min at 470g). Red blood cells were lysed using RCL buffer (155 mM NH4Cl, 10 mM KHCO3, 0.1 mM EDTA) for 10 min at room temperature and bone marrow cells were washed (centrifugation 5 min, 470g) and resuspended in preparation buffer. Malignant plasma cells were freshly isolated using CD138 MicroBeads, human (Miltenyi Biotec) according to the manufacturer's instructions and frozen in 90% FCS (Sigma-Aldrich) supplemented with 10% DMSO and stored in liquid nitrogen until further use. Non-plasma bone marrow mononuclear cells were frozen after cell counting at 1×10^7 cells per aliquot in 90% FCS (Sigma-Aldrich) supplemented with 10% DMSO and stored in liquid nitrogen until further use.

Cell lines

$CD8^+$ Jurkat reporter cell line was cultured in GlutaMAX-containing RPMI supplemented with 10% heat-inactivated FBS and 1% penicillin-streptomycin. B lymphoblastoid cell lines (B-LCL) were grown in GlutaMAX-containing RMPI 1640 Medium supplemented with 10% FBS, 1% penicillin-streptomycin, 50 mM β-mercaptoethanol, 1 mM sodium pyruvate and 1× MEM Non-Essential Amino Acids, further referred to as B cell media. HEK293T cells were cultured in DMEM supplemented with 10% FBS and 1% penicillin-streptomycin.

METHOD DETAILS

Antigen-agnostic screening of tumor-reactive T cells

BMTs were isolated as described above. Dead cells were removed using a dead cell removal kit (Miltenyi Biotec). Untouched T cells were isolated using a T cell isolation kit, human (Miltenyi Biotec) according to the manufacturer's instructions. Patient-autologous CD138+ plasma or leukemia cells were isolated from thawed bone marrow mononuclear cells using CD138 or CD33 MicroBeads, human (Miltenyi Biotec), respectively. Tumor-reactive T cells were identified in single cell interaction assays on the Lightning™

optofluidic system (Bruker Cellular Analysis). A full clean workflow was carried out on the Lightning system using BLI cleaning solution (PhenomeX) and double distilled water (ddH2O). An OptoSelect™ chip (Bruker Cellular Analysis) was wetted with wetting solution (Bruker Cellular Analysis) according to the manufacturer's instructions. Human IFN-γ, IL-2, and TNFα capture beads (BioLegend) were loaded into the NanoPen™ chambers of the OptoSelect™ chip using opto-electropositioning technology. Subsequently, single T cells and patient matched tumor cells were transferred into each NanoPen™ of the OptoSelect™ chip. As a negative control, one of 12 field of views (FOVs) of the OptoSelect™ chip was loaded with T cells and cytokine capture beads only. As a positive control, a different FOV was loaded with T cells and human T-Activator beads (ThermoFisher Scientific). Cells were co-cultured on the OptoSelect™ chip with cell culture media at 36°C and 5% CO_2 for 12 h. The OptoSelect™ chip was perfused with a detection antibody mix (72 L LEGENDplex human Th panel detection antibodies, 4 L Brilliant Violet 421-*anti*-hCD137 antibody and 4 L FITC anti-human CD8 antibody, all from BioLegend) for 30 min. Cells and cytokine capture beads were washed with cell culture medium for 45 min. Subsequently, the OptoSelect™ chip was perfused with a streptavidin-PE solution (8 L LEGENDplex Streptavidin-PE (BioLegend) in 72 L PBS) for 30 min. Cells and cytokine capture beads were washed with cell culture medium for 45 min. Fluorescence and bright-field images (DAPI, FITC, CY5, PE, OEP filter) of the cells and cytokine capture beads were acquired at 10× magnification. Fluorescence images were analyzed with Image Analyzer 2.4.16.6 (Bruker Cellular Analysis).

Export and TCR sequencing of tumor-reactive T cells

Reactive T cells were unloaded from the respective NanoPens™ of the OptoSelect™ chip using OEP™ and exported into 10 L of TCL (2×) buffer (Qiagen) in a 96-well PCR plate (Eppendorf). 30 L of mineral oil (Sigma-Aldrich) was layered on top of each T cell export and cells were centrifuged at 1000*g* for 5 min at RT. RNA was isolated using 20 L of RNAClean XP magnetic beads (Beckman Coulter). Magnetic beads were washed twice with 80% ethanol (Sigma-Aldrich), dried at RT for 2 min and resuspended in 4 L of ice-cold RT mix 1 (1.0 L/well TCRseq primer 1, 1.0 L/well dNTP mix, 0.2 L/well RNase inhibitor, 1.8 L/well ddH_2O, all from PhenomeX). The export plate was incubated at 72°C for 3 min, followed by a gradual cool to 4°C. 3 L of ice-cold RT mix 2 (0.5 L/well TCRseq primer 2, 1.3 L/well RT buffer, 1.0 L/well RT additive, 0.1 L/well RNase inhibitor, 0.1 L/well RT enzyme, all from PhenomeX) was added to each well of the export plate. First-strand cDNA was synthesized using a thermal cycler (50 min at 42°C, 10 cycles of 2 min at 50°C and 2 min at 42°C, followed by 5 min at 85°C) and purified using 20 L of MagBind Total Pure NGS magnetic beads (Omega Bio-tek). Magnetic beads were washed twice with 50 L of 80% ethanol, dried at RT for 2 min and cDNA was eluted by adding 30 L of nuclease-free water. Agarose gel electrophoresis and DNA quantification (Qubit 4 fluorometer, ThermoFisher Scientific) were performed to verify TCR recovery of each exported T cell. A new PCR plate was prepared on ice (5.0 L/well PCR enzyme K, 0.4 L/well TCR amp primer mix (PhenomeX), 3.6 L/well ddH_2O, 1.0 L/well purified cDNA) and V(D)J regions of the TCR alpha and beta chains were amplified using a thermal cycler (3 min at 96°C, 23 cycles of 20 s at 98°C, 30 s at 70°C, 20 s at 72°C, followed by 5 min at 72°C). A reaction mixture, containing unique index pairs for each TCR amplicons, was set up in a new 96-well plate on ice (5.0 L/well PCR Enzyme K, 0.5 L/well TCR Index (N7XX and S5XX, Illumina), 4.0 L/well ddH_2O, and 0.5 L/well amplified TCR). Different TCR amplicons were barcoded in an indexing PCR (3 min at 96°C, 10 cycles of 20 s at 98°C, 30 s at 70°C, 20 s at 72°C, followed by 5 min at 72°C). 2 L of each PCR reaction mixture was pooled and the indexed library was purified using 0.8 volumes of MagBind Total Pure NGS magnetic beads. DNA was washed twice with 80% ethanol; magnetic beads were dried at RT for 3 min and the indexed library was eluted from the beads. The indexed TCR amplicon multiplex was sequenced at a concentration of 10 nM on an Illumina MiSeq system (paired-end 300 bp). TCR V(D)J and CDR3 sequences were identified using MiXCR. TCR sequences with more than 100 reads and productive CDR3 region (no stop codon and in-frame junction) were analyzed. Uncovered sequence regions of full-length TCRα and TCRβ sequences were reconstructed with published TCR sequences exhibiting the highest sequence homology aligned with IMGT/V-QUEST.

HLA class I immunopeptidomics on CD138+ multiple myeloma cells

Low-input immunoprecipitation of HLA-I:peptide complexes

Immunoprecipitation of HLA-I molecules on tumor cells occurred in three batches. Pt-01 through Pt-08 constituted the first batch, while Pt-09 through Pt-12 constituted the second batch, and Pt-16 to Pt-21 constituted the third batch. Tumor cells isolated from bone marrow aspirates as described above were thawed on ice, lysed in 0.2 mL of lysis buffer at 4°C (20 mM Tris-HCl pH 7.5 (Invitrogen, Waltham, Massachusetts, USA, 15567027), 1 mM Ethylenediaminetetraacetic acid (EDTA) (Invitrogen, Waltham, Massachusetts, USA, 15575-038), 100 mM NaCl (Sigma-Aldrich, St. Louis, Missouri, USA, 71386-1L), 6 mM $MgCl_2$ (Sigma-Aldrich, St. Louis, Missouri, USA, 63069-100ML), 60 mM Octyl β-*d*-glucopyranoside (Sigma-Aldrich, St. Louis, Missouri, USA, O8001-25G), 1 mM phenylmethylsulfonyl fluoride (PMSF) (Sigma-Aldrich, St. Louis, Missouri, USA, 93482-250ML-F), 0.2 mM Iodoacetamide (Thermo Fisher Scientific, Waltham, Massachusetts, USA, A39271), 1.50% Triton X-100 (Sigma-Aldrich, St. Louis, Missouri, USA, T9284-500ML), 1× C0mplete protease inhibitor tablet-EDTA free (Sigma-Aldrich, St. Louis, Missouri, USA, 11873580001), 10 mM NaF (Sigma-Aldrich, St. Louis, Missouri, USA, S7920), 1:100 dilution Phosphatase Inhibitor Cocktail II (Sigma-Aldrich, St. Louis, Missouri, USA, P0044), 1:100 dilution Phosphatase Inhibitor Cocktail III (Sigma-Aldrich, St. Louis, Missouri, USA, P5726), 110 mM Sodium Butyrate (Sigma-Aldrich, St. Louis, Missouri, USA, B5887), 2 M suberoylanilide hydroxamic acid (SAHA) (Sigma-Aldrich, St. Louis, Missouri, USA, SML0061), 10 mM nicotinamide (Sigma-Aldrich, St. Louis, Missouri, USA, N3376), and 50 μM PR-619 (Lifesensors, Malvern, PA, USA, SI9619: PR-619) in pre-conditioned 0.6 mL Eppendorf tubes, and incubated for 30 min with 0.5 L benzonase (Sigma-Aldrich, St. Louis, Missouri, USA, E1014-25KU). Eppendorf tubes were pre-conditioned by rinsing twice with 500 L high-performance liquid chromatography (HPLC) water, incubating overnight with 500 L HPLC water, and then rinsing twice again with 500 L HPLC water. After incubating in lysis buffer, the lysates were centrifuged at 15,000 rcf for 20 min at 4°C.

To pre-clear the samples, the supernatants were transferred to another set of pre-conditioned 0.6 mL Eppendorf tubes containing ~10 L phosphate buffered saline (PBS)-washed Gammabind Plus Sepharose beads (Sigma-Aldrich, St. Louis, Missouri, USA, GE17-0886-01) and incubated by end-over-end rotation at 4°C for 1 h. Gammabind Plus Sepharose beads were pelleted at 1500 rcf for 1 min at 4°C. The pre-cleared supernatants were transferred to pre-conditioned 0.6 mL Eppendorf tubes containing PBS-washed Gammabind Plus Sepharose beads (Sigma-Aldrich, St. Louis, Missouri, USA, GE17-0886-01) and 5 g anti-HLA antibody (W6/32) (Bio X Cell, Lebanon, New Hampshire, USA, BP0079). HLA-I peptide complexes were captured on beads by end-over-end incubation at 4°C for 3 h. HLA-IP beads were pelleted at 1500 rcf for 1 min at 4°C.

HLA-IP beads were washed on top of a 10 m PE fritted filter plate (Agilent, Santa Clara, California, USA, S7898A) that was activated with 1 mL acetonitrile (ACN) and equilibrated with 3 × 1 mL PBS on a positive pressure manifold (Waters Corporation, Milford, Massachusetts, USA, 186006961). HLA-IP beads were transferred to the activated filter plate with 4°C 1 mL PBS. 500 L PBS was added to the HLA-IP tube to pick up any remaining beads and transfer them to the filter plate. Beads were washed 2× with 4°C 1 mL wash buffer (20 mM Tris pH 7.5 (Invitrogen, Waltham, Massachusetts, USA, 15567027), 1 mM EDTA (Invitrogen, Waltham, Massachusetts, USA, 15575-038), 100 mM NaCl (Sigma-Aldrich, St. Louis, Missouri, USA, 71386-1L), 60 mM Octyl β-*d*-glucopyranoside (Sigma-Aldrich, St. Louis, Missouri, USA, O8001-25G), and 0.2 mM Iodoacetamide (Thermo Fisher Scientific, Waltham, Massachusetts, USA A39271)) and 2× with 4°C 1 mL 10 mM Tris-HCl pH 7.5.

Low-input HLA-I peptide elution and desalting

All HLA IP samples were acid eluted and desalted in two desalting steps (primary and secondary). For the acid elution and primary desalt of the first batch of samples, Sep-Pak tC18 96-well plate with 40 mg sorbent per well (Waters, Milford, Massachusetts, USA, 186002320) was equilibrated with 2 × 1000 L methanol, 500 L 99% ACN/0.1% FA, and 4 × 1000 L 1% FA on a positive pressure manifold (Waters Corporation, Milford, Massachusetts, USA, 186006961). Beads were resuspended in 400 L 3% ACN/5% FA in the filter plate and the filter plate was stacked on top of the equilibrated Sep-Pak tC18 plate. At this step, 50 fmol of Retention Time Standards (iRTs) (JPT Peptide Technologies, Berlin, Germany, RTK-1-10pmol) were spiked into each sample. The HLA-IP beads were washed 2 × 200 L 1% FA. HLA-I peptides were acid eluted from the beads by three, five-minute incubations with 500 L of 10% acetic acid. The peptides were desalted by 4 × 1000 L 1% FA (after the first FA wash, the filter plate was removed) and eluted from the plate with 250 L 15% ACN/1% FA and 2 × 250 L 50% ACN/1% FA, frozen at −80°C, and lyophilized.

For the primary desalt of the second batch of samples, a μElution Sep-Pak tC18 96-well plate with 5 mg sorbent per well (Waters Corporation, Milford, Massachusetts, USA, 186002318) was equilibrated with 2 × 900 L methanol, 500 L 99% ACN/0.1% FA, and 4 × 900 L 1% FA. HLA-IP beads were washed in 200 L 3% ACN/5% FA in the filter plate which was placed on top of the equilibrated Sep-Pak tC18 plate. At this step, 50 fmol of Retention Time Standards (iRTs) (JPT Peptide Technologies, Berlin, Germany, RTK-1-10pmol) were spiked into each sample. The HLA-IP beads were washed 2 × 200 L 1% FA. HLA-I peptides were acid eluted from the HLA-IP beads by three, five-minute incubations with 500 L of 10% acetic acid. The peptides were desalted by 4 × 900 L 1% FA (after the first FA wash, the filter plate was removed) and eluted from the plate with 250 L 15% ACN/1% FA and 2 × 250 L 50% ACN/1% FA, frozen at −80°C, and lyophilized.

The dried HLA-I peptides were stored at −80°C until reduction and alkylation were performed on the second batch of samples. HLA-I peptides were reconstituted in 100 L 10 mM Tris-HCl pH 7.5 (Invitrogen, Waltham, Massachusetts, USA, 15567027). 2 L of 250 mM dithiothreitol (DTT) (Thermo Fisher Scientific, Waltham, Massachusetts, USA, A39255) was added to the sample for a final concentration of 5 mM and incubated for 20 min at 50°C while shaking at 1000 rpm. 6 L of 250 mM iodoacetamide (IAA) (Thermo Fisher Scientific, Waltham, Massachusetts, USA, A39271) was added to the sample for a final concentration of 15 mM and incubated for 30 min at room temperature while shaking at 1000 rpm in the dark. The reaction was quenched with 2 L of 250 mM DTT, for a final concentration of 5 mM, and incubated for 15 min at room temperature while shaking at 1000 rpm. The sample was brought to 3% ACN/5% FA by adding 90 L of 6.67% ACN/11% FA.

For all three sets of samples, a secondary desalt was performed on the sample by mirco-scaled basic reversed phase separation on SDB-XC stage tips. Stage tips were set up with two punches of SDB-XC material (CDS analytical, previously Empore 3M, Oxford, Pennsylvania, USA, 98-0604-0223-1). Stage tips were equilibrated with 2 × 100 L methanol, 100 L 50% ACN/1% FA, and 3 × 100 L 1% FA. The lyophilized peptides were resuspended in 200 L 3% ACN/5% FA, loaded onto the equilibrated stage tip, and ran through twice to maximize peptide retrieval. HLA-peptides were desalted with 3 × 100 L 1% FA. HLA-peptides were eluted from the SDB-XC stage tips with 60 L 5% ACN/1% FA, 60 L 10% ACN/1% FA, and 60 L 50% ACN/1% FA. Combined elutions were frozen at −80°C, lyophilized, and stored at −80°C.[102,103]

LC-MS/MS analysis

HLA-I immunopeptidome data collection by LC-MS/MS was performed as described previously.[104] The first batch of HLA-I peptides were resuspended in 5 L 3% ACN/5% FA and 4 L were injected onto a timsTOF SCP (Bruker, Billerica, Massachusetts, USA). HLA-I peptides were loaded onto a 30 cm analytical column with 1.9 m ReproSil-Pur C18 silica beads (Dr. Maisch HPLC GmbH, Ammerbuch, Germany), packed in-house into a PicoFrit 75 m diameter fused silica column with a 10 m emitter (New Objective, Littleton, Massachusetts, PF360-75-10-N-5). HLA-I peptides were eluted using a stepped gradient on a nanoElute LC (Bruker, Billerica, Massachusetts, USA) ranging from 2 to 15% Solvent B (0.1% FA in ACN) over 60 min, 15–23% over 30 min, 23–35% over 10 min, 35–80% over 10 min and held at 80% for 10 min at 400 nL/min. MS1 scans were acquired from 100 to 1700 m/z and 1/K0 = 1.70 Vs/cm^2 to 0.60 Vs/cm^2 in DDA-PASEF mode. Ten PASEF ramps were acquired with an accumulation and ramp time of 200.0 ms. Precursors above the minimum intensity threshold of 1000 were isolated with 2 Th at <700 m/z or 3 Th at >800 m/z and re-sequenced until a target intensity of 20,000 cts/s followed by a dynamic exclusion of 20 s. The collision energy was lowered linearly as a function of increasing

ion mobility from 55.00 eV at 1/K0 = 1.60 Vs/cm^2 to 15.00 eV at 1/K0 = 0.60 Vs/cm^2. Standard tryptic precursor isolation polygon placement was optimized for HLA-I peptide species by extending the polygon to include singly charged precursors with >600 m/z.[104]

The second and third batch of samples were acquired on a modified timsTOF SCP, with a higher capacity tims cartridge (Bruker, Billerica, Massachusetts, USA). Peptides were loaded onto a 25 cm Aurora Ultimate CSI nanoflow analytical column with 1.7 m particle size (IonOpticks, Fitzroy, Victoria, Australia). Peptides were eluted using a stepped gradient on a Vanquish *Neo* UHPLC System (Thermo Fisher Scientific, Waltham, Massachusetts, USA, VN-S10-A-01). The gradient ranged from 0 to 15% Solvent B (0.1% FA in ACN) over 60 min, 15–23% over 30 min, 23–35% over 10 min, 35–85% over 10 min and held at 85% for 10 min at 200 nL/min. DDA-PASEF data acquisition parameters are identical to the timsTOF SCP HLA-I parameters described above.

HLA-I peptide database search

Raw mass spectra were interpreted with the Spectrum Mill (SM) software package, version 8.01 (Broad Institute; proteomics.broadinstitute.org). Only MS/MS spectra with a precursor sequence MH+ in the range of 700–2000, a precursor charge of +1 to +3, and a minimum of <5 detected peaks were extracted. Similar spectra with the same precursor m/z acquired in the same chromatographic peak were merged. MS/MS spectra with a sequence tag length >1 (i.e., minimum of three masses separated by the in-chain masses of two amino acids) were searched with no-enzyme specificity. MS/MS spectra were searched against a database comprised of human reference proteome Gencode 42 (ftp.ebi.ac.uk/pub/databases/gencode/Gencode_human/release_34/42) with 50,872 non-redundant protein coding transcript biotypes mapped to the human reference genome GRCh38, 602 common laboratory contaminants, 2043 curated smORFs (lncRNA and uORFs), 237,427 nuORF DB v1.037, and the JPT iRT peptides (JPT Peptide Technologies, Berlin, Germany, RTK-1-10pmol) for a total of 290984 entries.[50] Patient-specific predicted neoepitope peptides (see STAR Methods: NeoEpitope Prediction) were appended to the sequence databases used for searches that are included in the MassIVE deposit. Parameters for SM MS/MS HLA-I search module for the first batch of samples included: ESI-QEXACTIVE-HCD-HLA-v3 30 scoring; fixed modifications: carbamidomethylation of cysteine; variable modifications: protein N-terminal acetylation and deamidation, oxidized methionine, pyroglutamic acid at peptide N-terminal glutamine, deamidation of asparagine, cysteinylation; precursor mass shift range of −18 to 81 Da; precursor mass tolerance of ±15 ppm; product mass tolerance of ±15 ppm; and a minimum matched peak intensity of 40%. For the second batch of samples, parameters for SM MS/MS HLA-I search module differed in: variable modifications: protein N-terminal acetylation and deamidation, oxidized methionine, pyroglutamic acid at peptide N-terminal glutamine, deamidation of asparagine; precursor mass shift range of −18 to 33 Da. Peptide spectrum matches (PSMs) within <1% false discovery rate (% FDR) were confidently assigned for individual spectra via the target decoy estimation of the SM Autovalidation module. PSMs were filtered for precursor charges of +1 to +3, sequence lengths ranging between 8 and 11 amino acids, and a minimum backbone cleavage score (BCS) of 5. BCS is a metric of peptide sequence coverage to enforce uniformly higher minimum sequence coverage for each PSM. The score is a sum after assigning a 1 or 0 between each pair of adjacent amino acids in the sequence (maximum score is peptide length −1) given all ion types, with the goal of decreasing false positive spectra having fragmentation in a limited portion of the peptide by multiple ion types. PSMs were consolidated to peptides through the SM Protein/Peptide Summary module in the file case sensitive mode. A distinct peptide is determined by the highest scoring PSM of a peptide detected for each sample. If different modification states were observed for a peptide, each were reported with a lowercase letter indicating a variable modification (i.e., "C"-carbamidomethylated, "c"-cysteinylated).

Subset-specific FDR filtering for nuORFs

Subset-specific FDR was performed as previously described.[102] The aggregate FDR was set to <1% as described above. FDR for the subset of nuORF peptides requires more stringent score thresholding to reach a suitable subset specific FDR of <1%. Subsets of nuORF types were thresholded independently from the HLA dataset through a two-step approach. First, PSM scoring metrics thresholds were tightened on the nuORF subset: minimum SM score of 7, minimum percent scored peak intensity (SPI) of 50%, precursor mass error of ±5 ppm, minimum backbone cleavage score (BCS) of 5. This allows nuORF distributions for each metric to meet or exceed the aggregate distributions. Second, remaining nuORF type subsets with FDR estimate above 1% were further subjected to a grid search to determine the lowest values of BCS and SM score that improved the FDR to <1% for each ORF type in the dataset.

Identification of CAAs

Each HLA-peptide maps to a parent protein, with an associated gene symbol. From preexisting lists of known cancer-associated antigens (CAAs),[31,39,103,105] the gene symbols of the identified peptides were cross-referenced to identify CAAs in the immunopeptidome.

Healthy tissue presentation of CAAs

The previously identified CAA peptide sequences were evaluated for expression in healthy tissues using the HLA Ligand Atlas (https://hla-ligand-atlas.org).[40]

Antigen-dependent screening of tumor and virus-specific T cells

A modified version of the MANAFEST assay was used to evaluate T cell responsiveness to tumor and viral antigens.[31] 350,000 tumor cell-depleted BMTs containing T cells from patients Pt-04 to Pt-12 were stimulated *in vitro* with HLA class I-restricted CMV, EBV, Influenza A and Sars-CoV-2 peptide pools (jpt Peptide Technologies) as well as with personalized tumor antigen pools (HLA immunopeptidome-derived; synthesized at >90% purity by GenScript), a shared tumor antigen pool (HLA immunopeptidome-derived; synthesized at >90% purity by GenScript) and without peptide for 10 days. BMTs were cultivated in culture medium (X-VIVO 20 (Lonza) containing 5% of human serum) with 1 g/mL of each tumor antigen, viral antigen or without peptide (as a reference for non-specific or background clonotypic expansion). On day 3, half of the medium was replaced with fresh medium containing

cytokines at a final concentration of 50 IU/mL recombinant human IL-2 (Novartis), 25 ng/mL recombinant human IL-7 and 25 ng/mL recombinant human IL-15 (both from Biolegend). On day 7, half of the medium was replaced with fresh medium containing cytokines at a final concentration of 100 IU/mL IL-2, 25 ng/mL IL-7 and 25 ng/mL IL-15. On day 10, cells were harvested, washed twice with PBS and the cell pellets were snap-frozen. gDNA isolation and UltraDeep TCRB sequencing using the Immunosequencing hsTCRB_v4b workflow were performed by Adaptive Biotechnologies.

Validation of tumor-reactivity by autologous co-cultures

IVT and mRNA production of V(D)J coding gene fragments

V(D)J-coding gene fragments were synthesized by Twist Biosciences. 25 ng gene fragment DNA coding for the V(D)J regions of TCR alpha and beta chains flanked by BsaI restriction sites was mixed with 50 ng of plasmid T7-alpha-TRAC, 50 ng of plasmid T7-beta-TRBC and 10 L BsaI (New England Biolabs) and Golden Gate Reaction Mix was incubated in a thermocycler (30 cycles of 1 min at 42°C, 1 min at 16°C, followed by 5 min at 60°C). 0.5 L of the reaction mixture was incubated with 1 L of 1:10 diluted forward primer, 1 L of 1:10 diluted reverse primer, 5 L of Clone Amp™ HiFi PCR Premix (ThermoFisher Scientific) and 3 L of ddH2O in a thermocycler (30 s at 98°C, 30 cycles of 5 s 98°C, 5 s 62°C, 10 s at 72°C, followed by 30 s at 72°C). The ligated DNA fragment was purified using 1.8 volumes of MagBind Total Pure NGS magnetic beads (Omega Bio-tek) and eluted in 10 L of ddH2O. The ligation of the DNA fragment was verified by Sanger sequencing (Eurofins Genomics) and 1 g of DNA was *in vitro* transcribed using the T7 mScript™ standard mRNA production system (Cellscript). 5′-capped, 3′-polyadenylated mRNA was purified using 1.8 volumes of RNAClean XP magnetic beads (Beckman Coulter) and eluted in 40 L ddH2O.

Rapid T cell expansion for tumor specificity validation

PBMC were thawed and 0.5×10^6 $CD8^+$ T cells were sorted using a $CD8^+$ T cell isolation kit, human (Miltenyi Biotec). $CD8^+$ T cells were co-cultured with feeder cells (10×10^7 PBMCs irradiated at 40 Gy with Gammacell 1000 Elite irradiator) in X-VIVO™ 15 hematopoietic cell media supplemented with 2% human AB serum, 300 U/mL recombinant human IL-2 (Novartis Pharmaceuticals) and an initial concentration of 30 ng/mL CD3 antibody (OKT3, ThermoFisher Scientific) in T25 cell culture flasks (Cellstars). Half of the cell culture media was replenished with fresh media 3 times a week. At day 14 post start of co-culture, T cells were used for electroporation with IVT-transcribed mRNA of respective TCRA and TCRB chains to be tested.

mRNA transfection and functional testing of transgenic TCR-expressing T cells

2×10^6 expanded T cells in 20 L nucleofector P3 solution (Lonza) were transfected with 1 g of TCR coding mRNA in each well of a 96-well unit using an 4D-Nucleofector™ electroporator (EO-115 program, Lonza). Cells were rested for 10 min at RT, 180 L of pre-warmed TexMACS™ Medium (Miltenyi Biotec) was added and electroporated cells were incubated for 24 h in a 48-well plate. 50,000 electroporated autologous T cells and 50,000 tumor cells were co-cultured in 200 L cell culture media in a 96-well U-bottom plate for 16 h at 37°C. As controls, TCR-transgenic T cells were cultured with autologous CD8-depleted PBMCs, 1 g/mL CEFT peptide pool (JPT Peptide Technologies), or alone. As positive control, T cells were stimulated with human T cell TransAct™ (Miltenyi Biotech) according to the manufacturer's instructions. In addition, all former conditions were tested for mock electroporated autologous T cells (without TCR encoding mRNA). Flu-specific TCR mRNA-transfected autologous $CD8^+$ T cells were co-cultured with tumor cells and the aforementioned controls. Cells were washed twice with staining buffer (DPBS, 3% FBS, 2 mM EDTA), incubated with human Fc block™ (BD Biosciences) for 10 min at RT and stained with CD8-FITC, mTRBC-PE, CD69-PE-Cy7 and CD137-APC antibodies (all from BioLegend) for 20 min on ice in the dark. A 1:1000 diluted live/dead blue viability dye (Life Technologies) was used. Compensation was performed using OneComp eBeads™ (ThermoFisher Scientific). Fixed cells were acquired on the BD Canto II (BD Biosciences) running BD FACSDiva Software. Data were analyzed using FlowJo (v.10.8.1; Tree Star).

Testing of cytotoxicity of tumor-reactive T cells

PCR amplification and in vitro *transcription of TCR constructs*

Fully assembled TCRαβ sequences were ordered as custom gene synthesis from Twist Bioscience and delivered in a third-generation pLVX-EF1α-IRES-Puro lentiviral expression vector (631253, Takara Bio). To generate linear DNA templates for *in vitro* transcription, TCR-encoding inserts were amplified by polymerase chain reaction (PCR). Briefly, 1 L of vector DNA (10 ng) was combined with 25 L of Q5® Hot Start High-Fidelity 2× Master Mix (New England Biolabs), 1.25 L each of 20 M forward and reverse primers, and 21.5 L of nuclease-free water in a total reaction volume of 50 L. The following primers were used: forward, 5′-TAATACGACTCACTATAGGGACCGGTGAATTCTAGCCAC-3′ (incorporating the T7 promoter sequence); reverse, 5′-CGGGATCCACGCCTATCA-3′. Thermal cycling was performed as follows: initial denaturation at 98°C for 30 s, followed by 30 cycles of 98°C for 10 s, 68°C for 30 s, and 72°C for 75 s, with a final extension at 72°C for 30 s. PCR amplicons were purified using 1.8 volumes of MagBind TotalPure NGS magnetic beads (Omega Bio-tek) and eluted in 10 L of nuclease-free water. DNA concentration and purity were assessed using a Qubit 4 fluorometer (Thermo Fisher Scientific).

One microgram of purified amplicon DNA was used as template for *in vitro* transcription (IVT) using the T7 mScript™ Standard mRNA Production System (CellScript), which generates 5′-capped and 3′-polyadenylated mRNA in a single workflow. The resulting mRNA was purified using 1.8 volumes of RNAClean XP magnetic beads (Beckman Coulter) and eluted in 30 L of nuclease-free water. mRNA concentration was quantified by Qubit 4 fluorometry, and quality was assessed by capillary electrophoresis.

LDH release cytotoxicity assay with patient-autologous primary myeloma cells

To assess the capacity of TCR-transgenic T cells to kill patient-autologous primary myeloma cells, an LDH release-based cytotoxicity assay was established. On day 1, peripheral blood mononuclear cells (PBMCs) were thawed and processed as described above (see Processing of human bone marrow samples). T cells were enriched by negative selection using a human Pan T cell Isolation Kit (Miltenyi Biotec) according to the manufacturer's instructions. For electroporation, 2×10^6 enriched T cells were resuspended in 18 L of P3 Primary Cell Nucleofector™ Solution (Lonza), prepared according to the manufacturer's protocol. Cells were mixed with 2.5 g of TCR-encoding IVT mRNA (in 2.5 L volume) and electroporated using a Lonza 4D-Nucleofector™ system with the EO-115 pulse program. Immediately after electroporation, 100 L of pre-warmed TexMACS™ medium (Miltenyi Biotec) was added to the cuvette, and cells were gently transferred into 24-well plates containing 2 mL of TexMACS™ medium supplemented with 30 IU/mL recombinant human IL-2. Electroporated T cells were incubated overnight at 37°C in a humidified atmosphere with 5% CO_2.

On day 2, cryopreserved autologous bone marrow mononuclear cells (BMNCs) were thawed, and $CD138^+$ plasma cells were isolated by positive magnetic selection using human CD138 MicroBeads (Miltenyi Biotec) according to the manufacturer's instructions. Purified plasma cells were resuspended at a concentration of 2×10^5 cells/mL in RPMI 1640 medium supplemented with 5% fetal bovine serum (FBS) and 30 IU/mL IL-2. Co-cultures were established in 96-well flat-bottom plates by seeding 1×10^4 plasma cells per well in 50 L of IL-2-supplemented medium. For the MART-1 positive control condition, target cells were pulsed with MART-1 peptide (1 g/mL) for 1 h at 37°C prior to T cell addition; unpulsed control wells received an equivalent volume of medium only. Electroporated T cells were harvested, washed with PBS, and resuspended at 1×10^6 cells/mL in IL-2-containing medium. A total of 50 L of T cell suspension (5×10^4 T cells) was added per well to achieve an effector-to-target (E:T) ratio of 5:1. Co-cultures were incubated at 37°C with 5% CO_2 for 24 h.

On day 3, cytotoxicity was assessed by lactate dehydrogenase (LDH) release. Co-culture plates were centrifuged at $250 \times g$ for 10 min, and 100 L of cell-free supernatant was carefully transferred to a fresh flat-bottom 96-well plate. LDH reaction mix was prepared according to the manufacturer's instructions and 100 L was added per well. After incubation for up to 30 min at room temperature protected from light, absorbance was measured at 490 nm (with a 680 nm reference wavelength) using a SpectraMax iD3 microplate reader (Molecular Devices). Spontaneous LDH release from target cells cultured alone and maximum LDH release (target cells lysed with the provided lysis buffer) served as negative and positive controls, respectively. Specific cytotoxicity was calculated as: % Cytotoxicity = [(Experimental - Spontaneous)/(Maximum - Spontaneous)] $\times$ 100.

Flow cytometric assessment of T cell activation and target cell viability

Following supernatant removal for LDH quantification, remaining cells were washed once with PBS, transferred to 96-well U-bottom plates, and prepared for multi-parameter flow cytometry. Cells were incubated with Fixable Viability Stain 780 (FVS780; BD Biosciences) and a panel of fluorochrome-conjugated antibodies directed against CD138 (clone RB780), CD3 (clone BV510), CD69 (clone RB613), and CD137/4-1BB (clone BV750) for 20 min at 4°C in the dark. T cell surface expression of the transfected murine TCRβ constant region was assessed using an anti-mouse TCRβ constant region (mTRBC) antibody conjugated to PE. After washing with FACS buffer (PBS, 2% FBS, 2 mM EDTA), Annexin V-FITC staining was performed in Annexin V Binding Buffer for 15 min at room temperature in the dark to assess early apoptosis of target cells. Samples were acquired on a Cytek Aurora spectral flow cytometer (Cytek Biosciences) using a standardized fixed acquisition volume to enable quantitative comparisons between conditions. Spectral unmixing was performed using single-stained UltraComp eBeads™ (Thermo Fisher Scientific). Data were analyzed using FlowJo software (v.10.10; BD Biosciences). T cell activation was assessed by CD69 and CD137 co-expression on $mTRBC^+CD3^+$ T cells, and target cell death was quantified by Annexin V positivity within the $CD138^+$ plasma cell gate.

Epitope mapping of tumor-reactive TCRs

B cell isolation and EBV immortalization to generate B-LCLs

PBMCs were thawed and diluted to 1×10^7 cells/mL in B cell isolation buffer (PBS+2% FCS+ 1 mM EDTA). B cell isolation was performed by negative selection with the EasySep Human B cell Isolation Kit (17954, StemCell Technologies) following manufacturer's guidelines. Isolated B cells were counted and diluted in B cell media to 0.3×10^6 cells/mL. Epstein-Barr virus-containing supernatant from B95-8 cells is added to the cell suspension to reach a final cell density of 0.25×10^6 B cells/mL. EBV-induced immortalization was further supported by holo-transferrin (30 g/mL, T0665, Sigma-Aldrich) and CpG ODN 2006 (2.5 g/mL, tlrl-2006, InvivoGen). B cells were plated in round-bottom 96-well plates at a cell density of 5×10^4 per well and expanded for subsequent analyses.

Generation of TCR-transgenic jurkat cell lines

Fully humanized TCRs were ordered as custom synthesis from Twist Bioscience in a third-generation pLVX-EF1α-IRES-Puro lentiviral expression vector (631253, Takara). HEK293T were cotransfected with a VSV-G envelope expression plasmid (pMD2.G) and a packaging plasmid (psPAX2) following the TransIT-Virusgen Transfection (MIR6700, Mirus) guidelines. Viral supernatants were harvested 48 h post transfection and filtered supernatants were added onto Jurkat reporter T cells. The following day viral supernatant was replenished with fresh T cell media and selection of TCR-transgenic Jurkat T cells with puromycin (1 g/mL) was started 96 h after transduction.

Epitope mapping assays and analysis

Co-cultures were performed with the T-FINDER platform as previously described.[51] In brief, TCR-transgenic Jurkat T cells were plated with patient-derived B-LCLs in a 3:1 ratio in 96-well U-bottom plates. Peptides were synthesized at GenScript (>90% purity) and added in a final concentration of 10 M. Co-cultures and T cell activation were analyzed after 16 h. Staining solution was prepared in flow cytometry buffer (PBS, 2% FCS and 2 mM EDTA) and the following antibodies were diluted 1:200: anti-human CD2 PerCP-

Cy5.5 (RPA-2.10, 300216, Lot: B399713, B382499), anti-human CD20 PE (2H7, 302306, Lot: B380281), anti-human CD69 APC-Cy7 (FN50, 310912, Lot: B260870), anti-human CD3 PE-Cy7 (UCHT1, 300420, Lot: B368934) and anti-HA.11 APC (16B12, 901524, Lot: B362222). All samples were acquired on a SonyID7000 spectral analyzer and data was analyzed using FlowJo (10.6.1). The proportion of CD69-positive cells was determined by calculating the integrated area under the histogram that did not overlap with control samples, employing FlowJo's population comparison (Overton) technique.

Antigen HLA promiscuity testing using tetramers

The following HLA tetramers were used: Flex-T™ HLA-A*01:01 Monomer UVX, 280001, Biolegend; Flex-T™ HLA-A*02:01 Monomer UVX, 280004, Biolegend; Flex-T™ HLA-A*03:01 Monomer UVX, 280005, Biolegend; Flex-T™ HLA-A*11:01 Monomer UVX, 280007, Biolegend. Tetramer:peptide complexes were prepared according to the manufacturer's instructions. 20 L Flex-T™ monomer UVX (200 g/mL, Biolegend) was mixed with 20 L peptide solution (500 M, synthesized at >95% purity by GenScript Biotech) in PBS. Monomers were illuminated with UV light (365 nm, 8 Watts, 5 cm) for 30 min on ice. Monomers were subsequently incubated for 30 min at 37°C in the dark. 4.4 L of PE-streptavidin or APC-streptavidin solution (0.2 mg/mL, Biolegend) were added, mixed and incubated for 30 min on ice in the dark. A blocking solution was prepared by mixing 1.6 L 50 mM D-Biotin (Biolegend) and 192.4 L PBS. After incubation of HLA-matched BMT samples with tetramers, 2.4 L of blocking solution was added and tetramers were incubated on ice for at least 30 min in the dark. Cells were washed twice with staining buffer (PBS, 3% FBS, 2 mM EDTA), incubated with human Fc block™ (BD Biosciences) for 10 min at RT and stained with 100 L 1:100 diluted Flex-T™ complex for 30 min on ice in the dark. Cells were co-stained with anti-CD3-Pacific Blue™ and anti-CD8-FITC antibodies (both from Biolegend) as well as 1:1000 diluted live/dead™ fixable yellow dye (Life Technologies) for 30 min on ice in the dark. Compensation was performed using OneComp eBeads™ (ThermoFisher Scientific). Fixed cells were acquired on the BD Canto II (BD Biosciences) running BD FACSDiva Software. Data were analyzed using FlowJo (v.10.8.1; Tree Star).

Single-cell transcriptome/V(D)J analyses

Single-cell sequencing and data preprocessing

For single-cell RNA (scRNA), V(D)J, and CITE-seq analyses, bone marrow T cells (BMTs) were counted and divided into eight aliquots per patient sample. For the NDMM cohort, each aliquot was stained with TotalSeq™ hashtag antibodies (BioLegend) and fluorescently labeled antibodies prior to pooling. Viable $CD45^+CD3^+$ cells were isolated using fluorescence-activated cell sorting on a BD Aria Fusion™ system (Figure S1A). Single-cell capture, reverse transcription, and library preparation were performed on the Chromium platform (10× Genomics) using the Single Cell 5′ Reagent Kit v2, following the manufacturer's protocol, with 40,000 cells loaded per channel. Library quality was assessed, and final libraries were paired-end sequenced (26 and 92 bp) on an Illumina NovaSeq 6000 S2 lane. Raw sequencing data encompassing gene expression, V(D)J, and cell hashing information were processed using Cell Ranger (v7.1) with the 'multi' command, referencing the GRCh38 genome (2020-A) and V(D)J reference (v7.1.0). The newly diagnosed AML T cell datasets were aligned using Cell Ranger (v10.0) with the 'multi' command, referencing the GRCh38 genome (2024-A) and V(D)J reference (v7.1.0).

Quality control and normalization

Demultiplexing of single-cell data was performed using the HTODemux function in Seurat (v5.0.1),[80] classifying cells as singlets, doublets, or unassigned based on hashtag oligos. Heterotypic doublets were identified with the scDblFinder package and, along with hashtag-identified doublets, removed from further analysis. Cells lacking a productive alpha/beta TCR were excluded. All datasets were normalized using SCTransform[82,83] and mapped to a reference dataset of pre-annotated bone marrow scRNA-seq profiles from newly diagnosed MM patients. This step facilitated removal of contaminating $CD3^-$ cells, likely arising from sorting artifacts. Mapping was performed using the MapQuery function in Seurat, following the SCTransform v2 vignette (https://satijalab.org/seurat/articles/sctransform_v2_vignette.html). For the newly diagnosed myeloma samples only cells with >200 detected genes, <10% mitochondrial content, and identified as singlet $CD3^+$ T cells were classified as high-quality and retained for analysis. For the newly diagnosed AML T cell dataset only cells with >300 and <5000 detected genes, <10% mitochondrial content, and identified as singlet $CD3^+$ T cells were classified as high-quality and retained for analysis. Whenever not noted otherwise, only cells with productive TCR annotation were retained for further analysis.

scVDJ analysis

TCR clonotypes were defined based on the CDR3 amino acid sequences of paired alpha and beta chains as annotated by Cell Ranger. In cases where multiple alpha or beta chains were detected, the top-expressed chain was retained. Unique TCRs were identified per patient and assigned stable IDs across analyses. Diversity indices were computed in R using the vegan package (v2.6-4) (https://vegandevs.github.io/), and clonotype proportions were calculated within each post-QC dataset per patient.

Back-projectiodn of antigen-specific TCRs to single-cell transcriptomes

Tumor-reactive TCRs identified via functional screening were mapped to single-cell RNA/TCR datasets based on exact CDR3 amino acid sequence matches. When a match was observed for both TRA and TRB - or for TRB alone - the single-cell clonotype was annotated as tumor-reactive. TCRs expanded in MANA-stimulated conditions were identified using ImmunoSeq UltraDeep sequencing (Adaptive Biotechnologies) and analyzed using the FEST tool[31] (http://www.stat-apps.onc.jhmi.edu/FEST/) with an odds ratio threshold of 2, assuming 250,000 cells per well. TCRs with >1% abundance at baseline were excluded. Expanded TCRs were back-projected onto single-cell datasets via exact CDR3 TRB amino acid matching. Publicly annotated virus- and tumor-reactive TCRs were mapped by matching TRB CDR3 sequences to the VDJdb[90] (downloaded January 25, 2024) and McPAS-TCR[91]

(downloaded February 1, 2024) databases, respectively. Tumor-reactive TCRs targeting TP53 and RAS were included based on literature from Levin et al. (2021),[106] Kim et al. (2022),[107] and Malekzadeh et al. (2019).[108] HLA-matched TCRs were filtered and mapped to single-cell populations according to their restriction: HLA class I TCRs were assigned to CD8/NKT (initial labeling) cells, and HLA class II TCRs to $CD4^+$ T cells. Ambiguously annotated TCRs (e.g., with dual virus/tumor specificity) were flagged in all outputs.

Module scores of T cell dysfunction and cytotoxicity[52]

The following module scores were added to single cell dataset using Seurat's AddModuleScore(., assay = "RNA"):

T cell dysfunction score:

"LAG3","HAVCR2","PDCD1","PTMS","FAM3C″,"IFNG","AKAP5","CD7","PHLDA1","ENTPD1","SNAP47","TNS3","CXCL13","RDH10","DGKH","KIR2DL4","LYST","MIR155","RAB27A","CSF1","CTLA4","TNFRSF9","CD27","CCL3","ITGAE","PAG1","TNFRSF1B","GALNT1","GBP2","MYO7A".

T cell cytotoxicity score:

"FGFBP2","CX3CR1","FCGR3A","S1PR5","PLAC8","FGR","C1orf21","SPON2","CD300A","TGFBR3","PLEK","S1PR1","EFHD2","KLRF1","FAM65B","C1orf162","STK38","SORL1","FCRL6","TRDC","EMP3","CCND3","KLRB1","SAMD3","ARL4C","IL7R","GNLY".

Integration of external and internal datasets and generation of a unified pan-entity reference map of cancer associated T cells

The internal cohorts of newly diagnosed myeloma patients (NDMM, $n = 20$), newly diagnosed AML patients (NDAML, $n = 15$) as well as external datasets of relapsed/refractory myeloma (RRMM, $n = 18$; Friedrich et al., (2023)[67]), relapsed/refractory AML (RRAML, $n = 8$; Abbas et al., (2021)[68]), healthy bone marrow samples (HBM, $n = 9$ samples, Hao et al. (2021)[81]) and an atlas dataset of cross entity tumor infiltrating T cells (TREF, Chu et al. (2023)[24]) were integrated to compute a unified pan-entity reference of cancer associated T cells with a specific focus on bone marrow resident T cells. To this end 50.000 cells from the NDAML, NDMM, RRMM, TREF and 10.000 cells from HBM and RRAML (fewer cells in dataset available) were randomly sampled and integrated per biological replicate (replicates with fewer than 200 cells excluded) as per the Seurat V5 integration vignette using the RPCA method after LogNormalisation and removal of ribosomal, mitochondrial and TCR genes from Variable features.

The top 30 integrated dimensions were used to identify clusters per the standard workflow (https://satijalab.org/seurat/articles/integration_mapping) using FindNeighbours(), FindClusters(…, resolution = 2) and RunUMAP(…, return.model = T). T cell subsets were identified using canonical marker expression as well as FindAllMarkers(). After integration a monocyte-Tcell doublette cluster (determined by parallel lineage marker expression) which survived QC was identified and retained to be used as a dump cluster. Subsequently cells mapping to this doublette cluster were removed from further downstream analysis.

Subsequently all datasets shown in this manuscript were mapped to the here generated T cell reference UMAP after LogNormalisation, standard per sample preprocessing (https://satijalab.org/seurat/articles/integration_mapping) and mapping via FindTransferAnchors(…, reference.reduction = "pca", dims = 1:30), TransferData(…, dims = 1:30) and MapQuery(…, reference.reduction = "pca",reduction.model = "umap").

Differential gene expression and signature derivation

Differential gene expression (DGE) analysis was conducted using the presto package (v1.0.0; https://github.com/immunogenomics/presto) via the wilcoxauc() function on raw assay data. TCR variable genes were excluded from the DGE analysis. Visualizations were generated using the pheatmap package (v1.0.12) with scaled average gene expression values (calculated via Seurat's AverageExpression() function), or Seurat-native plotting functions.

To derive the TFiT (Tumor-reactive Feature-inferred T cell) signature, we performed DGE in the establishment cohort after downsampling each TCR reactivity group to a maximum of 2,000 cells. Tumor-reactive cells were defined based on experimental evidence, literature-based annotation, and the MANA assay, and were compared to cells annotated as virus-reactive (CMV, EBV, Influenza A, SARS-CoV-2) or orphan T cells. Marker genes were filtered using thresholds of adjusted p-value <0.01 and log2 fold-change >0.5.

In the full cohort, a similar DGE workflow was performed with reactivity group sizes capped at 5,000 cells. Eight iterations of gene signature candidates were assessed, prioritizing genes ranked by AUC values. The final TFiT signature comprised the top 15 genes meeting the above statistical criteria and demonstrating robust performance across datasets. Notably for generation of the TFiT signature, the above mentioned reference based dump cluster removal was not carried out in order to maintain TFiT integrity for subsequent analyses.

To assess the predictive value of TFiT and other published gene signatures, we conducted gene set enrichment analysis (GSEA) using AUCell (v1.24.0),[86] following the method described in Lowery et al. (2022).[12] Area under the ROC curve (AUROC) metrics were computed with the pROC package (v1.18.5).[87] Tumor-reactive cells were assigned as the positive class (1), and all others as negative (0). AUCell enrichment scores were used as predictors in ROC analyses. The optimal threshold for the TFiT score was determined using the coords() function to achieve sensitivity and specificity >0.8 in the validation cohort (AUC: 0.8953; threshold: 0.48, specificity: 0.801, sensitivity: 0.807). In the establishment cohort, this threshold yielded an AUC of 0.9795, specificity of 0.938, and sensitivity of 0.952. This threshold (0.48) was applied throughout the study for binary classification of tumor-reactive T cells based on their gene expression signature.

CDR3 similarity and network analysis

After the identification of tumor-reactive and the annotation of virus-reactive TCRs as described above, the sequences from all different classes of TCRs were extracted from TCR and scRNA/VDJ sequencing data were used for similarity analyses. All analyses were implemented in custom R functions. TCR sequences of non-annotated clonotypes from scRNA/VDJ were used as bystander-TCRs. CDR3 TRA and TRB sequence similarities were evaluated using local alignment with BLOSUM45 and a gap opening cost of 10 as described previously[92,109–111] utilizing the msa package in R. To normalize local alignment scores, they were divided by the self-alignment score of the query-sequence. The separated scaled similarity was aggregated by calculating a geometric mean for scaled TRA and TRB similarity for each pairwise comparison. A bootstrapping methodology was employed to establish a similarity score significance threshold. In this method all pairwise comparisons of non-annotated TRA-TRB pairs were calculated using the same approach outlined above. This resulted in a background distribution from over 100.000 TCR sequences from TCR-clones found in the bone marrow. Two thresholds at either a 95% or 99% percentile of these background distributions were calculated. The normalized similarities of virus-reactive TCRs were analyzed with the same approach. Across patients, similarities of tumor-reactive TCR TRA-TRB were computed. Additionally, gliph[57] as implemented in the R package turbogliph (https://github.com/HetzDra/turboGliph) was used to identify clusters of TRA or TRB sequences. Gliph-based clusters were calculated using the turbogliph function independently for TRA and TRB chains of the included clonotypes. Visualization was rendered through heatmaps filtering values above the 95% bootstrapping limit using the ComplexHeatmap R package.[93] To show that gliph[57] was able to identify similarities in either TRA or TRB, each TRA or TRB identified gliph-cluster is shown together with the pairwise similarity analysis. A graphical representation of similarities filtered with the 99% threshold was created with the igraph[94] and ggraph (https://ggraph.data-imaginist.com/) R packages. Distinct clusters of TRA-TRB similarity had their sequence motifs for TRA and TRB illustrated using the msa[95] and ggseqlogo[96] R packages.

Analysis of newly diagnosed MM samples during induction therapy

Clinical response correlation of TFiT to induction therapy was conducted in n = 16 NDMM patients receiving quadruple induction therapy (see Table S1).

Paired scRNA-seq and scVDJ-seq data from n = 9 patients before and after induction treatment were used to trace clonotype dynamics. Clonal overlap was defined by matching paired TRA and TRB CDR3 sequences. Relative abundance of each clonotype was calculated per time point. To assess statistical significance of clonal dynamics, we applied a bootstrapping-based empirical cumulative distribution function (ECDF) analysis, as previously described.[67] This involved 10,000 resampling iterations of the TCR repertoire at each time point. ECDF-derived p-values were adjusted for multiple comparisons using the Benjamini-Hochberg method.

Clonotype dynamics were categorized into five groups: expansion (significant increase), contraction (significant decrease), stable, complete loss (absent post-treatment), and replacement (only detected post-treatment).

Analysis of longitudinal relapsed/refractory MM samples during bispecific antibody therapy

Bispecific antibody (bsAb)-treated scRNA-seq datasets[67] were mapped to the same integrated reference of pan-entity T cells. Only cells with productive TCRs were retained. GSEA was performed using AUCell[86](v1.24.0) with the previously defined TFiT signature and fixed enrichment thresholds.

Virus-reactive TCRs were annotated via exact TRB CDR3 sequence matching to VDJdb,[90] without HLA filtering. TCR overlap between timepoints was assessed based on CDR3 amino acid identity. Patients who relapsed before the end of cycle 4 were designated as clinical non-responders/bsAb-refractory.

Analysis of newly diagnosed AML samples during induction chemotherapy

NDAML patient datasets were generated as mentioned above and mapped to the same integrated reference of pan-entity T cells. Only bone marrow samples were carried on for further analysis (total of n = 15 patients, see Table S1). GSEA of the TFiT signature was conducted using AUCell with previously established thresholds.

Analysis of longitudinal r/r AML samples during AZA/nivolumab therapy

AML patient datasets[68] (kindly provided by Hussein A. Abbas) were mapped to the same integrated reference of pan-entity T cells.

GSEA of the TFiT signature was conducted using AUCell as described above. To correlate immune response with clinical parameters, TFiT dynamics and AML burden determined by flow cytometry were evaluated between timepoints A (pre-treatment) and B (post-initial exposure). Fold-changes in average TFiT expression and blast percentages were $\log_{10}$-transformed and compared via linear regression using R's lm() function.

Analysis of AML samples after allogeneic stem cell transplantation

AML patient datasets as preprocessed seurat objects (kindly provided by A. Mathioudaki) were mapped to the same integrated reference of pan-entity T cells. GSEA of the TFiT signature was conducted using AUCell as described above.

Deep TCRB sequencing of clinical trial samples (CARDAMON trial)

Genomic DNA was isolated from peripheral blood samples using QIAamp DNA isolation kit (QIAGEN) as per the manufacturer's instructions. TCR beta chain (TCRB) deep sequencing was performed on purified DNA from isolated bone marrow or blood

mononuclear cells to detect rearranged TCRβ gene sequences using hsTCRB Kit (Adaptive Biotechnologies) according to the manufacturer's protocol. The prepared library was sequenced on an Illumina MiSeq. TCR identification, error correction and CDR3 was performed using the *Decombinator* pipeline,[112] available at https://github.com/innate2adaptive/Decombinator. Samples with <2000 total TCR counts were removed. TCR α and β-chains were aggregated to clonotypes for each donor by amino acid CDR3 sequence. Clonality was defined as the inverse of diversity calculated using the Shannon diversity index and Rényi entropy as implemented by the *vegan* package (https://cran.r-project.org/web/packages/vegan/index.html). To account for differences in sample size, a weighted subsampled of 2000 counts was taken 100 times for each sample as the mean diversity calculated.

Whole-genome sequencing of tumor cells and germline controls

WGS was performed on an Illumina NovaSeq 6000 instrument with S4 flow cells in paired-end mode (2 × 151 bp). Previously described protocols were used for the extraction of nucleic acids, library preparation, and computational processing.[113]

Prediction of immunoglobulin-derived neoepitopes in multiple myeloma

To identify putative immunoglobulin-derived neoepitopes in MM, we developed a multistep bioinformatic workflow integrating somatic variant calling, HLA typing, and peptide binding prediction. Somatic variants were identified from tumor-enriched $CD138^+$ MM cells by comparing with matched germline data from PBMCs for exclusion of germline-encoded or non-somatic alterations. Variants located in non-coding regions were removed from downstream analyses. HLA class I haplotypes were inferred using OptiType[97] (v1.3.1), and candidate neoepitopes were predicted from non-synonymous SNVs and indels using NetMHCpan[98] (v4.1). To focus on HLA-presented ligands, only 8- and 9-mer peptides with a predicted eluted ligand rank $\leq$2% were retained. Variant allele frequency (VAF) was used to prioritize mutations with high clonal representation, minimizing artifacts due to tumor heterogeneity or subclonality. To mitigate the risk of selecting peptides with off-target reactivity, we filtered candidate neoepitopes against the UniProtKB[100] protein database using PeptideMatch[99] (v1.0). Peptides with sequence identity to known human proteins were excluded as potential self-antigens. The final list of predicted neoepitopes was ranked based on HLA-binding affinity and VAF of the underlying mutation, yielding a high-confidence set of immunoglobulin-derived neoantigen candidates for functional screening and validation.

Data visualization

Tabular data from single-cell sequencing analyses above were processed using the tidyverse suite of packages [https://CRAN.R-project.org/package=tidyverse] and visualized in the R programming environment using the ggplot2 package or the Python programming environment using the matplotlib package. Data from all other analyses were visualized using GraphPad Prism 10.0. Figures were produced using Adobe Illustrator 2026.

QUANTIFICATION AND STATISTICAL ANALYSIS

Data are represented as individual values or as mean ± SEM, as indicated. Group sizes (n) and applied statistical tests are indicated in figure legends. Statistical significance and multiple hypothesis testing corrections were assessed as indicated in figure legends. All reported *p* values are two-tailed. All analyses were performed using either R v4.5.0 (www.R-project.org) or GraphPad Prism 10.0.

For functional experiments, bone marrow samples were blinded to the experiment performers. Shannon and all others indices were calculated using diversity() vegan R package or Gini() as stated in methods above.

Due to the nature of this study, sample size determination was not applicable, as all available samples were included in this study. All cells passing QC were included in downstream analyses on a single-cell basis.